

**NASA
Technical
Paper
3279**

September 1992

1N-15
12/1/92
P.90

Phase I Final Report of the SITE Project: Continuous Data Bit-Error-Rate Testing

Gene Fujikawa
and Robert J. Kerczewski

(NASA-TP-3279) SITE PROJECT. PHASE
1: CONTINUOUS DATA BIT-ERROR-RATE
TESTING Final Report (NASA) 90 p

N93-11001

Unclass

H1/18 0121296

NASA

**NASA
Technical
Paper
3279**

1992

Phase I Final Report of the SITE Project: Continuous Data Bit-Error-Rate Testing

Gene Fujikawa
and Robert J. Kerczewski
*Lewis Research Center
Cleveland, Ohio*



National Aeronautics and
Space Administration
Office of Management
Scientific and Technical
Information Program

Contents

	Page
1.0 Summary	1
2.0 Introduction	1
3.0 Phase I Objectives	1
4.0 Test Results	2
4.1 Transponder Baseline Tests	2
4.1.1 Explanation of Transponder Baseline	2
4.1.2 RF Test Results	5
4.1.3 BER Test Results	16
4.1.4 Concluding Remarks—Baseline Tests	24
4.2 30-GHz Low-Noise-Receiver Tests	25
4.2.1 Receiver Design and RF Performance	26
4.2.2 Test Description	27
4.2.3 BER Test Results	29
4.2.4 Concluding Remarks—Receiver Tests	32
4.3 High-Power-Amplifier Tests	32
4.3.1 HPA Design and Performance	33
4.3.2 Test Description	34
4.3.3 BER Test Results	34
4.3.4 Concluding Remarks—Amplifier Tests	37
4.4 Interference Tests	38
4.4.1 Test Description	38
4.4.2 BER Test Results	40
4.4.3 Concluding Remarks—Interference Tests	45
4.5 Matrix Switch Tests	47
4.5.1 Matrix Switch Description	47
4.5.2 Matrix Switch CW Performance	48
4.5.3 BER Test Results	53
4.5.4 Concluding Remarks—Matrix Switch Tests	54
4.6 Amplitude Equalization Tests	57
4.6.1 Amplitude Distortions in Satellite Communications Systems	57
4.6.2 Induced-Distortion Tests	58
4.6.3 Link Equalization Tests	63
4.6.4 Concluding Remarks—Amplitude Equalization Tests	65
5.0 Conclusions	66
Acknowledgments	66
Appendixes:	
A—Complete Results of RF and BER Baseline Measurements	66
B—RF Measurement Methods	79
C—BER Measurement Methods	82
References	86
Bibliography	86

1.0 Summary

The Systems Integration, Test, and Evaluation (SITE) Project at the NASA Lewis Research Center encompasses a number of research and technology areas for satellite communications systems. Phase I of this project established a complete satellite link simulator system. Evaluating proof-of-concept microwave devices, radiofrequency (RF) and bit-error-rate (BER) testing of hardware, testing of remote airlinks, and other tests were performed as part of this first testing phase. This final report covers the test results produced in phase I of the SITE Project. The data presented include the results of 20-GHz high-power-amplifier testing, 30-GHz low-noise-receiver testing, amplitude equalization, transponder baseline testing, switch matrix tests, and continuous-wave and modulated interference tests. The report also presents the methods used to measure the RF and BER performance of the complete system. Correlations of the RF and BER data are summarized to note the effects of the RF responses on the bit error rate.

2.0 Introduction

A large part of the communications systems work over the past several years at the NASA Lewis Research Center has centered on the SITE test facility. This unique laboratory-based test bed, which was designed at Lewis, consists of a satellite communications system simulator integrated with high-data-rate digital Earth terminals to model a complete satellite communications system. The flexibility of the system allows for evaluation of advanced system design concepts and component performance, for development of hardware and software, and for inclusion of both networking and control. System experiments, such as bit-error-rate (BER) performance and degradation due to interference or signal distortions, can be performed. Major components that have been tested in the facility include high-power amplifiers and high-data-rate modems. The hardware development of the satellite link simulator established a commitment to 30/20-GHz communications research at Lewis. This simulator was tested extensively, both radiofrequency (RF) and digitally, to characterize the system test bed.

This report covers the continuous-data BER testing that was

performed in phase I of the SITE Project. The results that are presented include testing of major transponder components, such as 30-GHz low-noise receivers, intermediate-frequency (IF) matrix switches, and 20-GHz high-power amplifiers. The effects of amplitude equalization and interference (adjacent and cochannel) due to continuous-wave (CW) and modulated signals were also investigated. Determining how the RF responses affect digitally modulated signals and their BER's is important to satellite communications research, and therefore these results are also presented.

3.0 Phase I Objectives

The objective of the SITE phase I continuous-data BER testing was to perform quantitative BER measurements of a laboratory-based 30/20-GHz satellite communications system in transmitting continuous 220-Mbps serial-minimum-shift-keyed (SMSK) data for a variety of system parameters. Bursted-data transmission tests were not included in the phase I objective; they are planned as part of the phase II objectives. This objective was accomplished in the following manner: A large volume of RF test data was obtained from the RF test program for the 30/20-GHz, single-channel system. Measurements of the BER versus the ratio of energy per bit to noise power density E_b/N_0 for the 220-Mbps SMSK signal after transmission through the 30/20-GHz single-channel system were made under conditions identical to those for which the RF test data were obtained. The purposes were to correlate variations of the measured RF parameters with variations of the measured BER-versus- E_b/N_0 data and to determine how the system's RF parameters affect digital data transmission quality. The effects of the variation of signal power levels at critical points in the single-channel system on data transmitted through the system were measured by measuring the BER versus E_b/N_0 with the system adjusted to a number of power levels. The system performance in the presence of CW interferers, adjacent-channel modulated interferers, and cochannel modulated interferers was measured by introducing these effects into the system and measuring the resulting BER versus E_b/N_0 . These types of tests allowed the response of the 30/20-GHz, single-channel system to these perturbations to be measured.

4.0 Test Results

4.1 Transponder Baseline Tests

At the onset of the phase I testing we observed that when system operating parameters were changed, the measured system characteristics varied significantly. The parameters of particular importance were operating frequency, power level, amplifier operating point, and matrix switch crosspoint. The variation of the measured system characteristics has important implications in analyzing system performance. Without organizing and standardizing the important operating parameters, comparative analysis of measurement results would be meaningless. Therefore, a set of fixed transponder operating parameters and set points was established. This set of operating conditions became known as the transponder baseline. Once established, the baseline conditions were used for nearly all of the measurements described in this report.

Use of the transponder baselines allowed a large volume of useful measurement data to be obtained. Several important RF parameters, as well as a complete BER-versus- E_b/N_0 curve, were measured for each of the established baseline conditions. The resulting large body of test data was analyzed to assess the effects of RF parameter distortion on system BER, the effects of high-power amplifier (HPA) operating point on BER, the variation of system BER with matrix switch crosspoint, and other useful information.

In the following sections the development of the transponder baselines is explained, the final baseline operating conditions are given, and the results of RF and BER measurements are described. An analysis of these results, in terms of system RF performance, system BER performance, and the correlation of RF and BER data, is presented.

4.1.1 Explanation of Transponder Baseline

4.1.1.1 Variable Transponder Parameters

4.1.1.1(a) Baseline frequency bands.—Three 330-MHz primary frequency bands were chosen for baseline tests. As shown in figure 1, these bands were designated "A," "B," and "C." The 330-MHz bandwidth accommodates the

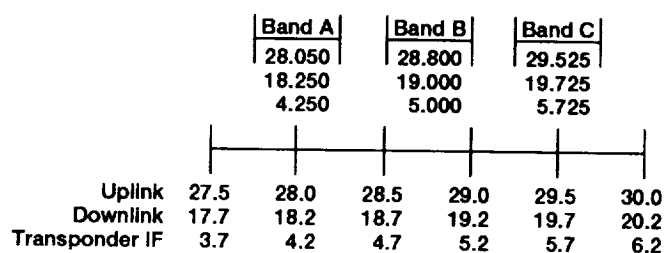


Figure 1.—Frequency bands of transponder baseline tests. Center frequencies are given for the uplink, downlink, and transponder IF. Each test band has a 330-MHz bandwidth. All frequencies are in gigahertz.

bandwidth requirement of the 220-Mbps SMSK-modulated signal. The bands were chosen to provide varying, rather than optimum, RF responses so that the effects of different types and degrees of distortion could be observed. Their location relative to the transponder's 2.5-GHz bandwidth resulted in varying RF parameters for each band.

The transponder's components, particularly the proof-of-concept (POC) hardware, exhibited degraded performance at their respective band edges and generally performed optimally at their band centers. Band B, which was located in the center of the 2.5-GHz bandwidth, thus exhibited the least distorted RF response. Band A, which was located at the lower end of the transponder bandwidth, suffered some distortion because of its location. Band C, which was located near the upper band edge, was the most severely distorted band, exhibiting in particular an amplitude rolloff that in some cases was as large as 10 dB.

4.1.1.1(b) Matrix switch crosspoints.—The microwave matrix switch built by Ford Aerospace and Communications Corporation was used exclusively in the transponder for baseline tests (refs. 1 and 2). Of 65 active crosspoints in the Ford matrix switch, 17 were chosen for baseline testing. Figure 2 shows the distribution of the crosspoints in relation to the 22-by-22 input-versus-output array. Crosspoint 7,6 was chosen as the primary baseline crosspoint; all of the baseline power settings were derived by using this crosspoint. The remaining 16 crosspoints were chosen in a 4-by-4 array that simulated the interconnection of four uplink and four downlink beams in a satellite-switched time-division multiple access (SS-TDMA) connection. For all of the baseline tests the transponder power levels were set with crosspoint 7,6. The

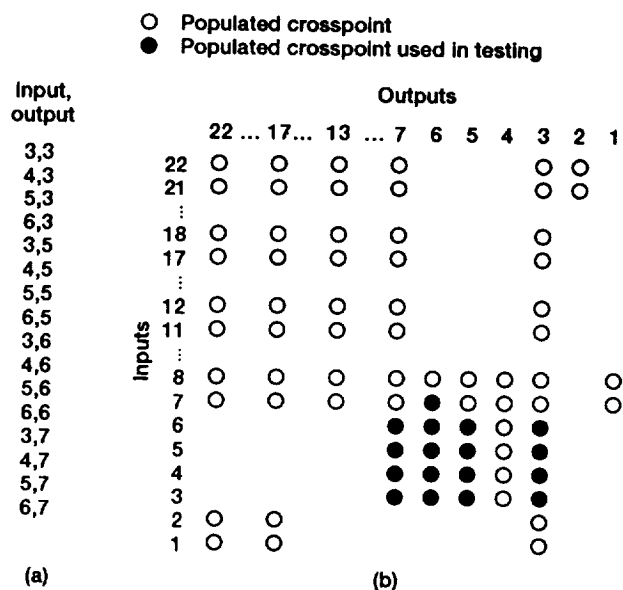


Figure 2.—Ford matrix switch crosspoints used in RF and BER testing. Primary test crosspoint: 7,6 (input, output).

settings remained unchanged when any of the other 16 crosspoints were used. Thus, some variation in transponder performance with varying matrix switch crosspoint was tolerated in order to keep the number of baselines at a manageable level.

4.1.1.1(c) Power amplifier modes and operating points.— Transponder baselines were developed for both the Texas Instruments (TI) gallium arsenide field-effect transistor (GaAs FET) HPA and the Hughes Electron Dynamics Division traveling-wave tube (TWT) HPA. For the TWT, three operating power modes are possible. Each mode (low, medium, and high) resulted in a different output power and gain, requiring different input powers and output attenuations. Therefore, a separate baseline was developed for each TWT mode.

In order to observe the effects of HPA operating point on system performance, the TI GaAs FET and the Hughes TWT (for all modes) were operated at three different points. The saturated operating point was determined by observing the highest output power attainable. When, upon increasing the HPA input power, the output power decreased, the saturation point was considered to be passed. The 1-dB-compression operating point was attained by recording and plotting the output power as a function of input power, in 1-dB increments (at the input). The 1-dB-compression point was defined as the point at which the output power fell 1 dB below a straight line drawn through points on the curve in the small-signal (linear) region. This point was easily determined from the output-versus-input power plots. The third operating point, known as the linear operating point, was also determined from the output-versus-input power curves and was defined as the point just before the power curve began to deviate from the straight line.

Figure 3 shows input-power-versus-output-power curves for the TWT and the GaAs FET, for band B. The saturation, 1-dB-compression, and linear operating points are indicated. For both the GaAs FET and the TWT the 1-dB-compression point occurred when the input power was backed off from the saturated operating point by 8 to 10 dB. The linear operating point occurred at an additional 8- to 10-dB input backoff from the 1-dB-compression point. A separate baseline was developed for each operating point.

As figure 3 shows, the TWT power curve never reached complete saturation for the low-power mode. The gain of the TWT decreased as it was changed from the high-power mode through the medium-power mode to the low-power mode. The low-power mode thus had the lowest gain and consequently required the highest input power to achieve saturation. The maximum output power of the driver amplifier was not great enough to saturate the TWT in the low-power mode. Thus, the TWT was not actually in saturation when the TWT low-power mode saturated baseline data were being taken but was approximately 3- to 4-dB input backoff from saturation. Similarly, the point chosen for 1-dB compression for the low-power mode was almost in the linear range, about 3 to 4 dB below the 1-dB-compression point. The third-order intermodulation tests indicate that significant signal compression

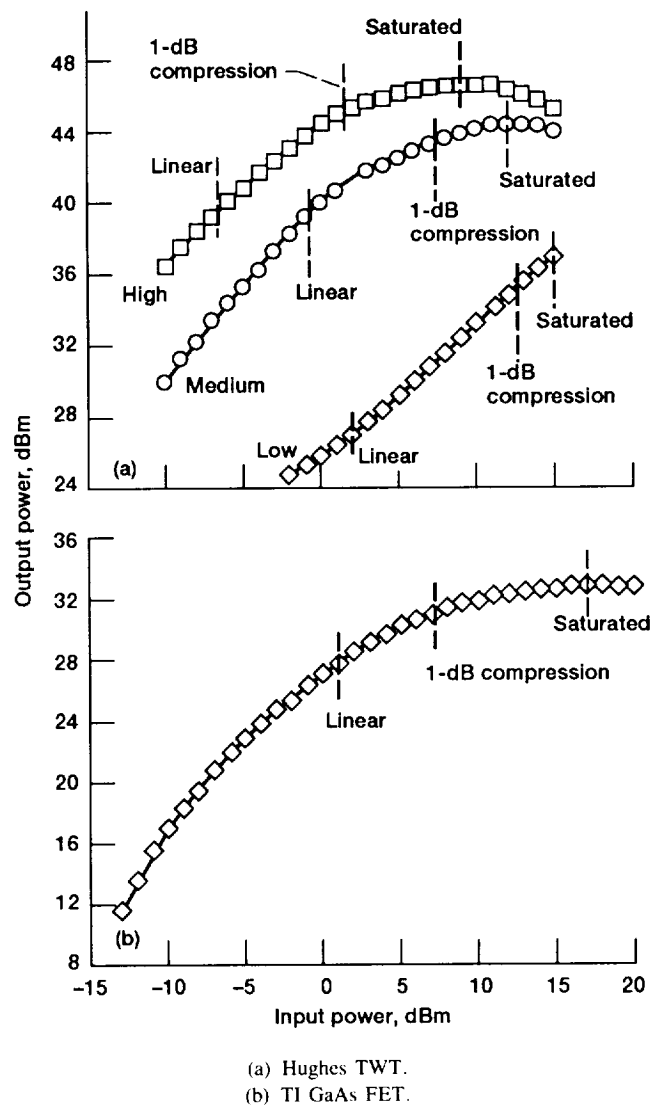


Figure 3.—Output power versus input power. Linear, 1-dB-compression, and saturated operating points are shown for each power mode.

was taking place at both the 1-dB-compression and saturated operating points, similar to that occurring in the other two power modes. The reason was that additional signal compression was taking place in the driver amplifier to get the maximum power into the TWT. Thus, baseline levels for the TWT low-power mode at saturation and at 1-dB compression were a reasonable approximation of saturated and 1-dB-compression levels.

4.1.1.2 Transponder Power Control and Monitoring

The phase I transponder contains five permanent power-monitoring points. An additional power monitor that is used to set transponder baseline parameters is located in the Earth terminal noise insertion subsystem. Six variable attenuators that are used to adjust power levels to obtain baseline settings are located throughout the transponder. Figure 4, a block diagram of the transponder, shows the location of the six

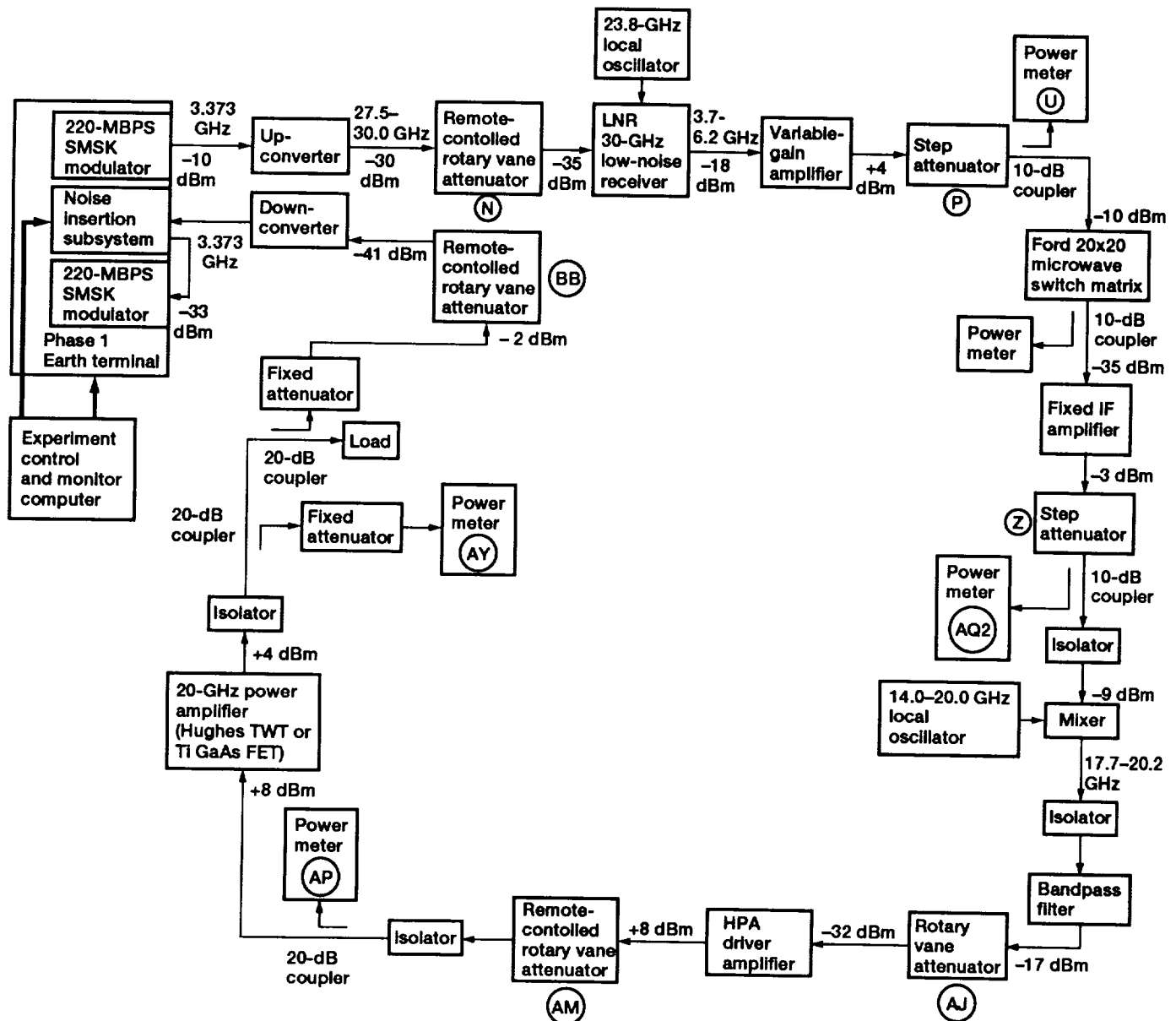


Figure 4.—Block diagram of phase I single-channel communications system simulator. Operating frequencies, approximate power levels, and baseline control and monitor points are shown.

attenuators and five permanent power monitors, the functions of which will now be explained.

The first variable attenuator in the transponder, designated "N," is located at the input to the 30-GHz, low-noise receiver and simulates the uplink transmission losses. This attenuator is a rotary vane attenuator (RVA) connected to a digitally indexed motor under computer control (ref. 3). The output power from the upconverter is constant at -30 dBm. The performance of the receiver as a function of input power is discussed in section 4.2. An operating input power level of -35 dBm was chosen for the transponder baseline. This power level ensures operation well above the noise floor of the receiver. Because the upconverter output is constant and the

required receiver input is constant, attenuator N was set to a constant 5 dB for all transponder baselines.

A variable-gain amplifier and a coaxial step attenuator (designated "P") are used at the output of the receiver to set the input power to the matrix switch. The matrix switch input power is set to -10 dBm and is monitored by power meter U. Because the receiver gain varies with frequency, the settings for attenuator P also vary with frequency band in order to maintain -10 dBm into the matrix switch. The variable-gain amplifier contains a continuously variable P-type intrinsic N-type (PIN) diode attenuator to control its gain. Slight adjustments (< 1 dB) were made to obtain a -19.2 -dBm reading on power meter AQ2 (through a 10-dB coupler).

Power meter AQ2 monitors the input power to the transponder upconverter mixer. An actual input power of -9.2 dBm is used because it is the highest power that can be read by the power sensor coupled to power meter AQ2. This is the highest mixer input power level that allows a linear IF-to-RF characteristic. A high power level into the mixer is desirable because it allows greater dynamic range at the input to the HPA driver amplifier. A coaxial step attenuator (designated “Z”) controls the input power to the upconverter; fine adjustments are made by using the variable-gain amplifier. Because the frequency response of the matrix switch varies with frequency, attenuator Z settings also vary with frequency.

Power meter AP monitors the input power to the 20-GHz HPA. The input power required varies with the amplifier, the power mode, and the operating point. Attenuator AJ, a manual RVA, controls the input power to the driver amplifier. Attenuator AM, a computer-controlled RVA, controls the final input power to the HPA. For most baseline cases attenuator AM is set to zero attenuation, and HPA input power control is attained by using attenuator AJ. In nearly all cases the driver amplifier is operated linearly. The exception is when the TWT is operated in the low-power mode, where the maximum available power from the driver amplifier is required to drive the TWT close to saturation. Power meter AY monitors the output power of the HPA.

The last attenuator in the transponder (designated “BB”) simulates the downlink transmission losses. This attenuator is set by observing the reading of the power meter located in the Earth terminal noise insertion subsystem. The input to the Earth terminal is required to be constant at -33 dBm in order for the BER measurement program to be used for all measurements. Attenuator BB is used to compensate for varying HPA output power levels.

4.1.1.3 Final Transponder Baselines Used for Testing

The final transponder baselines, including all of the variable parameters just described, are given in tables 1 and 2. Included in these tables are all of the attenuator settings and resulting power meter readings that were used to set and verify the transponder baselines. These settings were made and verified prior to each of the baseline RF and BER tests. Power meter readings are in decibels relative to 1 milliwatt, and settings for attenuators N, P, Z, and AJ are in decibels. Settings for attenuators AJ and BB are in motor indexer steps.

Considering all of the frequency bands, operating points, and matrix switch crosspoints used in baseline testing, a total of 468 different test configurations were obtained.

4.1.2 RF Test Results

Amplitude and phase distortions, noise, nonlinearities, and interference are the disturbances that have the greatest effect on the transmission quality of a communications channel. In the phase I baseline tests four of these five parameters were

investigated by performing unmodulated RF tests on the SITE system. The fifth parameter, interference, was investigated separately, as described in section 4.4.

Five RF measurements were made for the baseline configurations. Amplitude response and group delay response as a function of frequency were measured for all baseline configurations. Third-order intermodulation was measured for crosspoint 7,6 only, with all other parameters varied. The amplitude-modulation-to-phase-modulation (AM-PM) conversion coefficient was measured for all configurations, except the TI GaAs FET at the linear operating point because of time and equipment limitations. The output carrier-to-noise ratio C/N was measured for all configurations except the TI GaAs FET at the linear operating point. (C/N data for eight crosspoints in the TWT medium-power mode at saturation have been lost.)

A complete listing (1867 measurements) of all RF data obtained in the baseline testing is given in appendix A. The measurement methods for each of the five RF tests are described in detail in appendix B. Block diagrams of the hardware setups used are shown, along with examples of data outputs, plots, and graphs for each test. The method by which the reported data were extracted from the raw measurement results is also given. All the baseline measurements, including the BER measurements, are summarized in table 3. The values listed are the means over all crosspoints tested for the conditions stated in the table.

In the following sections the results of each RF test are described, and the correlation of measured RF characteristics to system operating parameters is analyzed. In the last section (4.1.2.7), correlations between relevant pairs of RF parameters are analyzed.

4.1.2.1 Results of Amplitude Response Measurements

The system output amplitude resulting from a frequency-swept CW input was measured on a spectrum analyzer. The results are presented in terms of the amount of amplitude variation, which was measured by subtracting the lowest from the highest amplitudes measured in the 330-MHz test band. The resulting number indicates the amount of amplitude variation for the system under the given test conditions. As shown in appendix A and summarized in table 3, a significant amount of amplitude variation was present in the system. In addition, the amount of variation varied considerably as baseline test parameters were varied. It is shown in section 4.6 that amplitude variation contributed significantly to degradation of the system's BER performance.

The amplitude response of the phase I single-channel system was primarily a function of three parameters: frequency band, HPA operating point, and matrix switch crosspoint. In table 3, amplitude variation is shown as a mean over all matrix switch crosspoints tested as HPA operating points and system test bands were varied. Variation as a function of matrix switch crosspoint can be observed in appendix A.

TABLE 1.—TRANSPONDER BASELINE FOR TWT

HPA operating point	Test band	Transponder control and monitor points: attenuator settings and power meter readings									
		Attenuator N, dB	Attenuator P, dB	Power meter U, dB	Attenuator Z, dB	Power meter AQ2 dB	Attenuator AJ (a)	Attenuator AM, dB	Power meter AP, dB	Power meter AY, dB	Attenuator BB (a)
Low-power mode											
Linear	A	5 ↓	14	-19.9	6	-19.2 ↓	16.0	0 ↓	-17.1	-10.7	37 800
	B		14	-20.1	6		13.0		-13.7	-10.1	38 600
	C		10	-19.9	5		13.0		-15.1	-15.4	52 800
1-dB compression	A		14	-19.9	6		9.0		-9.8	-4.5	22 400
	B		14	-20.1	6		7.0		-7.4	-4.8	25 800
	C		10	-19.9	5		2.5		-6.0	-7.0	25 400
Saturation	A		14	-19.9	6		1.0		-3.5	-0.9	16 400
	B		14	-20.1	6		1.0		-3.5	-2.2	20 000
	C		10	-19.9	5		0		-4.4	-5.6	23 000
Medium-power mode											
Linear	A	5 ↓	14	-19.9	6	-19.2 ↓	20.0	0 ↓	-21.3	-3.7	22 000
	B		14	-20.1	6		21.0		-21.4	-5.6	26 600
	C		10	-19.9	5		15.0		-16.9	-3.8	21 000
1-dB compression	A		14	-19.9	6		14.0		-14.7	1.6	13 400
	B		14	-20.1	6		12.2		-12.2	2.3	13 400
	C		10	-19.9	5		9.0		-12.2	0	13 200
Saturation	A		14	-19.9	6		7.0		-7.5	4.7	9 800
	B		14	-20.1	6		6.2		-6.8	4.1	11 200
	C		10	-19.9	5		2.0		-5.5	3.2	10 400
High-power mode											
Linear	A	5 ↓	14	-19.9	6	-19.2 ↓	21.0	76 000 ↓	-27.1	-2.4	19 000
	B		14	-20.1	6		22.0		-26.4	-2.4	20 400
	C		10	-19.9	5		17.0		-23.4	-1.9	17 600
1-dB compression	A		14	-19.9	6		15.0		-19.8	3.7	10 400
	B		14	-20.1	6		13.6		-18.4	4.0	11 600
	C		10	-19.9	5		10.1		-18.1	2.3	10 400
Saturation	A		14	-19.9	6		10.8		-10.8	7.4	6 800
	B		14	-20.1	6		9.3		-9.6	7.0	8 000
	C		10	-19.9	5		6.5		-9.3	6.2	7 200

^aUnits are motor indexer steps.

TABLE 2.—TRANSPONDER BASELINE FOR TI GaAs FET

HPA operating point	Test band	Transponder control and monitor points: attenuator settings and power meter readings									
		Attenuator N, dB	Attenuator P, dB	Power meter U, dB	Attenuator Z, dB	Power meter AQ2 dB	Attenuator AJ (a)	Attenuator AM, dB	Power meter AP, dB	Power meter AY, dB	Attenuator BB (a)
Linear	A	5 ↓	14	-19.9	6	-19.2	24.0	0 ↓	-25.2	-12.5	39 800
	B		14	-20.1	6	↓	25.0		-25.6	-13.6	47 800
	C		10	-19.9	5		26.0		-28.5	-16.8	54 400
1-dB compression	A		14	-19.9	6		14.4		-15.6	-4.8	20 400
	B		14	-20.1	6		14.5		-16.6	-6.3	26 800
	C		10	-19.9	5		19.6		-22.6	-11.9	37 400
Saturation	A		14	-19.9	6	↓	3.5		-5.6	-2.4	16 600
	B		14	-20.1	6		2.5		-5.4	-3.4	21 200
	C		10	-19.9	5		1.0		-5.2	-5.2	21 400

^aUnits are motor indexer steps.

TABLE 3.—SUMMARY OF SINGLE-CHANNEL RF AND BER MEASUREMENTS
[Mean values for all matrix switch crosspoints tested are given.]

High-power amplifier	Operating point ^a	Band	Amplitude variation, dB	Group delay variation, ns	AM-PM conversion, deg/dB	Output carrier-to-noise ratio, C/N, dB	Third-order intermodulation ^b dBc	Ratio of energy per bit to noise power density at BER of 10^{-6} , E_b/N_0 , dB
TWT low mode	Linear	A	2.09	1.44	1.15	22.55	25.10	1.09
		B	3.47	1.86	1.29	21.34	23.00	1.25
		C	9.37	7.20	3.95	23.76	28.90	5.14
		All	4.98	3.50	2.13	22.55	25.67	2.50
	1-dB compression	A	2.06	2.29	3.01	16.42	16.60	0.99
		B	2.86	2.24	3.50	15.68	13.70	1.07
		C	7.06	3.17	2.32	16.13	9.70	3.75
		All	4.00	2.57	2.94	16.08	13.33	1.94
	Saturation	A	1.78	7.03	4.75	14.80	6.60	0.98
		B	1.46	4.25	4.13	13.84	8.30	.90
		C	5.72	8.94	3.74	14.81	9.10	2.86
		All	2.98	6.74	4.20	14.48	8.00	1.58
	All data	All	3.68	4.51	3.39	16.21	15.67	1.85
TWT medium mode	Linear	A	3.24	1.83	1.35	22.06	20.80	2.55
		B	3.24	1.83	.78	21.12	26.10	2.18
		C	8.47	6.73	3.84	23.48	20.90	6.15
		All	4.99	3.47	1.99	22.22	22.60	3.63
	1-dB compression	A	4.38	1.80	3.58	16.66	14.50	1.41
		B	2.36	2.35	4.18	16.17	12.30	1.27
		C	6.83	7.36	2.20	16.36	10.80	5.67
		All	4.52	3.83	3.32	16.39	12.53	2.79
	Saturation	A	2.88	2.44	4.02	11.00	8.40	1.08
		B	2.17	2.42	4.19	14.20	5.90	.92
		C	2.32	3.54	2.39	14.41	1.50	2.32
		All	2.46	2.80	3.53	12.98	5.27	1.44
	All data	All	3.68	3.33	3.24	15.65	13.47	2.31
TWT high mode	Linear	A	5.34	2.26	0.88	22.12	22.40	2.80
		B	3.26	2.47	.61	20.84	27.40	1.95
		C	8.41	4.97	3.81	23.73	24.00	2.10
		All	5.67	3.23	1.77	22.23	24.60	2.28
	1-dB compression	A	2.43	4.57	2.18	16.25	15.70	3.37
		B	2.11	2.71	3.30	16.48	13.40	1.60
		C	7.01	4.98	2.00	16.43	12.10	3.86
		All	3.85	4.09	2.49	16.38	13.73	2.94
	Saturation	A	3.54	5.26	4.91	14.14	8.70	2.25
		B	1.74	4.00	3.96	11.66	7.40	1.44
		C	3.42	3.98	2.44	14.38	-.90	1.90
		All	2.90	4.41	3.77	13.39	5.07	1.87
	All data	All	3.67	4.12	2.96	15.83	14.47	2.39

TABLE 3.—Concluded.

High-power amplifier	Operating point ^a	Band	Amplitude variation, dB	Group delay variation, ns	AM-PM conversion, deg/dB	Output carrier-to-noise ratio, C/N, dB	Third-order intermodulation ^b dBc	Ratio of energy per bit to noise power density at BER of 10 ⁻⁶ , E_b/N_0 , dB
TWT	Linear	All	5.21	3.48	1.96	22.33	24.29	2.80
	1-dB compression		4.12	3.50	2.92	16.28	13.20	2.56
	Saturation		2.78	4.64	3.83	13.62	6.11	1.63
	All data	↓	3.68	3.99	3.20	15.90	14.54	2.18
GaAs FET	Linear	A	2.60	1.76	---	----	1.21	1.21
		B	3.81	2.05	---	----	----	1.01
		C	9.23	8.86	---	----	----	4.09
		All	5.21	4.22	---	----	----	2.10
	1-dB compression	A	1.59	1.25	3.88	17.68	12.30	1.08
		B	2.98	1.70	3.71	18.07	12.20	.89
		C	8.12	3.53	2.04	19.46	13.70	3.36
		All	4.23	3.16	3.21	18.40	12.73	1.78
	Saturation	A	1.42	2.91	4.48	17.80	8.00	0.92
		B	1.48	3.02	3.91	17.63	8.00	.83
		C	2.89	4.34	3.03	18.33	2.80	1.93
		All	1.93	3.42	3.81	17.92	6.27	1.23
	All data	All	2.69	3.41	3.51	18.16	9.50	1.58
TWT and GaAs FET	All data	A	2.61	3.23	3.58	16.25	14.46	1.53
		B	2.31	2.74	3.57	16.07	14.30	1.21
		C	5.86	5.23	2.65	16.98	12.05	3.36
		All	3.59	3.73	3.27	16.43	13.60	2.03

^aFor linear operating point, five crosspoints were tested. For 1-dB-compression and saturated operating points, 17 crosspoints were tested.

^bOnly one crosspoint tested.

The amplitude response of the system varied considerably between frequency bands. Band B had the flattest amplitude response, averaging 2.31 dB of variation. Band A was slightly worse, at 2.61 dB. Band C was significantly degraded relative to bands A and B, with an average variation of 5.86 dB, because of its location at the upper edge of the transponder bandwidth. Most of the amplitude variation in band C was in the form of a falling frequency slope. Figure 5 shows typical frequency responses for each band.

The variation of system amplitude response with matrix switch crosspoint was directly attributable to the matrix switch itself, in which performance varied considerably between crosspoints. The amount of variation between crosspoints is also a function of frequency band. The standard deviations, as a function of crosspoint, averaged about 0.5 dB in band A, 0.75 dB in band B, and 1.25 dB in band C. One crosspoint in particular, crosspoint 4,3, exhibited severely degraded performance in band C. Thus, the poorest band in terms of amplitude response also had the greatest variation from

crosspoint to crosspoint. The dependence of system performance on matrix switch performance is discussed further in section 4.5 and also in references 1 and 2.

Significant improvement in amplitude response was obtained by operating the HPA in compression rather than linearly. For the TWT HPA low-power mode the average amplitude variation was improved from 4.98 dB to 4.00 dB by moving from the linear operating point to the 1-dB-compression point. An additional improvement, to 2.98 dB, was obtained by moving to the saturated operating point. For the TWT medium-power mode the amplitude variation was improved from 4.99 dB to 4.52 dB to 2.46 dB as the operating point was changed from linear through 1-dB compression to saturation. In the TWT high-power mode the improvement was from 5.67 dB to 3.85 dB to 2.90 dB. For the GaAs FET HPA a similar improvement was noted. The amplitude variation was 5.21 dB at the linear operating point, but it improved to 4.23 dB at the 1-dB-compression point and improved further to 2.69 dB at saturation.

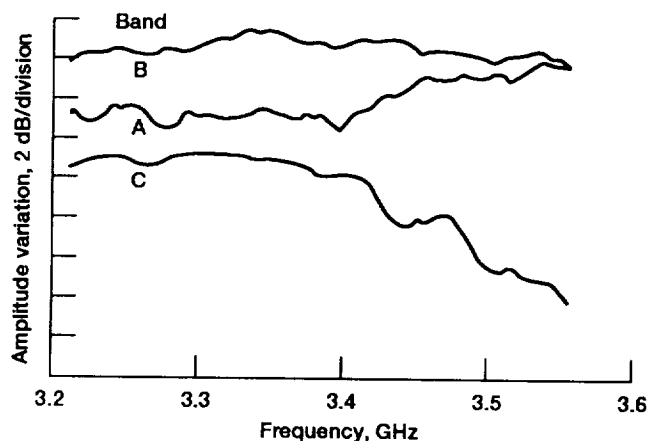


Figure 5.—Typical system frequency responses for test bands A, B, and C.

Finally, the data averaged over all conditions for both the TWT and GaAs FET HPA's indicate that the system amplitude response variation was about 1 dB better when the GaAs FET rather than the TWT was used as the HPA. For the TWT the average amplitude variation over all conditions was nearly identical for each of the three power modes.

These results indicate that the most of the amplitude variation in the system was due to the POC components, particularly the HPA's and the matrix switch's. Component testing done prior to the SITE phase I buildup and the subsequent phase I baseline testing, which showed a large variation in system amplitude response as matrix switch crosspoints were changed, indicates that the matrix switch was the largest contributor to overall amplitude variation. Additionally, the TWT appeared to add about 1 dB of additional amplitude variation relative to the GaAs FET. Driving the HPA's into saturation tended to flatten out the frequency response significantly. Smaller contributions to amplitude distortion were made by the receiver and other minor components of the system.

The hard-limiting effect produced by operating the HPA in saturation has several consequences. First, the highest HPA operating efficiency is obtained at the saturated operating point. Thus, this is often the operating point chosen for use in an operational satellite communications system because HPA power efficiency is of prime importance. As the baseline tests showed, hard limiting has the additional favorable effect of improving the system's frequency response in cases where amplitude distortions have been produced in the portions of the system before the HPA. The improved frequency response improves the BER performance, as shown in section 4.1.3.3. The problem with operating the HPA at saturation is intermodulation distortion, which is produced between adjacent channels, or side-lobe regrowth for single channels under certain modulation formats. The SMSK modulation used for the measurements described in this report is not susceptible to side-lobe regrowth, and thus no ill effects were noted. Adjacent channel measurements are presented in section 4.4.2.1.

4.1.2.2 Results of Group Delay Measurements

In a previous study group delay distortion was identified as a significant contributor to BER degradation for an SMSK-modulated channel (ref. 4). The study cited was based partially on results of phase I baseline measurements and on computer simulations.

The group delay data, summarized in table 3, indicate the amount of group delay variation, from highest to lowest measured group delay in the 330-MHz test band, similar to the amplitude variation. In appendix A, one can see considerable variation in the group delay data as system parameters are varied. However, the correlation of group delay distortion with baseline parameters is less clear than for the amplitude response data.

As with the amplitude response, the group delay variation appears to be a function of both frequency band and matrix switch crosspoint. The relationship to HPA operating point, however, is not clear. In some cases, the group delay variation improved as the HPA was driven into compression; in other cases it degraded. Also, the group delay data averaged over all conditions for the TWT and the GaAs FET show little difference in system group delay between the two HPA's.

In terms of frequency band dependence band B had the flattest group delay across the 330-MHz band, averaging 2.74 ns of variation. Band A was the second best, at 3.23 ns. Band C was the worst, with 5.23 ns of variation. Most group delay variation in band C was a rising response at the upper edge of the band that was coincident with the falling amplitude response also observed in this band. This ranking of performance by band exactly paralleled the amplitude response results. Thus, the transponder operating conditions that exhibited poor amplitude response were generally the same conditions that exhibited poor group delay response.

The system group delay response also varied significantly with matrix switch crosspoint because of the matrix switch performance variation between crosspoints. The average standard deviations as a function of crosspoint were 0.75 ns for band A, 0.54 ns for band B, and 1.89 ns for band C. This again reflected the overall degraded performance of band C. For group delay, band B slightly outperformed band A in terms of standard deviation; in contrast, for the amplitude response, band A was slightly better than band B.

The group delay response of the system was slightly better with the GaAs FET than with the TWT, with an average of about 0.5 ns less variation across the band. However, no conclusive results were found in terms of performance variation as a function of HPA operating point variation. In the TWT low-power mode the 1-dB-compression point had the best average group delay response, but in the medium-power mode the best response was at saturation and in the high-power mode the best response was in the linear region. For the GaAs FET the best response was at 1-dB compression. Thus, these tests indicate that the group delay response did not vary in any consistent way with the HPA operating point variation.

One primary source of group delay variation in an operational satellite system that did not exist in the SITE system is channel filtering. Channel filters, or demultiplexers, are used to separate frequency channels for processing and usually result in a parabolic group delay function with rapidly increasing group delay at the band edges. As demonstrated in reference 4, the effects of parabolic group delay distortion on an SMSK signal are negligible. The reason is that the SMSK spectrum has relatively low side-lobe levels. Only the main lobe of the spectrum is passed through the channel. Thus, the power level of the signal is quite low at the band edges, and parabolic distortions occurring at the edges because of channel filters have a negligible effect on the BER.

4.1.2.3 Results of AM-PM Conversion Measurements

Amplitude-modulation-to-phase-modulation (AM-PM) distortion occurs in nonlinear devices when amplitude fluctuations of the incident signal result in phase deviations of the output signal. If the signal has passed through components having a gain or group delay slope, the AM-PM conversion will result in phase distortion and contribute to BER (refs. 5 and 6). Thus, for the SITE system, in which we have already shown significant amplitude and group delay distortion, AM-PM distortion can be a significant source of BER degradation.

In the SITE system the only element that is operated nonlinearly is the HPA. Thus, the AM-PM conversion is a strong function of HPA operating point. It is not a strong function of the HPA itself, with nearly identical averages for the TWT and GaAs FET (considering that no data in the linear region were included in the GaAs FET average). There was some variation with matrix switch crosspoint and frequency band.

In terms of HPA operating point the AM-PM conversion was significantly lower in the linear region, as expected. The average AM-PM conversion factor measured in the linear region was less than 2.0 deg/dB. At 1-dB compression the average was 3.0 deg/dB, and at saturation the average was 3.8 deg/dB. Thus, the AM-PM conversion coefficient increased as the HPA was operated more nonlinearly. Note also that the average TWT AM-PM conversion was slightly lower in the high-power mode than in the medium-power mode and also slightly lower in the medium-power mode than in the low-power mode.

In terms of variation with matrix switch crosspoint the tables in appendix A show standard deviations ranging from 0.27 to 1.40 deg/dB. The measurements made with the HPA operating linearly had the lowest standard deviations, and band C at 1-dB compression and saturation and band B at saturation had the highest standard deviations. We believe that the variation of the amplitude response with frequency accounts for the variation in AM-PM data. The AM-PM measurements were made at the center of the band, and an amplitude variation of several decibels at the band center would result in a varying

level of nonlinearity in the HPA and thus a varying AM-PM conversion coefficient.

The dependence of AM-PM conversion on frequency was stronger for band C than for bands A and B. Bands A and B were nearly equal in terms of average AM-PM conversion coefficient, but in band C the average coefficient was nearly 1 deg/dB lower. Because band C exhibited a rolloff frequency, the measurement method (described in appendix B) yielded a lower AM-PM coefficient because of a smaller measured amplitude of the signal f_2 .

4.1.2.4 Results of Carrier-to-Noise Ratio Tests

The C/N tests measured the ratio of CW output signal power to output noise power in the 330-MHz test bandwidth, with the system operating at baseline power levels. The purpose of these tests was to ensure that adequate E_b/N_0 was available to perform a complete BER-versus- E_b/N_0 measurement for each baseline configuration.

The measurements showed that the output C/N ratios ranged from 26 dB to 9.5 dB. The C/N was found to be a function of HPA operating point for the TWT but not for the GaAs FET. There was little variation between TWT power modes and less than 1-dB difference between frequency bands on the average. The variation between matrix switch crosspoints was also small, with an average standard deviation as a function of crosspoint of about 1 dB, varying only slightly between frequency bands.

It was found that for the TWT the linear operating point afforded the largest output C/N for the system, averaging about 22.3 dB. As the TWT was driven to the 1-dB compression point, the C/N fell to 16.3 dB, and at saturation it fell further to 13.6. For the GaAs FET at 1-dB compression the C/N was 18.4 dB and at saturation it fell slightly to 18.2 dB. No measurements were made at the linear operating point for the GaAs FET.

Initially, it was believed that a minimum C/N of about 10.5 dB would be needed to achieve the minimum BER of 10^{-7} required to complete a BER measurement. However, measurements of C/N as low as 9.5 still allowed undegraded BER performance to be obtained. This led to the conclusion that the E_b/N_0 was higher when a modulated signal was transmitted than when a CW signal was transmitted. This was probably due to the spreading of the signal power across the band in the modulated case, which had the effect of suppressing noise across the band because of the small-signal capture effect. The fact the capture effect is occurring for the small-signal case can be seen from the baseline C/N data, which show that significant noise suppression is taking place in the TWT at the linear drive level, relative to the 1-dB compression and saturation cases. For the modulated signal the spreading of power across the 330-MHz band duplicates the small-signal capture effect and increases the real E_b/N_0 over that measured with a CW signal. In this were not occurring, the

C/N values measured for band A with the TWT in the medium-power mode at saturation (see appendix A, table 29(f)) would have led to significantly degraded BER. The measured BER for these cases, however, showed very little degradation. This indicates that the noise power generated by the TWT is decreased, relative to the CW case, when the transmitted signal is modulated.

4.1.2.5 Results of Third-Order Intermodulation Tests

Third-order intermodulation measurements were made for each system configuration, using only one matrix switch crosspoint, 7.6. The purpose of these tests was to quantify the amount of nonlinearity occurring in the system in terms of the relative level of third-order intermodulation products produced by two equal-strength CW signals input to the system at frequencies of 25 MHz above and below the band center frequency. The data given for third-order intermodulation are the difference in signal strength between the lowest fundamental signal and the highest third-order intermodulation signal measured at the output of the system.

The third-order intermodulation level is primarily a function of HPA operating point. The difference in third-order intermodulation between the TWT and the GaAs FET was negligible. In terms of frequency dependence some variation occurred between band C and bands A and B.

In the linear operating region the results varied between TWT power modes. (No measurements were made in the linear region for the GaAs FET.) In the low mode the average was 25.7 dB, in the medium mode the average was 22.6 dB, and in the high mode the average was about 22.3 dB. The data varied somewhat between frequency bands but not in a conclusive manner, especially since only one crosspoint was tested in each band. At the 1-dB-compression point the average third-order intermodulation product varied only slightly between power modes, measuring 13.3 dB in the low mode, 12.5 dB in the medium mode, and 13.7 in the high mode. Variation between frequency bands was significant and consistent. However, band A was 2.2 to 2.9 dB higher than band B in all cases, and band C was 1.3 to 3.9 dB lower than band B in all cases. At saturation the third-order intermodulation product averaged about 5.2 dB in the medium and high modes but was 8.0 dB in the low mode because the saturation level was not quite reached in this mode. Significant variation between frequency bands occurred in the medium and high modes, with band B about 1 dB lower than band A and band C 4.4 to 8.3 dB lower than band B. This large difference was due to the frequency response rolloff occurring in band C. In the low mode, band A had the lowest third-order intermodulation product and band C the highest.

For the GaAs FET, only slight variation occurred between frequency bands at 1-dB compression, with an average of 12.7 dB. At saturation band C was 5.2 dB lower than bands A and B (2.8 dB vs 8.0 dB). Averaged over both HPA's band C

averaged about 2.3 dB lower than bands A and B; most of this difference occurred with the HPA's at saturation.

As a measure of system linearity the third-order intermodulation measurements indicate that significant increases in nonlinearity occurred as the HPA's were driven from linear to 1-dB-compression to saturated operating points. The measurements indicate that the saturation point in the low-power mode was not quite reached for the baseline transponder settings used but was a relatively close approximation. In this mode the third-order signal at saturation was about 3 dB lower than in the medium and high modes on the average, but this difference was mostly due to band C data. For most cases, especially at saturation, band C appeared to be more nonlinear than the other two bands. This appearance was traced to the falling amplitude slope in band C, which reduced the amplitude difference between the higher frequency fundamental signal and the lower frequency third-order signal but does not necessarily mean a more nonlinear channel.

4.1.2.6 Interrelationships Between Measured RF Parameters

In the course of performing the RF measurements, it was noted often that certain configurations produced consistent results, either good or bad, for most RF tests. In particular, measurements made in band C usually produced the poorest results, whereas band B often produced the best results. However, the interrelationships between the RF parameters themselves were much less clear. For example, a system configuration in which a poor group delay response was noted did not necessarily exhibit a poor amplitude response or a high AM-PM coefficient. The relationships between pairs of the five RF parameters were analyzed by plotting the data point by point for each pair of parameters and by applying a linear regression curve-fitting analysis. In this section of the report we present observations on the correlation of the five RF parameters measured that are based upon this analysis. Only meaningful comparisons are presented. Regression analysis statistics for all comparisons are presented in detail in table 4.

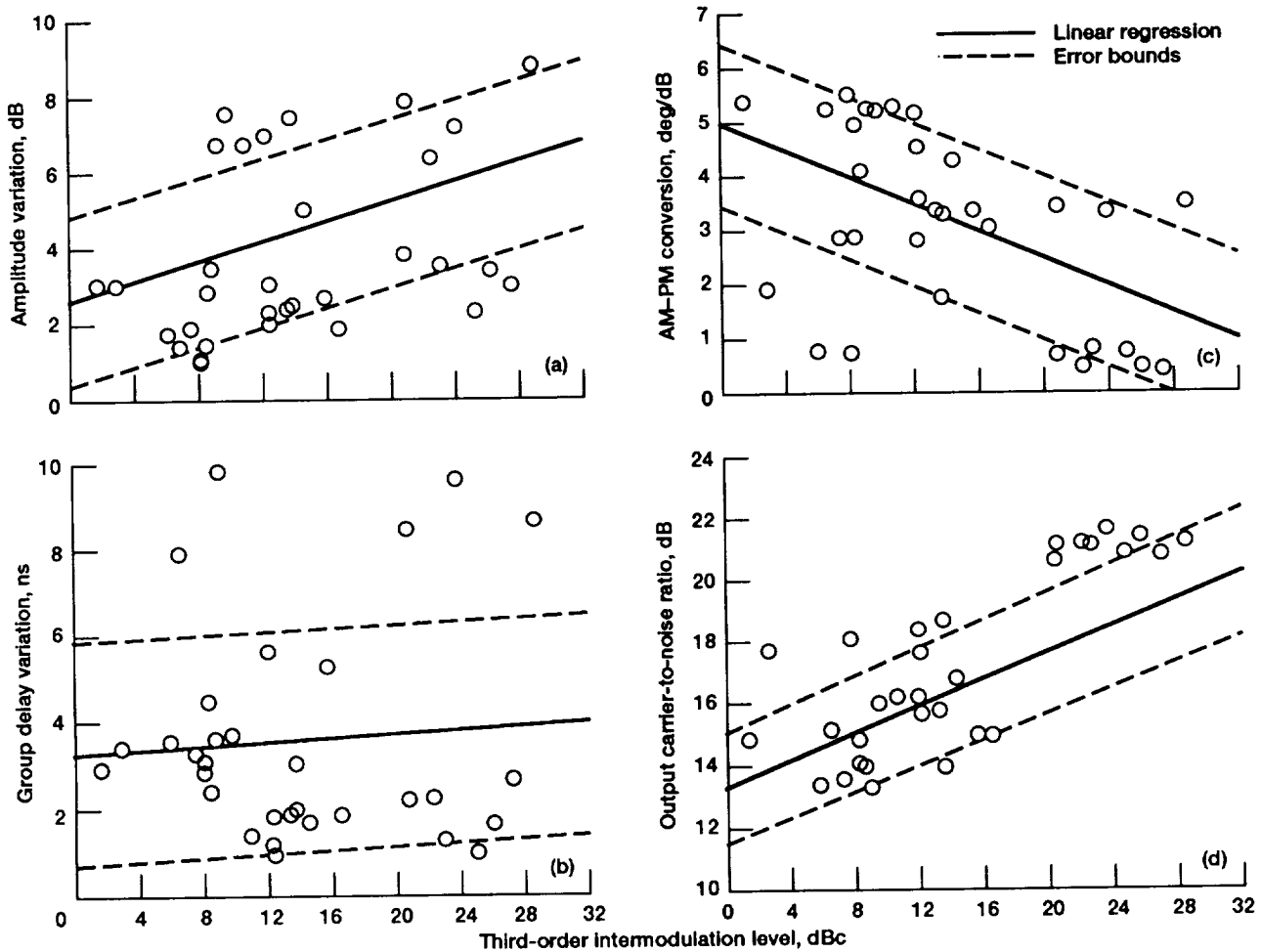
4.1.2.6(a) Comparison of third-order intermodulation with other parameters.—The third-order intermodulation measurement was the only one that directly measured the degree of system nonlinearity, and thus it was logical to compare the third-order results with the results of the other four measurements.

In figure 6 amplitude variation, group delay variation, AM-PM conversion, and C/N are plotted as a function of third-order intermodulation for all 34 test conditions. Also plotted are the calculated linear regression curves and error limits for each case.

The amplitude variation, as was noted earlier, was a function of the level of signal compression in the HPA. Hard limiting in the HPA tended to flatten out large amplitude variations resulting from other system components. Figure 6(a) shows the correlation of amplitude variation with third-order inter-

TABLE 4.—REGRESSION DATA FOR RF MEASUREMENTS

Data set	Independent variable, X	Dependent variable, Y	Y -intercept	Standard error of Y estimate	Coefficient of determination, R^2	Coefficient of X	Standard error of X coefficient
All data	Third-order intermodulation	Amplitude variation	2.55	2.21	0.113	0.10	0.050
		Group delay	3.32	2.60	.004	.02	.059
		AM-PM	4.81	1.51	.287	-.12	.034
		C/N	13.37	1.78	.603	.28	.041
GaAs FET	Amplitude variation	Group delay	1.81	1.49	.285	.35	.051
TWT	Amplitude variation	Group delay	2.28	2.39	.163	.46	.056
All data	AM-PM	Amplitude variation	5.01	2.27	.069	-.45	.078
		Group delay	3.43	2.40	.002	.09	.083
		Amplitude variation	-.42	2.25	.090	.24	.036
	C/N	Group delay	5.52	2.41	.017	-.11	.039
	C/N	AM-PM	5.40	1.32	.076	-.13	.021



(a) Amplitude variation.
(b) Group delay variation.

(c) AM-PM conversion.
(d) Carrier-to-noise ratio.

Figure 6.—Amplitude variation, group delay variation, AM-PM conversion, and carrier-to-noise ratio as a function of third-order intermodulation level for all test conditions.

modulation level. An increasing third-order intermodulation level, which indicates increasing system linearity, corresponds to an increasing amplitude variation, although the data are somewhat scattered and the error limits are rather large.

The group delay variation, as figure 6(b) shows, was a weak function of third-order intermodulation level and had considerable data scatter and little slope in the regression curve. Although, it has been noted that system configurations with large amplitude variations also generally contain large group delay variations, no strong, direct correlation was obtained between amplitude and group delay data. Therefore, the group delay was much less a function of third-order intermodulation than was amplitude response.

The AM-PM conversion coefficient was generally directly related to the system compression level. Figure 6(c) shows a significant correlation of the data; an increasing third-order intermodulation level corresponded to a decreasing AM-PM coefficient. Although several points fell outside the error limits, the AM-PM coefficient appeared to be a strong function of system linearity, as expected.

The C/N proved to be the strongest function of third-order intermodulation of the four RF parameters. The main reason is the TWT because signal backoff at the TWT input increased the C/N at the output. This is a characteristic of TWT's in general and was not observed for the GaAs FET HPA.

4.1.2.6(b) Correlation of group delay and amplitude response data.—A total of 468 data points for group delay and amplitude response were available for comparison. The data are plotted in figures 7(a) and (b) for the system with the TWT as the HPA and for the system with the GaAs FET as the HPA, respectively. The data were separated in this manner because the correlation between group delay and amplitude response was visibly greater for the GaAs FET than for the TWT.

In both cases it was clear that a rough correlation between amplitude variation and group delay variation existed, which was a logical and expected result. For the TWT data set (fig. 7(a)) data scatter was considerable and resulted in large error bounds. A large concentration of data occurred in the area bounded by 1 to 4 ns on the group delay axis and 1 to 4 dB on the amplitude axis. However, a discernible, if weak correlation existed, and showed that an increase in amplitude variation corresponded to an increase in group delay variation.

For the GaAs FET data set the correlation between the two parameters was much clearer. There was considerably less data scatter, with only a few points lying far outside the error bounds. The error bounds were much smaller for the GaAs FET data than for the TWT data. The reason for the better data correlation occurring in the GaAs FET data set was not clear but may be that the GaAs FET amplitude and group delay data exhibited less variation on the average than the TWT data.

4.1.2.6(c) Comparison of amplitude and group delay with AM-PM conversion coefficient.—A comparison of the amplitude and group delay results with the AM-PM conversion data is relevant because the combination of AM-PM conversion and amplitude or group delay distortions is believed to cause phase distortion resulting in bit errors (refs. 4 and 5). Thus, it was interesting to see whether increasing AM-PM conversion would correspond to increasing amplitude or group delay distortion and lead to a higher BER.

In figure 8(a) the amplitude variation is plotted against AM-PM conversion for all test cases. Although the data scatter is considerable, the linear regression curve shows a trend of decreasing amplitude variation with increasing AM-PM conversion. The reason is that whereas the AM-PM conversion generally increased with system nonlinearity, the amplitude variation decreased because of the hard-limiting effect of the

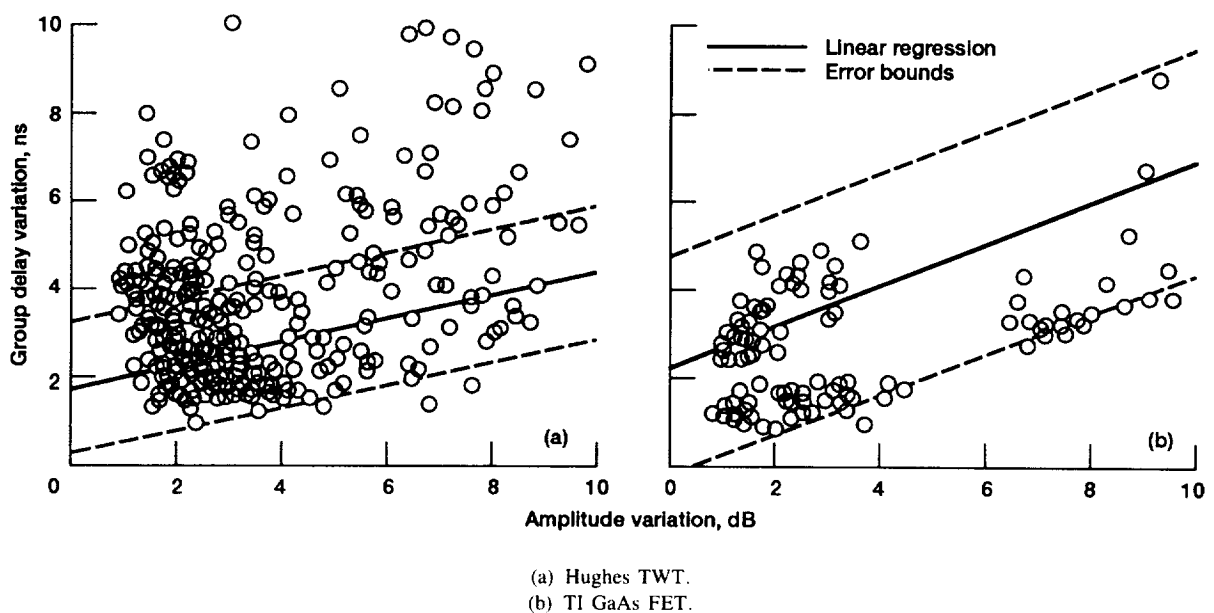


Figure 7.—Group delay variation as a function of amplitude variation for all test conditions.

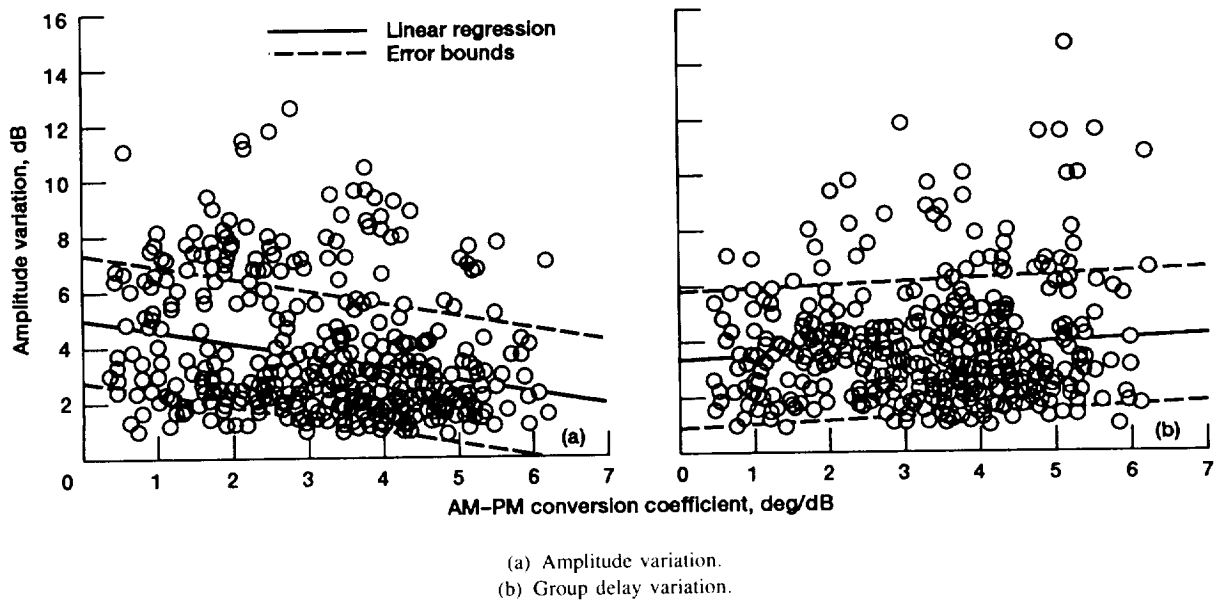


Figure 8.—Amplitude variation and group delay variation as a function of AM-PM conversion coefficient for all test conditions.

HPA, as was shown previously. Thus, the effect on BER caused by increasing AM-PM conversion was counteracted by decreasing amplitude distortion.

Figure 8(b), in which group delay variation is plotted against AM-PM conversion, suggests almost no data correlation. The small slope of the linear regression line indicates no trend in group delay distortion as AM-PM conversion increases. Also, considerable data scatter is present. Therefore, no substantial conclusions could be drawn in regard to relationships between group delay and AM-PM conversion for the SITE system.

4.1.2.7 Summary of RF Test Results

Five RF parameters were measured during SITE phase I RF testing. Amplitude response, group delay response, AM-PM conversion, C/N , and third-order intermodulation level were measured for all or part of some 468 system baseline configurations. A brief summary of these test results is now presented.

The system amplitude response was found to vary significantly with frequency band, HPA, HPA operating point, and matrix switch crosspoint. Band B had the flattest response and band C was the most severely distorted. The average variation of amplitude response over the 330-MHz test band was 1.0 dB lower when the GaAs FET was the system HPA than when the TWT was used. The standard deviation as a function of matrix switch crosspoint varied from 0.5 dB for band A to 1.25 dB for band C. The most significant result of the measurements was the flatter amplitude response obtained when the HPA was driven into the compressive, nonlinear region.

The group delay response of the system was found to vary with frequency band, matrix switch crosspoint, and HPA. Band B had the flattest group delay response over the 330-MHz

band, and band C had the most distorted response. The standard deviation as a function of matrix switch crosspoint ranged from 0.54 ns for band B to 1.89 ns for band C. The average group delay variation was about 0.5 ns less for the GaAs FET data than for the TWT data. No consistent variation of data was noted as the HPA operating point was varied.

The AM-PM measurements yielded no unexpected results. The AM-PM coefficient was found to be primarily a function of HPA operating point. Only slight variations existed as a function of HPA or matrix switch crosspoint. For frequency band C the average AM-PM coefficient was 1 deg/dB lower than for bands A and B. The average AM-PM conversion coefficient varied with HPA operating point. In the linear region the average AM-PM coefficient measured less than 2.0 deg/dB, at the 1-dB compression point it was 3.0 deg/dB, and at saturation it was 3.8 deg/dB.

For the C/N measurements the only significant variations were noted in the TWT data as a function of operating point. The measured C/N varied from 22.3 dB to 16.3 dB to 13.6 dB as the HPA operating point moved from linear to 1-dB compression to saturation. These results were apparently due to the characteristics of the TWT itself. Although C/N 's as low as 9.5 dB were measured, subsequent BER testing indicated that in all cases the C/N was high enough to provide an adequate SNR for successful BER testing.

Third-order intermodulation level measurements were made for a limited number of cases. Only slight variations were noted as a function of HPA, and only one matrix switch crosspoint was tested. In terms of frequency band, variations were noted but were not consistent between the various HPA's and power modes. Although the third-order intermodulation level varied between HPA's and power modes at a given operating point, the data indicated that significant compression was occurring

at the 1-dB compression and saturated power levels. The average third-order level was 23.5 dB in the linear region, 13.1 dB at 1-dB compression, and 5.7 dB at saturation.

The interrelationships between the five RF parameters were analyzed by plotting each pair of parameters against each other and performing and graphing a linear regression. We observed that the amplitude variation, the AM-PM conversion, and the C/N were relatively strong functions of third-order intermodulation level, whereas the group delay was a very weak function. Group delay correlated well with the amplitude data; increasing amplitude corresponded to increasing group delay variation. The effect was more pronounced for the GaAs FET cases than for the TWT cases. Finally, amplitude variation proved to be a function of AM-PM conversion, but group delay showed no such relationship.

4.1.3 BER Test Results

The establishment of the transponder baselines resulted in 468 different system configurations that were carefully categorized and characterized in terms of RF parameters, as has been described herein. In a second set of tests each system configuration was also characterized in terms of a BER-versus- E_b/N_0 curve. The results of these 468 BER measurements are described in this section.

4.1.3.1 Description of Baseline BER Measurement

A complete description of the method of measuring BER as a function of E_b/N_0 is contained in appendix C. In brief, the phase I digital Earth terminal was used as the modulated data source (ref. 7). An automated noise insertion and measurement subsystem calibrated and incremented the E_b/N_0 . Under control of the experiment control and monitor (EC&M) computer BER measurements were made for a number of E_b/N_0 's, starting at 5 dB. The noise and signal powers were measured and adjusted to vary the E_b/N_0 in 1-dB increments. Five BER measurements were made at each E_b/N_0 point, and an average result was obtained. If one or more of the five BER measurements were determined to be faulty, they were discarded and the remaining good measurements were reaveraged. As the E_b/N_0 was increased, the BER tended to decrease, requiring an appropriate increase in measurement time to obtain a measurement of consistent accuracy (ref. 8). When a BER of 10^{-8} was measured, a complete BER-versus- E_b/N_0 was considered to have been obtained and the measurement program was ended.

For each of the 468 baseline system configurations the transponder baselines were set according to tables 1 and 2, using a modulated signal as the system input. Each resulting BER-versus- E_b/N_0 curve was checked carefully at the conclusion of the measurement. When errors or anomalies were discovered, the data were discarded and the measurement was repeated. Acceptable BER-versus- E_b/N_0 data were entered into a computer program that stored and analyzed the data and

produced several types of graphical output to enable further analysis of the data.

4.1.3.2 Results of Baseline BER Measurement

The results of the baseline BER measurements are summarized in table 3 in terms of mean values for all baseline configurations over the several crosspoints tested. Results are presented in appendix A for each of the 468 baseline measurements.

In the following sections the BER results are compared with the major parameters of the SITE phase I system. System BER performance is described in terms of variation with frequency band, matrix switch crosspoint, HPA and HPA power mode, and HPA operating point. In section 4.1.3.2(f) the BER performance of the system in general is discussed. Additional details on BER performance are included in sections on matrix switch tests and 20-GHz HPA tests later in this report.

4.1.3.2(a) BER performance parameters.—The number used to represent the results of each BER measurement is the BER degradation at a BER of 10^{-6} , which is derived by measuring the difference in E_b/N_0 between the measured curve and the theoretical curve at a BER of 10^{-6} . This is shown graphically in figure 9 for a typical BER curve. The curve is produced by

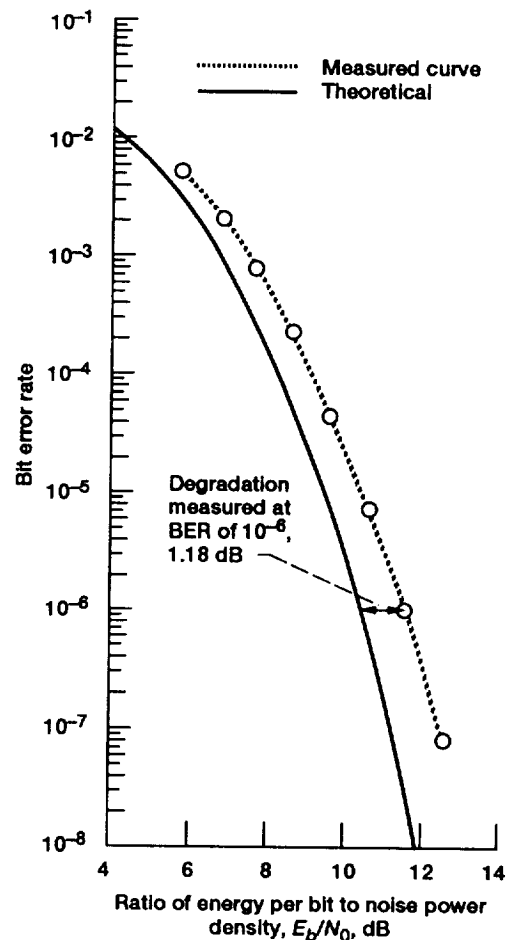


Figure 9.—BER as a function of ratio of energy per bit to noise power density.

the aforementioned computer program, which also calculates the BER degradation. Insofar as all BER curves measured during the SITE project have exhibited the same "waterfall" shape shown in figure 9, the BER degradation figure is a good indication of the transmission quality. The poorer the transmission quality of the system under test, the farther the measured BER curve will be from the theoretical curve. This separation normally occurs at all points along the curves; thus any arbitrary BER (other than 10^{-6}) could have been chosen, yielding the same relative performance comparison between any set of curves. A BER of 10^{-6} was chosen because it corresponds to data often published in the technical literature and thus allows for comparisons with other reported data. It also represents typical desired digital data transmission system performance. In addition, 10^{-6} falls far enough down the curve to allow good data resolution.

A BER curve for the back-to-back SMSK modulator-demodulator hardware connection is presented in appendix C. The degradation at a BER of 10^{-6} is 0.75 dB. This case represents the undistorted communications transmission channel, in which all degradation from the theoretical curve results from implementation losses occurring in the modulator and the demodulator. All additional degradation measured when using the SITE phase I transponder and Earth terminal in any configuration resulted from distortions created by the system hardware, which essentially represented the simulated communications transmission channel. It was the purpose of the phase I BER tests to quantify these distortions in terms of BER degradation.

4.1.3.2(b) System BER performance as a function of frequency band.—The BER performance of the system as a function of frequency band is detailed in table 3. Data averaged over the matrix switch crosspoints tested are given as a function of the HPA and the HPA operating point for each operating point. At the bottom of the table, average BER degradations are given as a function of frequency band for all system configurations.

Overall, the best BER performance was obtained in frequency band B, with an average degradation of 1.21 dB. Band A was only slightly worse at 1.53 dB. Band C was considerably degraded, with an average degradation of 3.36 dB, 2 dB worse than bands A and B and 2.61 dB worse than the distortionless (back-to-back modem) case. Measured BER curves displaying the typical variation between the three frequency bands are shown in figure 10. The curves shown are for the GaAs FET HPA operated at the 1-dB-compression point and using matrix switch crosspoint 7,6. The variation in BER performance between the frequency bands paralleled the RF measurement variation described earlier. This data correlation is investigated further in section 4.1.3.3.

When the data were broken down by HPA power mode and operating point, bands A and B continued to greatly outperform band C. An exception was noted for the TWT in the high-power mode. At both the linear and saturated operating points, band C performed comparably to bands A and B.

4.1.3.2(c) System BER performance as a function of matrix switch crosspoint.—In section 4.5 the system BER performance

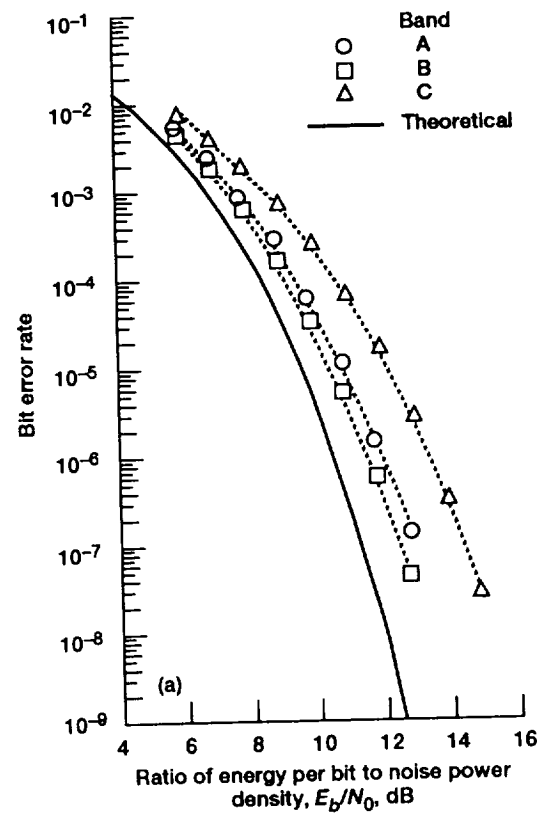


Figure 10.—Typical BER curves for frequency bands A, B, and C.

as a function of matrix switch crosspoint is presented in terms of comparing the performance of the Ford matrix switch with that of the GE matrix switch and in terms of assessing the contribution of the matrix switch to the total system distortion. In this section we discuss the variation in system BER performance as a function of the 17 Ford matrix switch crosspoints used in baseline testing.

In table 5 the BER degradation for each crosspoint is averaged over all test conditions (i.e., for all HPA modes, operating points, and frequency bands). Note that crosspoints 3,3, 4,5, 5,6, 6,7, and 7,6 were the only ones tested at the linear HPA operating point. The linear results, which usually had the poorest BER

TABLE 5.—BER DEGRADATION AS A FUNCTION OF MATRIX SWITCH CROSSPOINT

Cross-point	Mean, dB	Standard deviation, dB	Cross-point	Mean, dB	Standard deviation, dB
3,3	1.84	1.42	4,6	1.73	0.97
4,3	3.17	2.57	5,6	2.18	1.54
5,3	2.04	1.39	6,6	2.19	1.74
6,3	2.09	1.66	3,7	1.65	1.05
3,5	1.53	.74	4,7	1.78	1.15
4,5	2.09	1.30	5,7	1.88	1.28
5,5	1.92	1.13	6,7	1.96	1.52
6,5	2.18	1.42	7,6	2.04	1.01
3,6	1.65	.92			

performance, were averaged in with the 1-dB-compression and saturated results for these crosspoints. Nevertheless, table 5 shows that the range of variation was relatively small for these averages, from 1.53 to 2.19 dB, excluding crosspoint 4,3. Crosspoint 4,3 performed consistently worse than all others, averaging 3.17 dB of degradation. This was apparently due to the generally poor RF response of the system with crosspoint 4,3, particularly in band C.

Table 6 lists the standard deviation of the BER degradation data for each set of crosspoints. Thus, one can observe the system variation as the matrix switch crosspoint was changed while all other system parameters were held fixed. Band B had the smallest standard deviation in almost every case, ranging from 0.08 to 0.49 dB. Band A's was slightly worse, ranging from 0.10 to 0.69, excluding the TWT high-mode data. In the high mode, band A had a considerably higher standard deviation, from 0.80 to 1.38 dB. Band C's overall standard deviation ranged from 0.55 to 1.49 dB, and thus band C had not only the poorest average BER degradation but also the largest variation between crosspoints.

The standard deviations generally decreased as the HPA was driven from linear to saturated operating points. The GaAs FET HPA varied slightly less than the TWT. The TWT showed little variation between the three power modes, with the exception of band A, which exhibited a much higher standard deviation in the high mode than in the medium or low modes.

In summary, system BER performance as a function of matrix crosspoint varied slightly for bands A and B, particularly when

the HPA was in saturation, but varied significantly for band C in nearly all circumstances and for band A when the TWT was used in the high-power mode.

4.1.3.2(d) System BER performance as a function of HPA and HPA power mode.—The data summary in table 3 shows that on the average the system BER degradation was 0.6 dB lower with the GaAs FET amplifier than with the TWT. This significant difference is attributable to the better system RF response provided by the GaAs FET, as was noted in section 4.1.2.

The data also show some variation in system BER performance between the three TWT power modes. The average degradations were 1.85 dB in the low mode, 2.31 dB in the medium mode, and 2.39 dB in the high mode. The RF data yield no clues to the reason for these differing results. The average amplitude variation, for example, was virtually identical for the three modes, and the group delay variation was actually highest in the low mode. Thus, we only note this BER performance variation without attempting to explain it.

4.1.3.2(e) System BER performance as a function of HPA operating point.—The variation of system BER performance with HPA operating point is summarized by the data in table 7. In nearly every case, the average BER degradation decreased when the operating point was changed from linear to 1-dB compression and decreased still further as the operating point was moved to saturation. The exception was for the TWT high mode, where the degradation increased from linear to 1-dB compression. Examining the BER data in more detail (see table 3) shows that the effect of BER performance improvement held for all

TABLE 6.—STANDARD DEVIATION OF BER DEGRADATION FOR EACH GROUP OF CROSSPOINTS

High-power amplifier	Operating point	Band	Standard deviation, dB	High-power amplifier	Operating point	Band	Standard deviation, dB
TWT low mode	Linear	A	0.45	TWT high mode	Linear	A	1.38
		B	.28			B	.24
		C	.51			C	1.08
	1-dB compression	A	0.21		1-dB compression	A	1.34
		B	.23			B	.24
		C	1.23			C	1.03
	Saturation	A	0.10		Saturation	A	0.80
		B	.08			B	.49
		C	1.06			C	.87
TWT medium mode	Linear	A	0.69	GaAs FET	Linear	A	0.36
		B	.46			B	.15
		C	1.04			C	.46
	1-dB compression	A	0.22		1-dB compression	A	0.17
		B	.21			B	.10
		C	1.49			C	.91
	Saturation	A	0.14		Saturation	A	0.21
		B	.18			B	.10
		C	.85			C	.55

TABLE 7.—BER DEGRADATION AS A FUNCTION OF
HPA OPERATING POINT
[Average over all bands and crosspoints.]

High-power amplifier	Operating point		
	Linear	1-dB compression	Saturation
TWT low mode	2.50	1.94	1.58
TWT medium mode	3.63	2.79	1.44
TWT high mode	2.28	2.94	1.87
TWT (all data)	2.80	2.56	1.63
GaAs FET	2.10	1.78	1.58

frequency bands as well, again with the only exception being the TWT high mode, where for bands A and C the performance degraded when moving from linear to 1-dB compression.

In section 4.1.2 it was noted that the system's amplitude response improved dramatically when the HPA operating point was changed from linear to 1-dB compression or from 1-dB compression to saturation. The other RF parameters measured showed no consistent improvement as a function of HPA operating point. We therefore concluded that the improved BER performance obtained when operating the HPA in compression was primarily the result of improved amplitude response.

4.1.3.2(f) Summary of system BER performance.—The system BER performance was a strong function of operating frequency and HPA operating point. Frequency band B, which was at the center of the system 2.5-GHz bandwidth and had the best response in terms of RF parameters, produced the least BER degradation. Significantly better BER performance was obtained when the HPA was operated at saturation than at the 1-dB-compression or linear operating points.

Overall, the SITE system proved capable of transmitting digitally modulated data with very little degradation. In 16 percent of the cases tested, the measured degradation from theoretical

was ≤ 0.90 dB. Since 0.75 dB of degradation was due to modem implementation losses, the transmission channel actually contributed 0.15 dB or less of degradation in these cases—an indication of outstanding, nearly distortionless performance. In over one-third of the cases (34.4 percent), the degradation was ≤ 1.1 dB. A degradation figure of 2.0 dB (or 1.25 dB additional degradation caused by the transmission channel), which represents reasonably good performance, was achieved in nearly two-thirds (66.2 percent) of the test cases.

4.1.3.3 Correlation of BER Performance With RF Test Results

The relationship between the several types of transmission channel distortions and the resulting BER performance of the channel is of great importance in designing any data transmission system. The large body of test data produced during the baseline RF and BER tests allowed some conclusions to be drawn regarding the amount of distortion that can be tolerated in a system without significant degradation of the BER. In the following sections we compare the measured system BER performance with each of the five measured RF parameters. The data were analyzed by plotting the BER as a function of each RF parameter, point by point, and applying a linear regression analysis.

4.1.3.3(a) Comparison of BER performance and amplitude response.—It has been noted previously in this report that a clear relationship existed between the amount of variation in the system's amplitude response and the amount of BER degradation. Plots made of the BER degradation as a function of amplitude variation provide a qualitative confirmation of this relationship; the linear regression analysis indicates the quantitative relationship.

The regression statistics calculated for the BER degradation as a function of amplitude variation are presented in table 8. The data are broken down by TWT mode, TWT operating point,

TABLE 8.—REGRESSION STATISTICS FOR BER DEGRADATION AS A FUNCTION
OF AMPLITUDE VARIATION
[Amplitude variation is the independent (X) variable.]

Data set	Y-intercept	Standard error of Y estimate	Coefficient of determination, R^2	Coefficient of X	Standard error of X coefficient
TWT low mode	-0.14	0.67	0.813	0.54	0.024
TWT medium mode	-.60	1.12	.686	.79	.050
TWT high mode	1.26	1.70	.281	.31	.045
TWT linear	.45	1.31	.478	.45	.072
TWT 1-dB compression	.05	1.31	.544	.61	.045
TWT saturation	.37	.63	.574	.45	.032
TWT (all data)	.20	1.08	.565	.54	.025
GaAs FET linear	-.12	.68	.808	.43	.038
GaAs FET 1-dB compression	.23	.55	.804	.36	.026
GaAs FET saturation	.21	.33	.716	.53	.048
GaAs FET (all data)	.36	.53	.776	.36	.018
All data	.28	1.01	.573	.49	.019

and GaAs FET operating point. Because visual inspection of data plotted showed no discernible dependence on frequency band, this parameter was not included in the regression analyses. Comparing these data sets generally showed no large variation between the various modes and operating points. Two exceptions were noted. First, the TWT high-mode data showed a significantly higher Y-intercept value, corresponding to an overall higher average BER degradation in this mode. Second, the TWT medium mode showed a higher slope than the other cases because of a number of data points with large BER degradation. Overall, there did not appear to be any dependence of the BER-degradation-versus-amplitude-variation function on HPA, TWT mode, HPA operating point, or frequency band.

The regression curve calculated for the entire data set (last line in table 8) represents a characteristic BER-versus-amplitude-variation function for the SITE system, from which only two significant variations occurred for any subset of the data. The standard error for this curve was 1.01 dB, indicating that parameters other than amplitude variation also affected BER performance. The plot of BER degradation versus amplitude variation for the entire data set is shown in figure 11, along with the calculated regression curve. The x -coefficient value, or slope of the regression curve, is of particular importance. It indicates that each decibel of additional amplitude variation occurring in the transmission channel caused an additional 0.49 dB of BER degradation. This was a general result. As shown in section 4.6, the BER degradation was also highly dependent on the type of amplitude variation and its location in the frequency band relative to the modulated spectrum.

4.1.3.3(b) Comparison of BER performance and group delay response.—The effect of group delay on the BER has been studied previously (ref. 4). In that study a sample of the SITE phase I data indicated that each additional nanosecond of group delay variation resulted in 0.34 dB of additional BER degradation. Analysis of the entire data set showed that the sample used in the study was representative. The slope calculated for all data

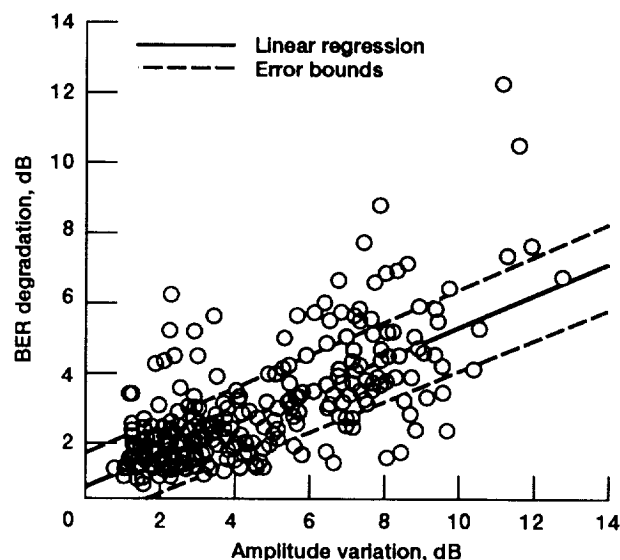


Figure 11.—BER degradation as a function of amplitude variation for all test conditions.

showed 0.31 dB of additional BER degradation per nanosecond of group delay variation.

The regression statistics are summarized in table 9. As with the amplitude variation analysis, the data are broken down by TWT mode, TWT operating point, and GaAs FET operating point. No dependence on frequency band was noted. In contrast to the amplitude response data (table 8), considerable variation is evident in the regression statistics. The y -intercept value varied from -0.49 to 1.49 dB, and the x -coefficient varied from 0.16 to 1.05 . The standard errors for the y -intercept and the x -coefficient were larger than those for the amplitude data, and the x -coefficient was smaller. All of these observations indicate that group delay variation was not as significant a contributor to BER degradation as was amplitude variation.

TABLE 9.—REGRESSION STATISTICS FOR BER DEGRADATION AS A FUNCTION OF GROUP DELAY VARIATION
[Group delay variation is the independent (X) variable.]

Data set	Y-intercept	Standard error of Y estimate	Coefficient of determination, R^2	Coefficient of X	Standard error of X coefficient
TWT low mode	1.04	1.44	0.138	0.18	0.042
TWT medium mode	.39	1.37	.529	.58	.051
TWT high mode	1.49	1.20	.097	.22	.062
TWT linear	1.19	1.34	.453	.48	.080
TWT 1-dB compression	.45	1.39	.484	.60	.051
TWT saturation	.88	.85	.227	.16	.024
TWT (all data)	1.03	1.45	.213	.29	.030
GaAs FET linear	.75	.91	.658	.32	.064
GaAs FET 1-dB compression	-.49	.57	.789	1.05	.077
GaAs FET saturation	-.47	.45	.449	.50	.079
GaAs FET (all data)	.47	.90	.346	.37	.048
All data	.88	1.34	.243	.31	.025

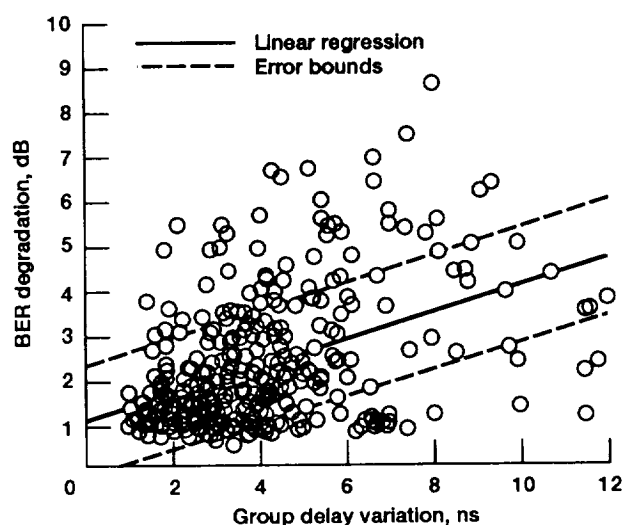


Figure 12.—BER degradation as a function of group delay variation for all test conditions.

The regression curve calculated for the entire data set (last line in table 9) represents the characteristic BER-versus-group-delay function for the SITE system. The function varied considerably between subsets of the data set, however. The data set and regression curve are plotted in figure 12. As noted, the x -coefficient, or slope of the regression curve, indicates that in general, each nanosecond of additional group delay variation resulted in an additional 0.31 dB of BER degradation. The group delay study of reference 4 shows that the amount of BER degradation is highly dependent on the type of group delay distortion and its location in the frequency band with respect to the modulated spectrum.

4.1.3.3(c) Comparison of BER performance and AM-PM conversion.—Published theory and results (refs. 5, 6, and 9) indicate that the AM-PM conversion can have a significant degrading effect on system BER performance for some modulation formats. The effect of AM-PM conversion on the

SITE system BER was studied in the same detail as the amplitude and group delay variation effects. The results give no indication that AM-PM conversion adversely affected the BER. Because the modulation used for these tests (SMSK) is a constant-envelope modulation, this is expected.

The calculated regression statistics for the BER degradation as a function of AM-PM conversion are given in table 10. They are broken down by TWT mode, TWT operating point, and GaAs FET operating point. Only slight variations were observed between frequency bands, but significant variations were observed in the regression statistics between the various parameters. The x -coefficient was negative in all but one case (TWT linear) and ranged from 0.80 to -0.91 dB. The standard error for the x -coefficient was more than twice as large as the error for the amplitude or group delay data. The y -intercept value ranged from 1.23 to 5.22 dB, with standard errors larger than those for the amplitude and group delay data.

The regression curve calculated for the entire data set represents a characteristic BER-versus-AM-PM-conversion curve for the SITE system. This curve is plotted in figure 13 along with the corresponding data. The negative slope of the curve indicates that increased AM-PM conversion actually improves (decreases) the BER degradation by a factor of 0.4 dB/dB-deg of AM-PM conversion.

The modulation format used for these tests (SMSK) is a constant-envelope modulation. The carrier is effectively modulated with a continuous-phase data signal; therefore the signal amplitude does not change with time. As a result there are no amplitude variations to the signal that would cause phase distortions due to AM-PM conversion in the transmission channel. The slight improvement in BER performance coinciding with increased AM-PM conversion can be explained as follows: The AM-PM coefficient was shown to be clearly coupled to system linearity through the RF test results. Decreased system linearity corresponded to increased AM-PM conversion (see fig. 6(c)). The RF results also showed that the amplitude variation of the system is closely coupled to the linearity, decreasing significantly

TABLE 10.—REGRESSION STATISTICS FOR BER DEGRADATION AS A FUNCTION OF AM-PM CONVERSION
[AM-PM conversion is the independent (X) variable.]

Data set	Y-intercept	Standard error of Y estimate	Coefficient of determination, R^2	Coefficient of X	Standard error of X coefficient
TWT low mode	2.55	1.53	0.030	-0.21	0.110
TWT medium mode	4.09	1.82	.157	-.55	.120
TWT high mode	3.23	1.19	.111	-.28	.075
TWT linear	1.23	1.41	.400	.80	.150
TWT 1-dB compression	5.22	1.64	.288	-.91	.117
TWT saturation	2.22	.94	.045	-.15	.058
TWT (all data)	3.36	1.55	.100	-.37	.059
GaAs FET 1-dB compression	3.88	.98	.398	-.66	.121
GaAs FET saturation	1.90	.58	.107	-.18	.073
GaAs FET (all data)	3.12	.88	.274	-.46	.075
All data	3.33	1.45	.123	-.40	.050

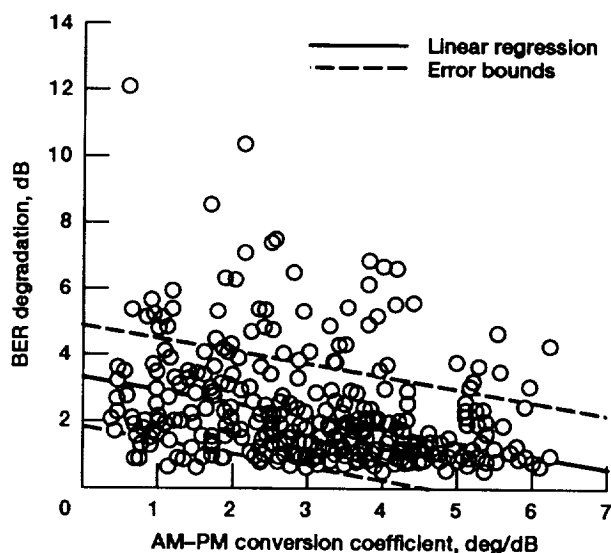


Figure 13.—BER degradation as a function of AM-PM conversion coefficient for all test conditions.

as the system is driven into nonlinearity (see fig. 6(a)). This led to an indirect relationship between the AM-PM coefficient and the amplitude variation, in which increased AM-PM conversion corresponded to decreased amplitude variation (see fig. 8(a)). Since the decreased amplitude variation corresponds to improved BER performance as shown earlier, the AM-PM data appear to show a slight improvement in BER for increasing AM-PM conversion. There is no basis for such a direct relationship, however.

4.1.3.3(d) Comparison of BER performance and output C/N .—The output C/N was measured to determine the ability of the system to provide the minimum E_b/N_0 required for a BER of 10^{-6} to be obtained. In the section on C/N test results (section 4.1.2.4), it was noted that in some cases where marginal C/N was measured, a good BER was nevertheless obtained. We

concluded that differences existed between the C/N measured with an unmodulated CW carrier and the actual SNR obtained when a modulated signal was transmitted. Thus, the value of analyzing the BER results as a function of C/N is probably not very great. We present these results anyway, with brief comments.

The regression analyses were performed in the same manner as for the amplitude, the group delay, and the AM-PM conversion; the results are tabulated in table 11. Note the large variation of the y-intercept values, along with the large standard error. A positive (albeit small) x -coefficient was obtained in all but one case. The BER-versus- C/N data and corresponding regression curve are plotted in figure 14. The positive slope of the curve contradicts the expectation that a higher C/N should provide an improved BER. This result may be due to the correspondence of increasing C/N to an decreasing third-order intermodulation level (see fig. 6(d)) and consequently to an increasing amplitude variation. The amplitude variation effect on BER dominated the C/N effect and lead to the appearance of increased BER degradation with increased C/N .

4.1.3.3(e) Comparison of BER performance and third-order intermodulation level.—The third-order intermodulation level indicates the degree of nonlinearity in the system. The data given represent the difference in amplitude between two fundamental CW signals and the resulting third-order signals. The smaller the difference, the greater the degree of nonlinearity. In general, for digital communications systems nonlinearity tends to degrade the BER performance. There are two primary causes for this. First, intermodulation distortion occurs when more than one modulated signal is transmitted through the system. The non-linearity generates interfering intermodulation products and increased side lobes that intrude into adjacent channels. Second, side-lobe regrowth can occur when a single signal is present in the channel. In this case, excess power that cannot be added to the power-limited main lobe is added to the side lobes. The higher side-lobe levels distort the demodulated signal and cause errors in detection.

TABLE 11.—REGRESSION STATISTICS FOR BER DEGRADATION AS A FUNCTION OF CARRIER-TO-NOISE RATIO

[Carrier-to-noise ratio is the independent (X) variable.]

Data set	Y-intercept	Standard error of Y estimate	Coefficient of determination, R^2	Coefficient of X	Standard error of X coefficient
TWT low mode	0.12	1.53	0.038	0.11	0.050
TWT medium mode	-1.36	1.91	.145	.23	.055
TWT high mode	1.48	1.25	.021	.06	.037
TWT linear	-5.88	1.70	.127	.39	.155
TWT 1-dB compression	6.37	1.92	.021	-.23	.130
TWT saturation	-.20	.96	.043	.13	.052
TWT (all data)	.09	1.61	.061	.13	.028
GaAs FET 1-dB compression	-3.70	1.16	.128	.30	.111
GaAs FET saturation	-5.08	.56	.147	.35	.121
GaAs FET (all data)	-4.63	.96	.147	.34	.081
All data	.47	1.54	.032	.09	.025

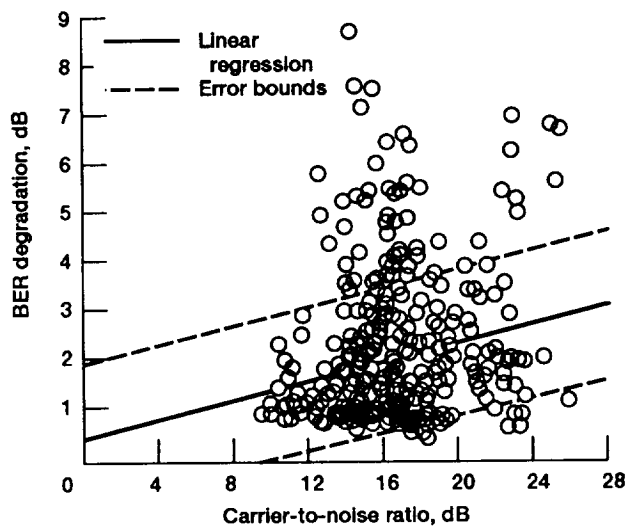


Figure 14.—BER degradation as a function of carrier-to-noise ratio for all test conditions.

For the SITE system neither of these problems occur. Except for the interference measurements, described in section 4.4, only one modulated signal is transmitted through the channel at any one time. In addition, the modulation type, SMSK, is not susceptible to the side-lobe regrowth problem. Thus, the major contributions of system nonlinearity to BER degradation do not exist in the SITE system. Instead, the system nonlinearity, as measured by the third-order intermodulation level, tends to indicate the level of other system distortions, particularly amplitude variation. The more nonlinear the system, the lower

the amplitude variation (see fig. 6(a)) and the better the BER performance. Thus, the relationship between third-order intermodulation level and BER is dominated by the effects of the corresponding amplitude variation.

The regression statistics for the BER as a function of third-order intermodulation level were calculated for all 33 third-order measurements. Thus, no breakdown for TWT modes, etc., was performed. The results are listed in the top entries in table 12, and the regression curve is plotted with the data points in figure 15. The positive slope indicates that BER degradation increased as the system became more linear, which was the opposite of the normally expected result and was due to the domination of the amplitude variation effect on BER.

4.1.3.3(f) Comparison of BER performance and groups of RF parameters.—Multiple regression analyses were performed for the BER as a function of combinations of RF parameters. The results of these analyses are listed in table 12.

The first analysis compared the BER with amplitude and group delay variation. The y-intercept for the resulting function was -0.08 dB, and the standard error of the y-estimate was 0.97 dB, smaller than the error for the single-parameter regressions. The amplitude coefficient was 0.45 , and the group delay coefficient was 0.14 . The standard errors for both coefficients were relatively small, at 0.021 . This analysis indicates the dominance of amplitude variation as the RF parameter with the most effect on BER, although group delay still contributed significantly. The large y-estimate error reduced the reliability of this analysis.

The second analysis compared the BER with all RF parameters except third-order intermodulation. Third-order data were

TABLE 12.—REGRESSION STATISTICS FOR BER DEGRADATION AS A FUNCTION OF SEVERAL GROUPS OF PARAMETERS

[BER degradation is the dependent (Y) variable; RF parameters listed are the independent (X) variables.]

	Y-intercept	Coefficient of determination, R^2	Amplitude variation	Group delay	AM-PM conversion	Carrier-to-noise ratio, C/N	Third-order intermodulation
Constant or coefficient	1.25	0.199					0.06
Standard error	.92						.021
Constant or coefficient	-0.08	0.617	0.45	0.14			
Standard error	.97		.021	.021			
Constant or coefficient	1.05	0.655	0.41	0.16	-0.24	-0.02	
Standard error	.92		.022	.021	.034	.017	
Constant or coefficient	-0.52	0.874	0.32	0.05	0.07	0.03	0.02
Standard error	.39		.041	.032	.057	.042	.015

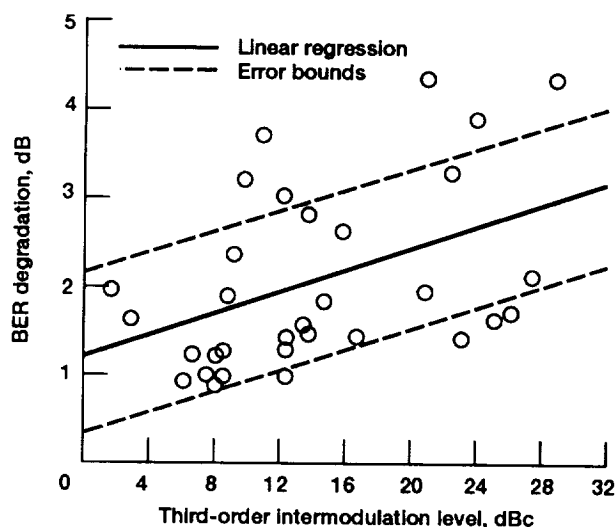


Figure 15.—BER degradation as a function of third-order intermodulation level for all test conditions.

excluded because only 33 measurements were made. This analysis thus includes several hundred data points. The y-intercept for these data was 1.05 dB, with a y-estimate error of 0.92 dB. The amplitude and group delay coefficients and errors were nearly identical to those calculated for the two-parameter case discussed in the preceding paragraph. The AM-PM conversion coefficient was -0.24 , as a result of amplitude variation effects described in section 4.1.3.3(c). The C/N coefficient was -0.02 dB, indicating very little C/N effect on BER. Overall, for this analysis amplitude variation still had by far the most effect on system BER, with group delay contributing to a lesser degree.

The third multiple regression was performed for the 33 system configurations for which all five RF parameters were measured. The results are listed as the last set of numbers in table 12. The y-intercept value is -0.52 dB, with a relatively small y-estimate error of 0.34 dB. The RF parameter coefficients were small except for the amplitude coefficient, which was 0.32. The amplitude variation, as in all previous cases, was the dominant RF parameter. The group delay was much less of a factor in this analysis. The AM-PM coefficient was negligible, as expected for a constant-envelope modulation format. The C/N and third-order intermodulation had a very small effect on the BER in this analysis.

4.1.3.3(g) Summary of correlation of BER results with RF parameters.—The one conclusive result obtained in the comparison of BER and RF data was that the amplitude variation had the greatest effect on BER rate for the SITE system. The several analyses presented indicate that each additional decibel of amplitude variation resulted in 0.32 to 0.49 dB of additional BER degradation.

Results for the other RF parameters were much less clear. Group delay variation appeared to have a definite effect on the BER, but the degree of effect was difficult to assess. The

several analyses indicated that each additional nanosecond of group delay resulted in anywhere from 0.05 to 0.31 dB of additional BER degradation.

The results of the AM-PM conversion analysis indicate that AM-PM conversion has a negligible effect on BER, as expected for SMSK modulation.

The output C/N analyses proved to be of little value. Because of the nature of the measurement, the C/N values did not accurately reflect the SNR available in the channel when transmitting a modulated signal. In addition, the calculated x -coefficients indicated that the C/N had only a small effect on BER.

Nonlinearities on BER, as measured by the third-order intermodulation level, had a small effect on the SITE system because of the type of modulation used and the fact that only a single signal is transmitted through the system. Because the third-order data closely corresponded to the amplitude variation data, we concluded that the effect revealed by two regression analyses was the result of amplitude variation and not nonlinearity.

4.1.3.4 Summary of BER Test Results

The SITE system proved to be capable of providing virtually distortionless transmission of a 220-Mbps SMSK digitally modulated signal. In most of the 468 cases tested the additional BER degradation attributable to the channel was less than 1.25 dB. Frequency band and HPA operating point were the most critical SITE operating parameters in terms of their effects on BER.

Comparison of BER results with corresponding RF measurement results indicated that the RF parameter with the most effect on BER was the amplitude variation. Group delay appeared to contribute to a lesser degree to BER degradation. AM-PM conversion, output C/N , and third-order intermodulation level (or system linearity) effects were not clearly discernible from the data and analyses that were performed.

4.1.4 Concluding Remarks—Baseline Tests

The SITE phase I baseline measurements were intended to fully exercise the system in terms of RF parameters and system operating parameters. In addition, the correlation of BER results with RF performance was a specific goal. These goals were successfully met, and a large volume of useful data was obtained. The analysis of these data provided insights into the performance of a 30/20-GHz digital satellite system as configured in the SITE simulated system.

In considering the data that are presented and analyzed in this section (4.1), it is important to remember the specific characteristics of the system and the applied signals that are unique to SITE and do not necessarily apply in a general sense to all satellite communications systems. Of these, the most important is the modulation format, SMSK, and the data rate, 220 Mbps. The side-lobe levels for the SMSK-modulated spectrum are quite low, and therefore only the main lobe of

the signal can be transmitted, at a channel bandwidth equal to 1.5 times the data rate (330 MHz). Transmitting in this fashion allows BER performance equal to that of quaternary phase shift keying (QPSK) modulation. The absence of significant side lobes leads to unique transmission properties, such as the absence of side-lobe regrowth problems during nonlinear system operation. The data rate and corresponding channel bandwidth represent a relatively wideband transmission system relative to satellite systems currently employed or planned for the future. Many of the results are nonetheless applicable to narrowband systems.

Other unique characteristics in system design and operation should be noted. In particular, the absence of narrowband channel filtering or demultiplexing in the transponder is unusual in comparison with operational systems. We feel that such filtering would have had negligible effect on the SMSK-modulated signal. However, such filters and demultiplexers are common in operational systems and often affect the performance of systems employing the more standard modulations such as QPSK or binary phase shift keying (BPSK). In terms of system operation the variety of operational configurations that were used during baseline testing represents most configurations seen in operational systems. The exception is the receiver input power level. In an operational system the input power to the receiver would be close to the minimum level required for adequate E_b/N_0 in order to optimize the system's economic performance and minimize interference with other spacecraft. For the LNR receiver that level would be about -60 dBm. Such a level in the SITE system would cause E_b/N_0 limitations imposed by the receiver to be a factor in system operation. This factor, which would have significantly complicated the evaluation of data taken during the course of testing, was eliminated by choosing a higher input level (-35 dBm). The higher input level also eliminated the interference of several low-level spurious responses occurring in the receiver (ref. 10). Thus, the high E_b/N_0 available at the output of the satellite's 30-GHz receiver is unusual in comparison with an operational system and should be taken into account when evaluating the system performance.

The system baselines that were developed for each combination of HPA, TWT mode, HPA operating point, and frequency band resulted in a large variety of system RF characteristics. This variety allowed significant variation of BER performance to be observed and consequently made possible an analysis of how RF distortions affect BER performance. Additionally, the optimum operating conditions for the SITE system could be observed in terms of BER performance.

In assessing RF performance we found that amplitude variation varied with frequency band, HPA, HPA operating point, and matrix switch crosspoint. Group delay varied primarily with frequency band, HPA, and crosspoint. AM-PM conversion varied primarily with HPA operating point, as did third-order intermodulation level. C/N varied with operating point for the TWT only.

In comparing RF parameters, we found that amplitude variation, AM-PM conversion, and C/N were strong functions of third-order intermodulation level. Group delay and amplitude variation were related. Amplitude variation was found to be somewhat a function of AM-PM conversion.

In 66 percent of the cases tested the system transmitted data with 2.0 dB or less of BER degradation as compared with the theoretical case. Accounting for modem losses, the transmission channel in these cases added less than 1.25 dB of degradation. The system performed best, in terms of both BER and RF parameters, in frequency band B. The optimum HPA operating point was saturation, and the GaAs FET slightly outperformed the TWT.

Comparing BER with the RF parameters showed that the BER was primarily a function of amplitude variation and, to a much lesser degree, of group delay variation. The other RF parameters showed effects that were either very small or were masked by the amplitude variation effects.

4.2 30-GHz Low-Noise-Receiver Tests

The low-noise receiver is a critical component of a satellite communications system in terms of the effects on system cost and performance. The satellite receiver's noise figure determines the magnitude of transmitted signal power needed to achieve the signal-to-noise ratio required for acceptable system performance. Therefore, the receiver is critical in determining such parameters as the size of satellite and Earth terminal antennas, the amount of power required from the uplink transmitter amplifier, requirements for uplink power control or data encoding during periods of signal fading, and other system parameters, all of which affect the cost-versus-performance tradeoffs for the system. Other important receiver parameters that affect the system's performance are the gain and phase as a function of frequency, the stability of the receiver's local oscillator, and the receiver's ability to reject image frequencies.

As part of the POC development program at NASA Lewis, two parallel contracts were let for low-noise receivers operating at an input frequency of 27.5 to 30.0 GHz and designed as satellite receivers for a 30/20-GHz satellite communications system. The contractors were LNR Communications, Inc. (Hauppauge, New York) and ITT Defense Communications Division (Nutley, New Jersey). Under a separate program sponsored by NASA's Goddard Space Flight Center (Greenbelt, Maryland), a similar development contract was let to Hughes Aircraft Company, Microwave Products Division (Torrance, California). The Hughes effort was started approximately 18 months after the LNR and ITT contracts began. The LNR and ITT contracts were completed late in 1982, at which time the POC models were delivered to Lewis (refs. 11 and 12). Three receivers

were delivered by LNR and two by ITT. The POC models were then tested extensively to determine their operating characteristics, under the direction of Martin Conroy (ref. 10). The Hughes receiver contract was completed in 1984, with resulting hardware delivered to NASA Goddard (ref. 13). In the fall of 1986 one of the Hughes receivers was given to NASA Lewis personnel for evaluation under the SITE Project. RF performance measurements were made for comparison with Hughes's published results.

As part of the phase I BER testing one POC receiver from each of the three contracts was evaluated by using digitally modulated test signals. We now describe these tests and their results.

4.2.1 Receiver Design and RF Performance

The LNR and ITT receivers are based on similar electrical designs, shown in figure 16(a) (refs. 11 and 12). Because at the time the contracts were let a 30-GHz amplifier with a suitably low noise figure was not technologically viable, both designs employ an image-enhanced diode mixer as the receiver front end. The required gain of the receivers is produced by the following stage, an IF amplifier circuit. The major difference between the two designs is in the local oscillator generation circuit. The LNR design has an internal 5.95-GHz voltage-controlled oscillator (VCO) phase locked to an external 500-MHz, high-stability reference crystal oscillator. The 5.95-GHz VCO output is multiplied by a factor of 4 (by using

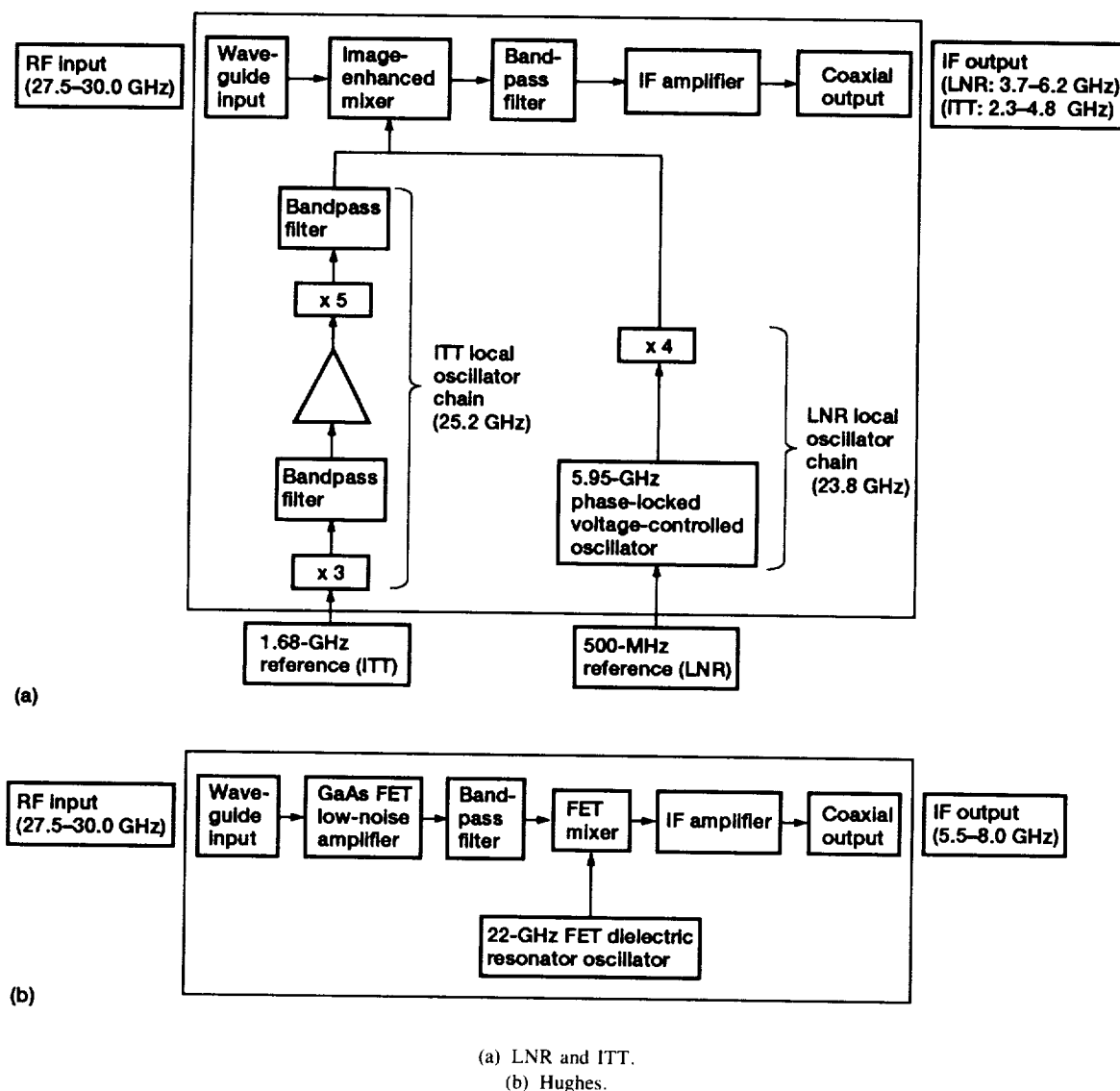


Figure 16.—Functional block diagrams of 30-GHz low-noise receivers.

a diode multiplier) to the required 23.8 GHz. All of the phase-lock circuitry resides inside the receiver housing. The stability of the local oscillator is determined by the stability of the reference oscillator. In the ITT receiver a 1.68-GHz external reference oscillator is used to obtain the local oscillator signal. The reference is multiplied by 3, filtered, amplified, and then multiplied by 5 to obtain the 25.2 GHz required. The stability of the local oscillator is directly related to the stability of the 1.68-GHz reference.

The electrical design of the Hughes receiver represents a major step forward in 30-GHz receiver technology (fig. 16(b)). The design incorporates three gallium arsenide microwave integrated circuits (GaAs MIC's) that were developed by Hughes specifically for this project. The MIC's produced were a 30-GHz FET low-noise amplifier (LNA), a dual-gate FET mixer, and a dielectric resonator oscillator (operating at 22 GHz). These three MIC's were combined with a commercially available IF amplifier in a hybrid circuit topology to produce a complete receiver package (ref. 13). In contrast to the LNR and ITT receivers, which use an image-enhanced mixer as the receiver's front end, the Hughes receiver employs the 30-GHz GaAs FET LNA as the front end. All of the electrical circuitry resides inside the receiver package, with no external frequency references used. The 22-GHz dielectric resonator local oscillator, while having the advantage of small size and simple design, is not phase locked to any stable reference. It is subject to a slow frequency drift and requires a long warmup time and manual tuning before it can be tested in a digital data transmission system.

Figure 17 shows the three completed receivers. (Power supplies and external frequency references are not shown.) The results of RF measurements made on the three receivers tested under the phase I BER testing are summarized in table 13. The IF frequency bands of the receivers varied from 2.3 GHz to 8.0 GHz, reflecting the different local oscillator frequencies chosen by each contractor. The design requirements for the Hughes contract differed from those for the LNR and ITT contracts, resulting in some significant differences in RF performance. The gain of the Hughes receiver was approximately 20 dB higher than that of the LNR and ITT receivers. The high gain of the Hughes receiver, derived from the front-end LNA as well as from the IF amplification stage, also had the effect of lowering the input 1-dB-gain-compression point by 20 dB. The use of a 30-GHz LNA as the front end for the Hughes receiver resulted in a significantly better noise figure than those for the LNR and ITT receivers. The LNA also has an inherently better input match than the image-enhanced mixer, resulting in a better input voltage standing-wave ratio (VSWR) for the receiver. However, the LNR and ITT receivers benefited from the use of an image-enhanced mixer front end in obtaining a much better image rejection performance than the Hughes receiver.

4.2.2 Test Description

Each receiver was subjected to a series of BER tests in which the input power to the receiver was varied from -70 dBm to -30 dBm. These tests were performed with the TWT as the satellite HPA. The TWT was operated in the high-power mode, and the receiver tests were repeated with the TWT set at the linear, 1-dB-compression, and saturated operating points. These conditions have been described previously in this report.

Figure 18 shows the operating frequency ranges of the three receivers in relation to the transponder IF operating band, as well as the specific 330-MHz bands used for receiver testing. The transponder IF operating band of 3.5 to 6.0 GHz is determined by the operating band of the Ford matrix switch, which is a fixed element of the transponder.

The LNR receiver's IF band closely matches that of the Ford matrix switch; that is why it was chosen as the permanent SITE phase I transponder receiver. As a result of this frequency band match, five 330-MHz test bands were specified for the transponder. The testing of the LNR receiver occurred early in the phase I BER testing, before the decision was made to restrict testing to only three bands. Therefore, LNR receiver test data are available in five frequency bands, and all of those data are presented in this report. The test bands located at the LNR receiver band center, particularly bands B and D, benefited greatly from their collocation with the transponder's band center. Nearly all of the transponder's components operated best near the center of their design bands. Thus, the center test bands represent the most nearly ideal operating characteristics obtainable from the SITE phase I system. On the other hand, bands A and C, which are located at the lower and upper edges (respectively) of both the LNR receiver and the transponder, exhibited degraded transmission characteristics, with band C being the most severely degraded

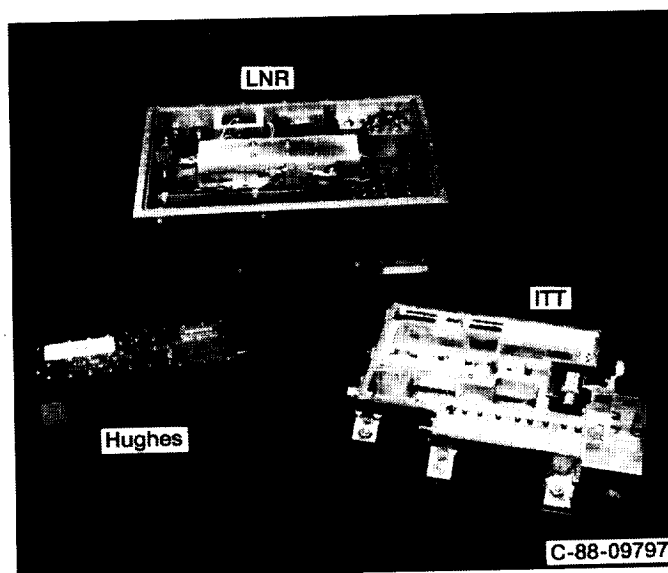


Figure 17.—Completed 30-GHz low-noise receivers.

TABLE 13.—RF PERFORMANCE OF 30-GHz LOW-NOISE RECEIVER

Parameter	Receiver		
	LNR Communications S/N 1	ITT Defense Communications S/N 2	Hughes Microwave Products Division S/N 1
Input band, GHz	27.5–30.0	27.5–30.0	27.5–30.0
Output band, GHz	3.7–6.2	2.3–4.8	5.5–8.0
Local oscillator frequency, GHz	23.8	25.2	22.0
Gain (midband), dB	20	18	41
Gain variation over 2.5 GHz, dB	3.8	4.8	5.2
Noise figure (minimum), dB	5.8	6.8	3.7
Noise figure variation over 2.5 GHz, dB	2.7	2.4	0.6
Input voltage standing wave ratio (VSWR) (maximum over 2.5 GHz)	2.3:1	3.4:1	^a 1.3:1
Output VSWR (maximum over 2.5 GHz)	1.7:1	1.4:1	2.3:1
Group delay variation over 2.5 GHz, ns	6	5	5
1-dB compression point midband (input/output), dBm	13/–7	>10/–8	14/–27
Image rejection, dB	64	57	>25
Design topology	Hybrid	Hybrid	Hybrid-MIC

^aHughes measurement.

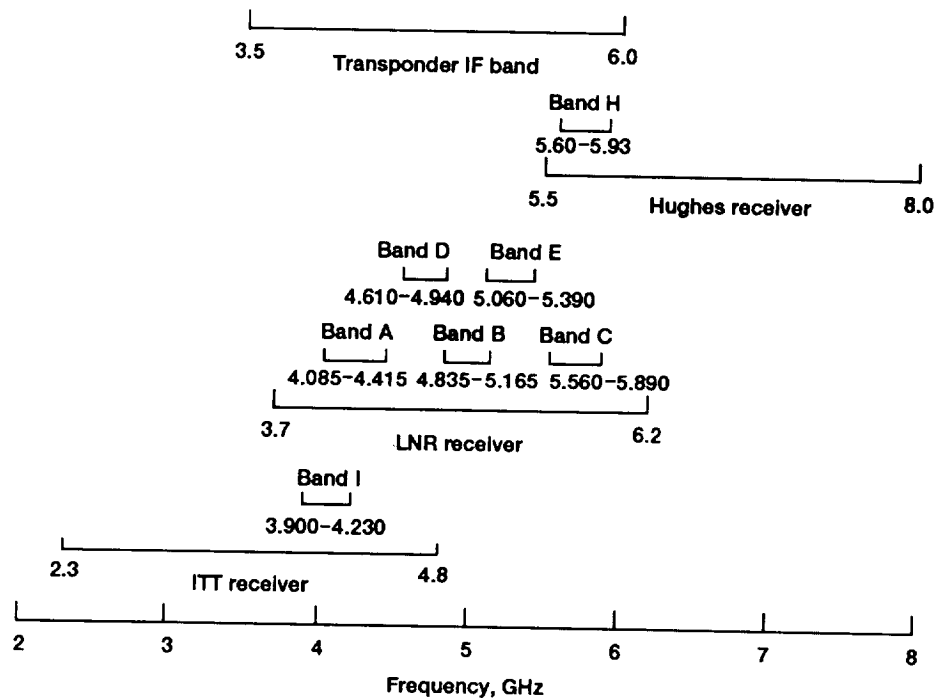


Figure 18.—30-GHz low-noise receiver IF bands and BER test bands in relation to SITE transponder IF operating band.

of the LNR test bands. LNR band E, located off the center frequency, suffered to a smaller degree from the upper band edge effects.

The ITT receiver's IF output band had an overlap of 1.3 GHz with the transponder operating band. This overlap

occurred at the lower edge of the transponder band and the upper edge of the ITT receiver band. Degraded performance characteristics occurred at these band edges, relative to the band centers of the receiver and transponder. The 330-MHz band was chosen for ITT receiver testing to minimize the

cumulative degradation caused by overlapping the two band edges. However, the performance was still less than ideal when compared with, for example, the test bands for the LNR receiver located at the receiver's band center, which coincides with the transponder's band center. This unavoidable less-than-ideal situation must be taken into account when considering the test results for the ITT receiver.

The output IF band for the Hughes receiver has only a 500-MHz overlap with the transponder operating band. The overlap occurs at the lower end of the Hughes receiver band and the upper end of the transponder band. Although the Hughes receiver had almost no degradation at its band edge, the transponder had significant degradation at its upper band edge. With only 500 MHz in which to place a 330-MHz test band, little can be done to optimize the receiver's performance by moving the test band around. Therefore, the test band was placed approximately in the middle of the 500-MHz band, and as with the ITT results, this less-than-ideal situation must be accounted for when considering the Hughes results.

Despite all these frequency band placement problems the results of the receiver testing provide significant insight into the relative performance of the receivers, as well as the effect of a receiver on the overall system performance. These test results are discussed next.

4.2.3 BER Test Results

The results of the receiver BER tests are summarized in table 14. For each receiver test band, a BER curve measurement was attempted at receiver input powers of -30 , -40 , -50 , -60 , -65 , and -70 dBm. For all the receivers, -70 dBm was below the minimum input power required for demodulation. Therefore, no data are given in the table at this input power level. An input signal level of -65 dBm was below the minimum input power required for the ITT and LNR receivers, but a measurement was possible for the Hughes receiver. All receivers were able to operate at -60 -dBm input power, but for two cases (LNR bands C and E with the HPA saturated) the BER curve was so severely degraded that no useful results could be stated.

For all of the test cases in which useful data were obtained, table 14 lists the degradation of the measured BER curve relative to the theoretical ideal BER curve for SMSK modulation. The parameter used to describe this degradation is the difference between the measured E_b/N_0 and the ideal E_b/N_0 at a BER of 10^{-6} .

4.2.3.1 Receiver Performance as a Function of Receiver Noise Figure and System Noise Contributions

As the input power to the receiver was decreased, eventually a point was reached where an E_b/N_0 high enough to obtain a BER of 10^{-6} could not be obtained. This input power limitation was primarily due to the noise figure of the receiver. A higher noise figure required a higher receiver input power to maintain a constant output E_b/N_0 . Other components of the

system also had some effect on the system output E_b/N_0 obtainable for a given receiver input power. An understanding of how the system performance is affected by the receiver noise figure requires a further explanation of these effects.

The total noise power available in a 50-ohm system at a temperature of 290 K can be easily calculated from reference 14 as

$$P = kTB$$

where

k Stefan-Boltzmann constant (1.38×10^{-23}) J/K)

T temperature (290 K)

B noise bandwidth, Hz

$$\begin{aligned} P &= (1.38 \times 10^{-23})(290)B = 4.002 \times 10^{-21} \text{ W/Hz} \\ &= -174.0 \text{ dBm/Hz} \end{aligned}$$

For the SITE phase I system the noise bandwidth of the test bands is 330 MHz. Therefore, the total noise power over the test band is $-174.0 \text{ dBm} + 10 \log(330 \times 10^6) = -88.8 \text{ dBm}$. Because the noise figure of a receiver is measured relative to an input noise temperature of 290 K, the actual noise power referenced to the receiver input can be obtained by adding the measured noise figure to the calculated noise power at 290 K. For example, for LNR band A the measured noise figure of 7.5 dB (table 14) indicates a noise power referenced to the receiver input of $-88.8 \text{ dBm} + 7.5 \text{ dB} = -81.3 \text{ dBm}$. Thus, in order to obtain an output SNR ratio of 10 dB, the input signal power to the receiver must be -71.3 dBm .

For the communications system overall, components other than the receiver add small amounts of noise to the system. An estimate of the quantity of additional noise added by the system is available from SNR degradation measurements as listed in table 14. The measurements represent the difference between the output SNR (see section 4.1.2.4) and the input C/N measured in the same manner at the system input. Because these measurements were made at a receiver input power of -30 dBm, it was assumed that the noise contribution of the receiver for this measurement is negligible. Thus, the SNR degradation result can be considered a reasonable estimate of the noise contribution of the system excluding the receiver.

The bottom row of numbers in table 14 is an estimate of the maximum E_b/N_0 obtainable at the system output (demodulator input) for a receiver input power of -60 dBm. These numbers were obtained by the following formula:

$$(E_b/N_0)_{\max} = -88.8 \text{ dBm} + \text{NF} + \text{SNR degradation} + 1.8 \text{ dB}$$

The final term in the equation, 1.8 dB, is the ratio of the test bandwidth to the bit rate ratio and is required to derive E_b/N_0 from SNR (ref. 8).

How the maximum system output E_b/N_0 affects the measured BER curves is demonstrated in figure 19. As explained previously, BER curves are measured by adding a calibrated amount of noise to the system output signal, precisely measuring the BER and the E_b/N_0 , and then decrementing the amount of E_b/N_0 noise in 1-dB steps until the curve is completed. However, when the system output signal contains a significant amount of noise to begin with, the actual E_b/N_0 at the demodulator input is lower than the measurement indicates.

As an example, assume that because of a low input signal level at the receiver, the maximum E_b/N_0 available at the system output is 10 dB. The measurement system, which is simulating a varying input power (and thus a varying E_b/N_0) at the Earth terminal receiver, adds known amounts of noise to the system output signal, which already contains a significant amount of noise. The maximum E_b/N_0 that the demodulator will see is

10 dB. Thus, as the measurement system's added noise is removed, the BER curve begins to converge to the minimum BER attainable, which in this example is a BER corresponding to an E_b/N_0 of 10 dB.

This effect is clearly seen in figure 19. From table 14 the maximum system output E_b/N_0 for a receiver input of -60 dBm in band D is 16.3 dB. By assuming a normal-shaped BER curve at -60 dBm and drawing the BER line that intersects this curve at an E_b/N_0 of 16.3 dB, the convergence of the measured BER curve to the BER limit is apparent. For the -50-dBm input the maximum output E_b/N_0 can be estimated to be 26.3 dBm (10 dB higher than for a -60-dBm input). The BER measurement would have to be carried much farther down the curve before a convergence to the corresponding BER limit could be observed. (Such a measurement would take several

TABLE 14.—BER RESULTS FOR 30-GHz LOW-NOISE RECEIVERS

Parameter	Receiver						
	LNR Communications					ITT Defense Communications	Hughes Microwave Products Division
	Band A	Band B	Band C	Band D	Band E		
	E_b/N_0 degradation from ideal at BER of 10^{-6} , dB						
HPA (saturation):							
-30-dBm input	0.95	1.06	3.06	0.88	1.61	2.02	2.59
-40-dBm input	1.17	.97	2.80	.92	1.74	2.10	1.47
-50-dBm input	1.55	1.25	4.74	1.18	3.94	2.50	2.48
-60-dBm input	10.51	3.80	-----	7.25	-----	6.60	2.54
-65-dBm input	-----	-----	-----	-----	-----	-----	5.19
HPA (1-dB compression):							
-30-dBm input	1.91	1.76	3.56	1.73	2.13	2.82	3.66
-40-dBm input	2.19	1.46	2.80	1.83	2.22	2.51	3.19
-50-dBm input	2.58	1.53	4.74	1.55	2.42	2.72	3.26
-60-dBm input	12.67	3.62	17.09	3.95	10.54	6.68	4.29
-65-dBm input	-----	-----	-----	-----	-----	-----	6.93
HPA (linear):							
-30-dBm input	2.12	1.49	4.04	2.14	4.98	3.33	4.35
-40-dBm input	2.42	1.56	3.86	2.03	5.26	2.88	3.32
-50-dBm input	2.75	1.78	4.04	1.99	6.97	3.23	3.66
-60-dBm input	12.43	4.22	9.32	4.41	13.55	6.69	4.87
-65-dBm input	-----	-----	-----	-----	-----	-----	8.91
BER measurement band center frequency, GHz:							
Receiver input	28.050	28.8	29.525	28.575	29.025	29.265	27.775
Receiver output	4.250	5.0	5.725	4.775	5.225	4.065	5.775
Measured receiver noise figure average over 330-MHz band, dB	7.5	7.2	8.3	6.7	7.9	7.8	3.8
Measured input-to-output SNR degradation at band center, dB	4.0	5.1	4.1	7.6	5.4	4.0	4.1
Estimated maximum system-output E_b/N_0 at -60-dBm receiver input, dB	19.1	18.3	18.2	16.3	17.3	18.8	22.7

^aEstimated from band A data.

^bEstimated from band C data.

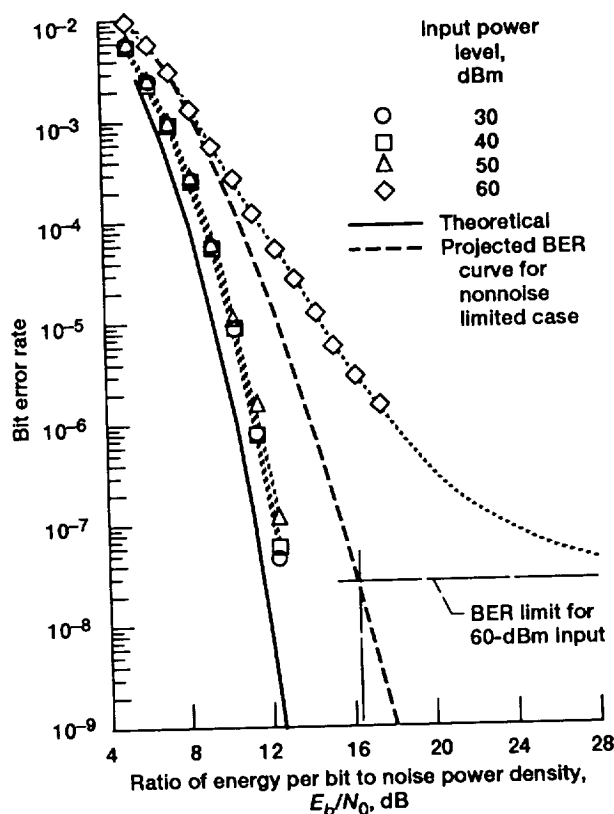


Figure 19.—BER curves for LNR receiver, band D, with TWT in saturation, at four receiver input power levels.

months to complete.) Similarly, for the -40 -dBm and -30 -dBm curves the convergence does not appear for the measurement range shown in figure 19.

The data in table 14 clearly show how the receiver's noise figure affects the system's ability to operate at low receiver input powers. The Hughes receiver, which has the lowest noise figure, is able to operate effectively at an input power of -65 dBm, but the other two receivers cannot. Note also that the receiver test bands that are located at the center of the transponder operating band, especially LNR bands B and D, benefit from the improved transmission characteristics of the entire system at the band center and thus perform better at lower input powers than the other test bands.

4.2.3.2 Receiver Performance as a Function of Input Power

The effect of receiver noise figure on the system BER performance has been discussed in the previous section and can be observed in the test results presented in table 14 and by comparing figures 20(a) and (b), particularly in terms of the minimum receiver input power required for acceptable transmission quality (i.e., a BER of 10^{-6} or better). The LNR and ITT receivers can perform with little or no additional degradation down to an input level of -50 dBm. At -60 dBm considerable degradation was observed. The degradation when

the input power level was decreased from -50 dBm to -60 dBm was approximately 2 to 6 dB for the ITT receiver and for the LNR receiver in bands B and D. In the other three LNR test bands the additional degradation ranged from 6 to 12 dB. The degraded RF transmission characteristics that have been observed and measured for these bands enhanced the degradation effects caused by reducing the input power. As the receiver input power was reduced still further, to -65 dBm, neither the ITT receiver nor the LNR receiver in any of its five bands was able to transmit data with a BER approaching 10^{-6} .

The Hughes receiver demonstrated some minor degradation (0.5 to 1.0 dB) at an input power of -30 dBm relative to -40 dBm. The input 1-dB-compression point of the Hughes receiver has been measured at -27 dBm (table 13). Thus, a small amount of signal compression occurred at an input level of -30 dBm, which we believe accounted for the observed BER degradation. The receiver continued to perform with no more than 1.5 dB of additional degradation down to an input level of -60 dBm. At -65 dBm additional degradation of 2.5 to 4.0 was observed. At -70 dBm operation at a BER of 10^{-6} could not be achieved.

4.2.3.3 Receiver Performance as a Function of Frequency

The frequency responses of the receivers by themselves exhibit some variation (refs. 11 to 13). Additional variations resulted from the frequency response of the rest of the transponder. These effects were primarily responsible for the variation in BER test results between the different test bands.

The best BER results were obtained for LNR band B. The BER degradation from the ideal case never exceeded 1.78 dB for any of the HPA operating points for input levels of -50 dBm and above in this test band. This was a result of band B's location at the center of the 2.5-GHz bandwidth of the overall transponder, yielding transmission characteristics superior to the other test bands. As the test bands were moved away from the transponder band center, BER degradation increased. Thus, the worst BER performance was observed for the Hughes and ITT receivers and for LNR band C, all of which are located at the band edges. For the LNR and ITT receivers the frequency responses of the receivers themselves contributed significantly to the degradation at the band edges. The Hughes receiver, however, had a reasonably flat response at its lower band edge; therefore, most of the degradation measured for the Hughes test band can be attributed to the band edge problems of the rest of the system.

4.2.3.4 Performance Comparison of the Three Receivers

Each of the receivers has demonstrated a capability of transmitting digital data without severe degradation. The LNR receiver, when tested near its band center, allowed transmission with a BER degradation of as little as 0.88 dB. The ITT receiver's best degradation performance was 2.10 dB. Because the measured RF performance of the ITT receiver was approximately equal to that of the LNR receiver, it is

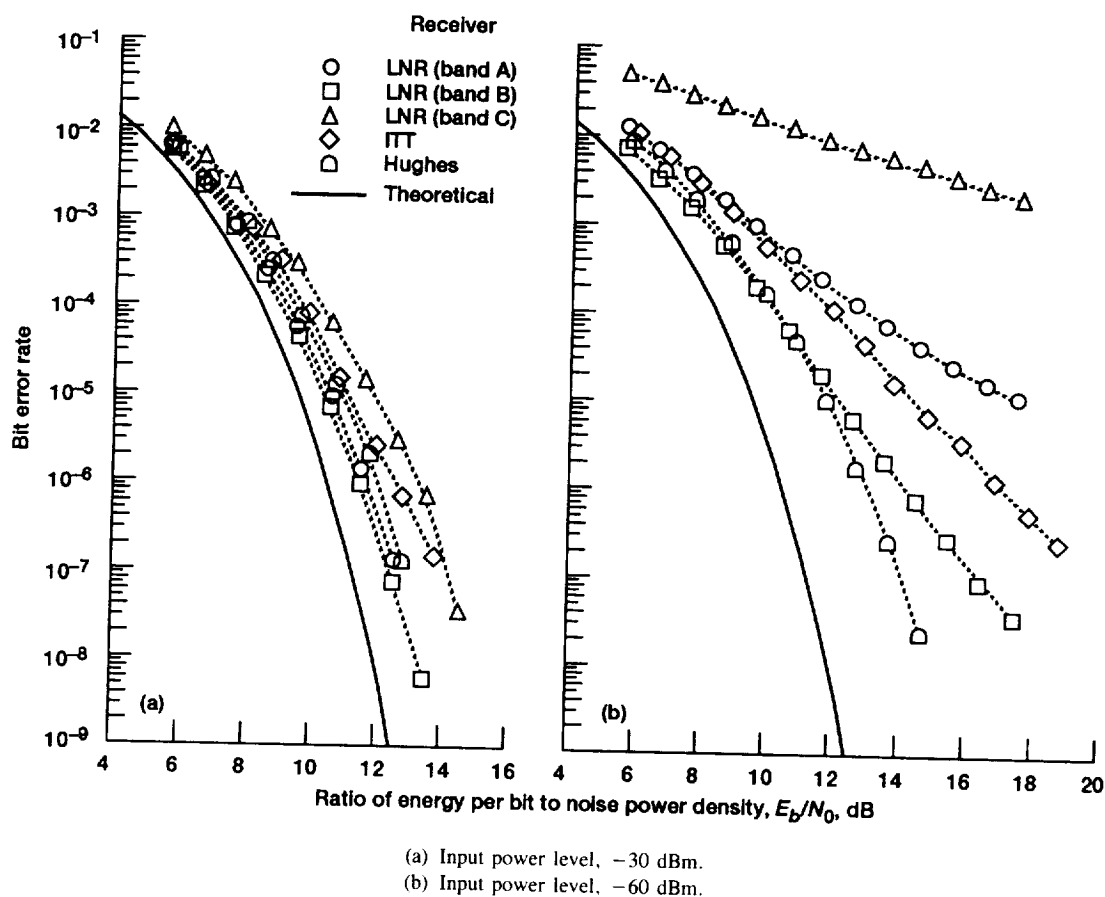


Figure 20.—BER curves for three receivers at two input power levels with TWT saturated.

reasonable to expect that a BER measurement made at the center of the ITT receiver's 2.5-GHz bandwidth, if it were possible, would yield comparably good performance. The Hughes receiver was able to provide a BER degradation as low as 1.47 dB, despite the fact that it was operating at the extreme upper edge of the transponder bandwidth. A measurement made at the Hughes band center would most probably yield a BER measurement as good as or better than those of the LNR or ITT receivers.

The Hughes receiver clearly outperformed the LNR and ITT receivers in terms of noise figure. This is evidenced by both noise figure measurements and the ability of the Hughes receiver to operate at input power levels 5 dB lower than those of the LNR and ITT receivers. In terms of gain, all of the receivers met their design goals of 20 dB for the LNR and ITT receivers and 40 dB for the Hughes receiver. A gain of 20 dB is considered adequate for most 30/20-GHz satellite transponder applications, so that the additional 20-dB gain that the Hughes receiver generates is not considered a major advantage. Other differences in RF performance, as shown in table 13, did not manifest themselves in the BER measurements made in the SITE system.

4.2.4 Concluding Remarks—Receiver Tests

All of the receivers tested are capable of providing digital data signal transmission in a 30/20-GHz satellite system with little or no degradation. Best results were obtained when using the receivers at the center of their operating bandwidths when possible. The Hughes receiver design was preferred because of its low noise figure, better input VSWR, and much smaller packaging. All receivers would benefit by having a flatter frequency response, particularly at the band edges.

4.3 High-Power-Amplifier Tests

The phase I testing employed two high-power amplifiers developed as downlink transmitters for the NASA Lewis 30/20-GHz POC Program. The frequency range of operation of these amplifiers was 17.7 to 20.2 GHz. Two contractors provided the high-power amplifier devices used in the program: Hughes Electron Dynamics Division, which developed a multimode traveling-wave-tube amplifier

(TWTA), and Texas Instruments (TI), which developed a GaAs FET solid-state amplifier. The use of both the TWTA and the GaAs FET solid-state amplifier within the phase I system allowed for a performance comparison of the two devices.

The 20-GHz downlink amplifier is a critical component of the satellite transponder. The inherent characteristics of the downlink amplifier, such as bandwidth, noise figure, gain flatness, and linearity, will all contribute to the performance of the overall system. Less-than-ideal amplifier characteristics will result in some signal degradation within the system. The available output power from the downlink amplifier is very important when determining system requirements to close the satellite link. System tradeoffs include the antenna gain and size and the use of power-efficient modulation schemes. These tradeoffs need to be studied when choosing the best amplifier for the application.

The obvious difference between solid-state amplifiers and TWTA's is their output power and efficiency, especially when output power levels of greater than 25 W are required. It is reasonable to assume that for output power below 10 W, the GaAs FET solid-state devices may offer the best performance in terms of reliability, cost, and reductions in size, power, and weight. For high output power requirements at frequencies above 20 GHz, the TWTA remains the best amplification device.

As part of the phase I BER program the Hughes TWTA and the TI GaAs FET solid-state amplifier were evaluated by using SMSK digitally modulated signals. BER measurements were taken and evaluated for a number of input power drive conditions. The test results are described in the following sections.

4.3.1 HPA Design and Performance

The Hughes 918HA helix type of TWTA was developed to demonstrate high efficiency and multipower level capability in a TWTA. Such a device was deemed beneficial for use as the downlink transmitter in a satellite communications system operating in the frequency range 17.7 to 21.2 GHz. Key design

features of this TWTA included a diamond-supported, electro-polished helix and a five-stage depressed collector. A diagram and electrical design features of the TWTA are shown in figure 21.

A TWTA amplifies by causing the RF signal to propagate along a slow-wave structure such as a helix and allowing it to interact with an electron beam traveling along its axis. An electron gun generates a stream of electrons that are drawn through an anode and focused by a magnetic field into a narrow beam, so that the electrons travel along the length of the tube. The electrons are then dissipated as heat in the collector. An interaction between the RF signal and the electron beam causes electrons to be slowed down or accelerated and "electron bunching" occurs. Thus, the phase velocity of the electromagnetic RF signal wave will move slightly slower than the velocity of the electron beam. A near-synchronous condition occurs where the RF wave and the electron beam are continuously interacting. The electron bunches couple direct-current energy to the slowed RF wave, and an exponential amplification of the signal occurs. The use of diamond support rods in this design reduced the dielectric loading of the helix circuit and also minimized the RF losses. A five-stage depressed collector was used to obtain high efficiencies over the full multimode operating range. The multiple stages allow for velocity sorting of the electron beam into groups so that the recovery of average kinetic energy is greater. The five-stage collector also has the advantage of substantial power savings during small-signal (backed-off) operation. The anode control of beam current allows the TWTA to achieve a multipower mode capability. Table 15 lists the main operational data of the TWTA.

A solid-state, high-power amplifier (TI GaAs FET) was developed by Texas Instruments to demonstrate the feasibility of an efficient, reliable GaAs FET transmitter for use in 30/20-GHz communications systems. The general approach of the TI design is shown in the block diagram of figure 22. The output power goal of this device was 6.0 to 7.5 W over a 17.7- to 20.2-GHz frequency range. The approach used a 16-way waveguide power divider/combiner where the wave-

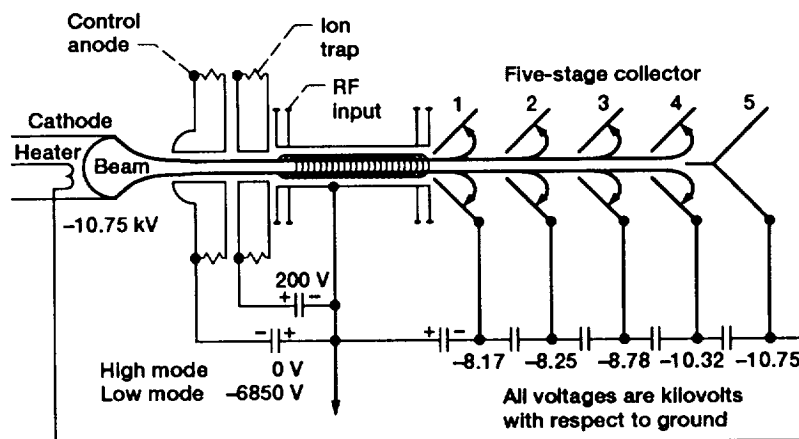


Figure 21.—Features of Hughes TWT design. High mode, 72 mA and 7 W saturated; low mode, 16 mA and 7.5 W saturated.

TABLE 15.—DESIGN FEATURES OF
HUGHES TWT
[Saturation frequency, 18.5 GHz]

TWTA mode	Beam current, mA	Anode voltage, kV	Cathode voltage, kV	Output power, W
Low	22.5	−5.2	−9.8	5.1
Medium	42.3	−2.4	−9.9	18.6
High	57.9	−.7	−10.1	34.7

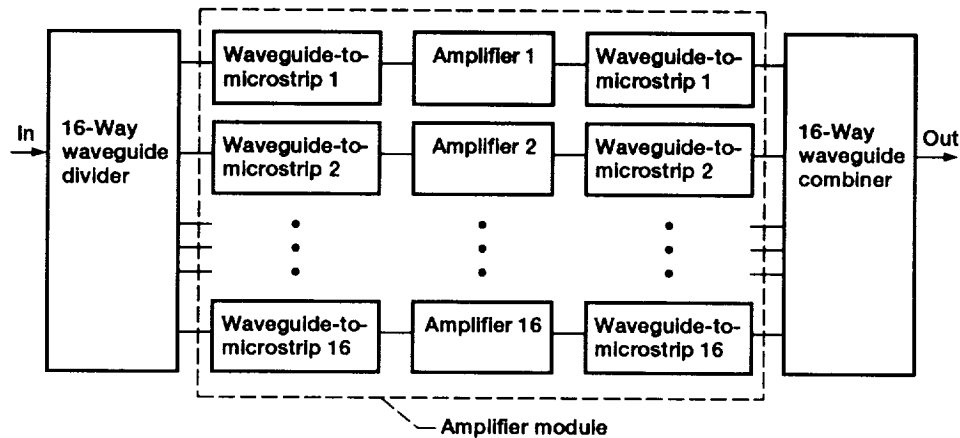


Figure 22.—Block diagram of TI GaAs FET design approach.

TABLE 16.—GOALS OF TEXAS
INSTRUMENTS GaAs FET

Parameter	Required	Actual
RF band, GHz	17.7–20.2	17.5–20.2
Output power, W	6.0–7.0	3.0
Gain, dB	30	30

guide was used to minimize insertion loss of the structure over the 2.5-GHz bandwidth. Circuit-level power combining was employed because of the limited saturated output power of each FET module. A direct waveguide-to-microstrip finline transition with less than 0.5-dB insertion loss was also developed for this design. Each amplifier module was designed to provide 30-dB gain and 0.5-W power output. However, the amplifier failed during testing and the failure resulted in a substantial power output reduction. Table 16 shows the required and actual performance of the amplifier as tested by TI.

4.3.2 Test Description

The two HPA devices were subject to BER tests where the input power of each high-power amplifier was backed off from saturation (0 dB). The input power drive level was reduced in increments of 2 dB to a level that was 16 dB below the saturation point. An overdrive condition of 2 dB above saturation was also observed. All other transponder system power levels were maintained at the baseline settings throughout each

test. The switch matrix crosspoint path used in the system test also contributed to the frequency response of the test. Therefore, to eliminate the possibility of crosspoint variations, a single IF switch matrix crosspoint (input port 7, output port 6) was used for all of the tests. For the Hughes TWT, tests were done in the three (low, medium, and high) power modes of operation. The TI GaAs FET operated at a constant output power and was tested for this single case. The input power variation test was operated over three frequency bands of the transponder (bands A, B, and C). These test bands are described in section 4.2.2.

4.3.3 BER Test Results

A summary of the bit-error-rate results is shown in table 17. Table 17 lists the E_b/N_0 degradation from the ideal E_b/N_0 value at a BER of 10^{-6} for all of the tested conditions. Each of the three power modes of the Hughes TWT and the single mode of the TI GaAs FET were evaluated. For each test band of the transponder a BER curve was taken at input power drive

TABLE 17.—SUMMARY OF BER RESULTS

Frequency band	Power backoff, dB	Amplifier			
		Hughes TWT			TI GaAs FET
		Low mode	Medium mode	High mode	
		E_b/N_0 degradation from ideal at BER of 10^{-6} , dB			
A	2	1.38	0.92	0.82	1.05
	0	1.31	.85	1.29	1.11
	-2	1.62	1.01	1.32	1.25
	-4	1.19	1.11	1.98	1.28
	-6	1.46	1.25	2.03	1.35
	-8	1.66	1.40	2.94	1.52
	-10	1.96	1.55	3.01	1.56
	-12	1.74	1.59	3.66	1.60
	-14	-----	1.65	3.57	1.88
-16	-----	-----	4.30	1.81	
B	2	0.93	0.71	0.97	0.76
	0	1.15	.88	1.19	.86
	-2	1.24	1.05	1.35	.97
	-4	1.33	1.10	1.83	.91
	-6	1.39	1.11	1.92	.86
	-8	1.37	1.28	1.30	.94
	-10	-----	1.41	1.45	.98
	-12	-----	1.49	1.60	.84
	-14	-----	1.46	1.79	.90
-16	-----	-----	2.72	.92	
C	2	2.50	1.89	1.71	1.75
	0	3.43	2.41	1.96	1.88
	-2	3.73	2.72	1.99	2.11
	-4	3.90	3.14	2.36	2.29
	-6	4.03	3.42	2.86	2.27
	-8	4.21	3.71	2.98	2.57
	-10	4.06	3.87	3.35	2.86
	-12	-----	-----	3.56	2.92
	-14	-----	-----	3.92	3.20
-16	-----	-----	3.80	3.48	

conditions from 2-dB to 16-dB power backoff relative to the saturation point. Several data points are not listed in table 17; these data points were either unobserved or where the BER tests ran exceptionally long in time to reasonably obtain a data point.

4.3.3.1 Performance as a Function of Frequency

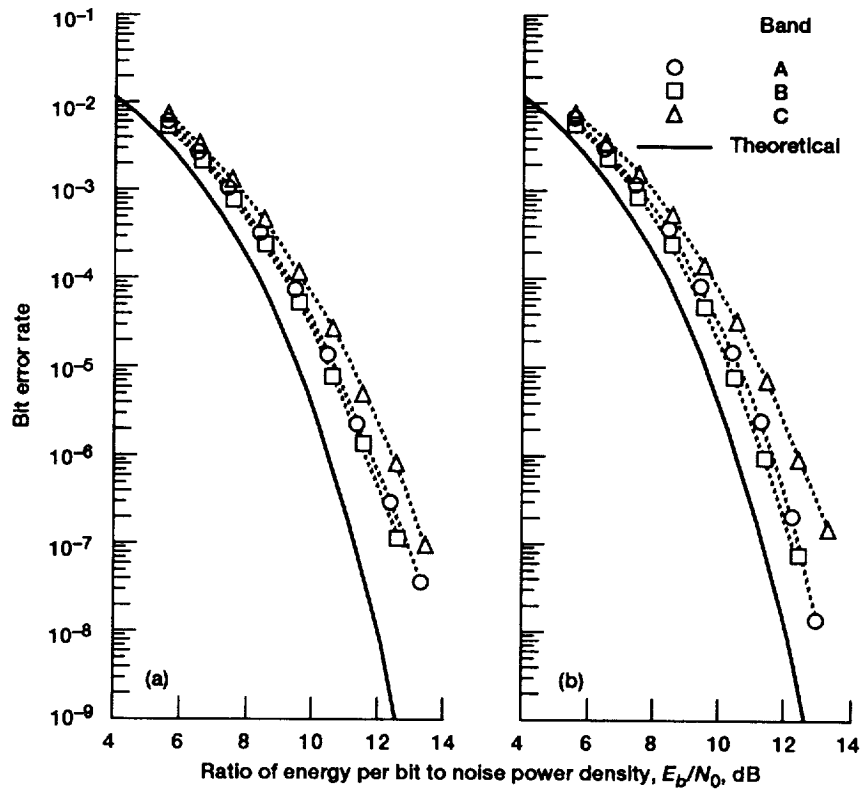
An amplifier's own frequency response will certainly contribute to the BER attainable from the system. Of course, one should not discount the many frequency variations resulting from the other devices present in the transponder system. The variations of the transponder, with the downlink amplifier included, thus are responsible for the BER variations between test bands. The BER curves of figure 23 show the effect of varying input power to the amplifiers for the three frequency bands for both the Hughes TWT and the TI GaAs FET.

Figure 24 plots the E_b/N_0 degradation from ideal at a BER of 10^{-6} versus the input power backoff for bands A, B, and

C for the TI GaAs FET and for all modes of the Hughes TWT. The best BER for a given operating condition in all cases was obtained in band B. As mentioned previously in section 4.2.3.3, the location of band B at the center of the 2.5-GHz bandwidth of the overall transponder yielded superior transmission characteristics over the other frequency bands. The worst BER performance was observed in band C, where the poorer amplitude response within the band contributed to the increased BER degradation.

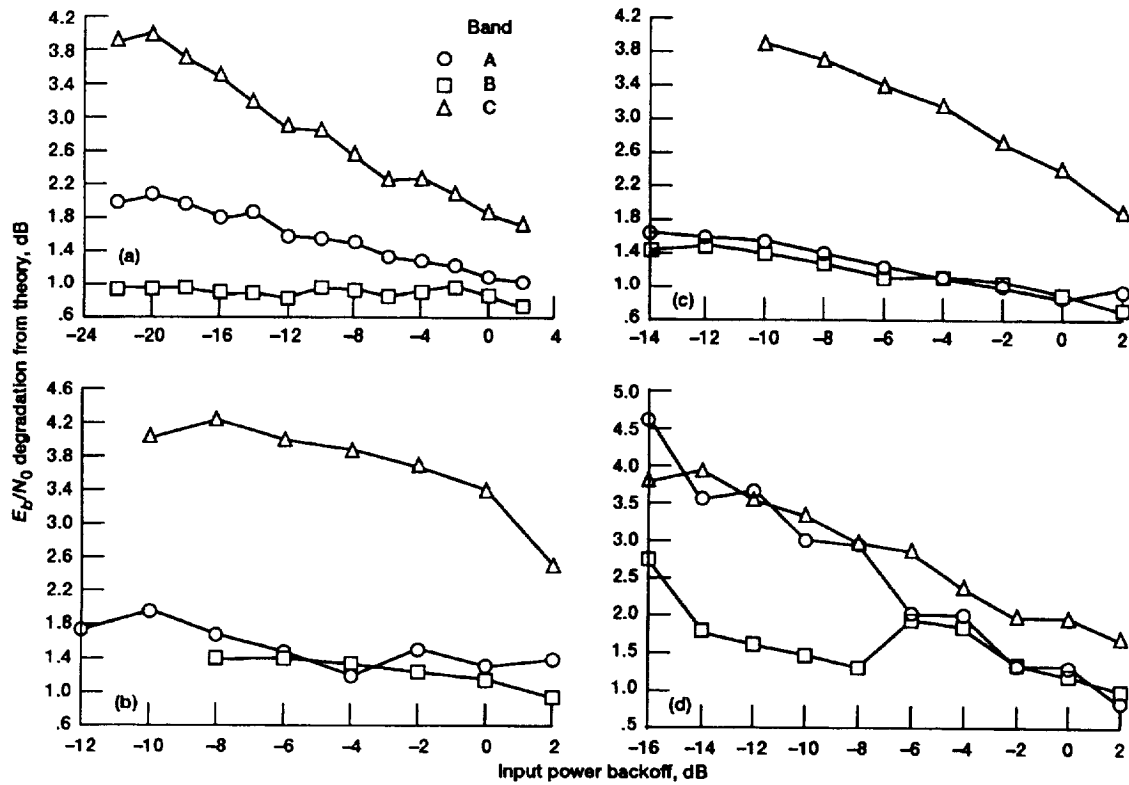
4.3.3.2 Performance as a Function of Input Drive Power

As the input power of the amplifier was increased, a direct linear gain occurred in output power until saturation was reached and further increases in input power no longer produced a substantial increase in output power. Nonlinear amplification resulted near the region of maximum output power. This is an important point to consider; if multiple carriers (FDMA) are present, intermodulation distortion will



(a) Hughes TWT.
(b) TI GaAs FET.

Figure 23.—Frequency band comparison. Drive level, 0 dB.



(a) TI GaAs FET.
(b) Hughes TWT (low-power mode).

Figure 24.—Input power variation for BER of 10^{-6} .

occur. In this case only a single input signal was present; therefore, no carrier distortion occurred as the saturation point was approached.

As shown in the figures on Hughes TWT input power variation (fig. 24(b) to (d)), in every power mode and for every band tested, the degradation was clearly minimum at the 2-dB overdrive point or at saturation. The E_b/N_0 degradation at a BER of 10^{-6} tended to increase as the input power was backed off. A similar result occurred in tests with the TI GaAs FET. As shown in figures 25 and 26 the minimum E_b/N_0 degradation from theory also occurred at the overdrive or saturated power point.

4.3.3.3 Performance Comparison of Hughes TWT Versus Solid State

Both the Hughes TWT and the TI solid-state amplifier demonstrated the capability of transmitting SMSK digital data without major BER degradation. The obvious difference in the design of these two transmitters is the available output

power. The Hughes TWT easily outperformed the solid-state design by exhibiting an output power approximately 10 dB above that of the TI amplifier. The TI GaAs FET, however, exhibited the best BER performance for a single test condition. Operating in band B, the TI amplifier was able to transmit data with degradation no worse than 0.98 dB for all input drive conditions. In general, the BER performances of the two types of amplifiers were not substantially different.

4.3.4 Concluding Remarks—Amplifier Tests

The Hughes TWT and the TI GaAs FET solid-state amplifier were evaluated by using SMSK digitally modulated signals. Each of these amplifiers was capable of transmitting digital data with very little BER degradation. The best BER performance was obtained when the amplifiers were at their saturated or overdriven condition. Generally, as the input drive power was decreased, the bit error rate increased for a given test condition. Signal degradations as low as 0.71 dB from theory were observed at a BER of 10^{-6} .

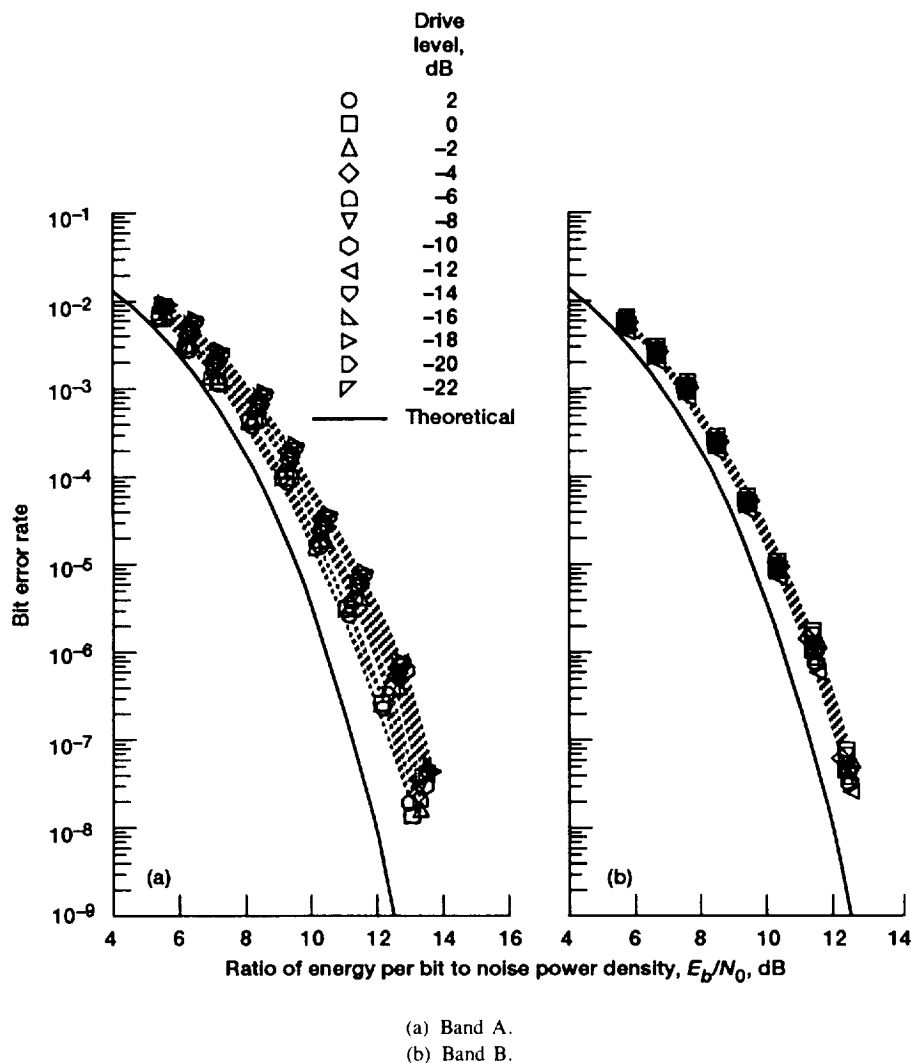


Figure 25.—Input power variation for TI GaAs FET.

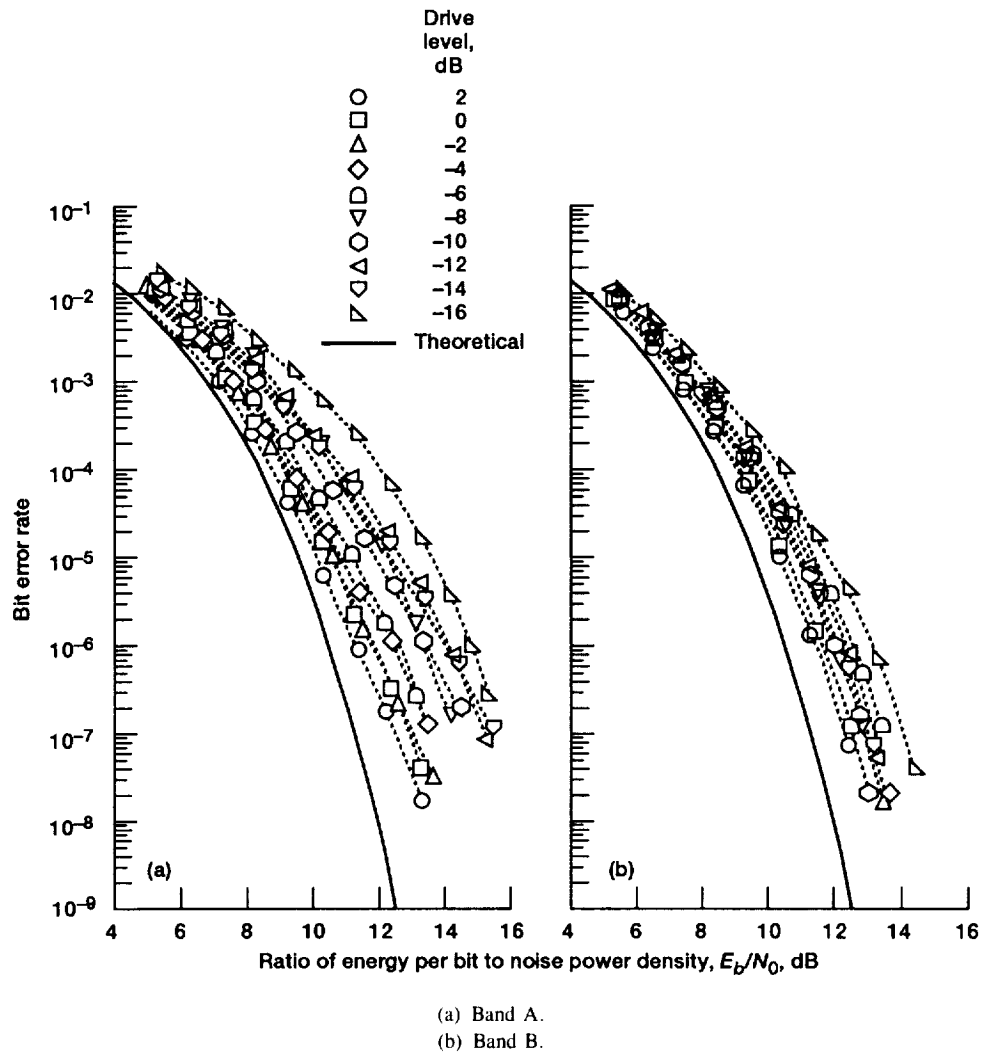


Figure 26.—Input power variation for Hughes TWT.

4.4 Interference Tests

The effects of interference on satellite channels are of primary concern in maintaining reliable communications. The increased frequency reuse employed in present-day satellite systems and limitations of the radio spectrum indicate that interference may be a major contributor in degrading system performance. The BER performance may be substantially degraded because of stray radiofrequency interference (RFI), cochannel interference (CCI), and adjacent channel interference (ACI). Possible causes include accidental or unauthorized transmissions, insufficient polarization discrimination, and side-lobe energy spillover. Adjacent channel and cochannel interferences were studied in the phase I testing. Adjacent channel interference is characterized by the injection of signal energy from other frequency channels into the channel of interest. For example, in frequency-division-multiplexed (FDM) channels the proximity at which channels can be located in frequency is determined by their main-lobe spectrum and the spectral rolloff of the modulation used.

Cochannel interference is defined here as the interfering channel occupying the same bandwidth as the desired communications channel. Phase I testing included tests to determine the degradation that interference can have on a satellite communications system. SMSK modulators and demodulators were employed to test the capability of the modulation scheme in effectively dealing with adjacent channel and cochannel interference. Both CW and modulated interferers were investigated.

4.4.1 Test Description

A number of parameters were varied in these tests to obtain the data described in this section. Both 20-GHz downlink amplifiers were separately tested within the system for comparison: the Hughes TWTA (operated at saturation and at the 1-dB-compression point) and the TI GaAs FET. Two types of interferers were employed in the tests, single-tone CW and 220-Mbps modulated spectrum. Tests were done for both uplink channel interference and downlink channel

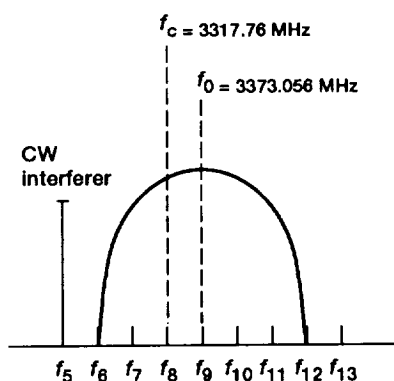


Figure 27.—CW interference test.

interference cases. For the uplink cases tests were performed with and without automatic gain control (AGC). The interfering signal's power level and frequency relative to the communications channel were varied as well. The parameters varied in these tests are described next.

4.4.1.1 Continuous-Wave Interference

A single CW tone was injected at various frequencies with respect to the offset SMSK carrier, and the system BER effects of this signal were measured. The power level of the CW interferer was varied relative to the test channel carrier power. Figure 27 shows the CW tone at its starting point f_5 . The interference signal began at the lower side of the frequency spectrum and was systematically incremented across the band over nine distinct frequencies. The cochannel interference test was performed at frequency f_9 . A BER curve was taken at each of the nine frequencies. The CW power level was also varied at each frequency. The power level of the interferer was varied from -5 to -40 dB above the carrier reference level. The tests were performed over frequency band B and across matrix switch crosspoint 7,6. The downlink amplifier configurations tested were the GaAs FET and TWT in the high-power mode at the 1-dB-compression point and at saturated levels.

4.4.1.2 Modulated interference

The modulated interference test was similar to the CW test, except that a modulated spectrum at 220 Mbps was used as the channel interferer. Figure 28 illustrates the modulated interference spectrum as it appeared relative to the test channel. This test required the use of a second SMSK modulator that generated a modulated spectrum identical to the test spectrum. A pseudorandom data sequence was provided to obtain the modulation, but in this case no acquisition and timing information was necessary for demodulation. Note that the main-lobe bandwidth of the SMSK spectrum was 1.5 times the data rate, 330 MHz. The modulated interferer was varied across the band over 17 different frequencies and over six power levels, 5 to -20 dBc, in 5-dB increments. The

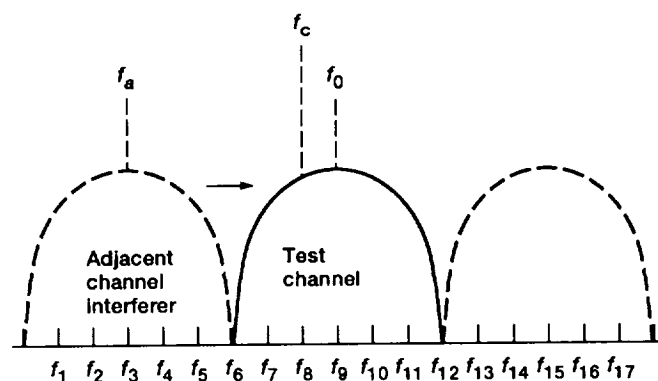


Figure 28.—Modulated interference test.

cochannel interference was performed at f_9 . A BER curve was generated for each test point. The tests were performed for the same cases as the single-tone CW interferer tests.

4.4.1.3 Uplink Tests

The uplink tests were a set of tests done to characterize the transponder system in the presence of an uplink interferer. Diagrams of the test setup are shown in figure 29. The interferer signal was summed at the IF with the communications signal, upconverted, and transmitted through the transponder. These tests were done to determine the BER degradation of the communications signal as it was transmitted through the transponder with interference. The effects of the interference on key transponder components, mainly the receiver and the high-power amplifier, could then be evaluated. It was determined that intermodulation of the two signals would inherently cause some BER degradation because the TWT was operated in the nonlinear region.

For the uplink interferer tests the interferer was present at the input to the 30-GHz receiver. Two types of tests were done in this mode, with and without AGC. Transponder settings were normally at baseline values throughout each test, as described in section 4.1.1.1(a). The power of the interferer was often in band; therefore, the power meter readings were off in value by the added power of the interfering signal. Thus, for tests performed with AGC the input power to the receiver was adjusted to maintain baseline power readings. For the tests performed without AGC the input power to the receiver was left as is. No adjustments were made to maintain a baseline power level.

4.4.1.4 Downlink Tests

The downlink tests were also done with the interferer present at the IF input to the demodulator. The test setup is shown in figure 30. This test bypassed any effects the interferer had on the transponder system. The primary objective of the test was to determine the demodulator's response in handling both CW and modulated interference. The BER degradation was measured over a set number of frequencies and power levels.

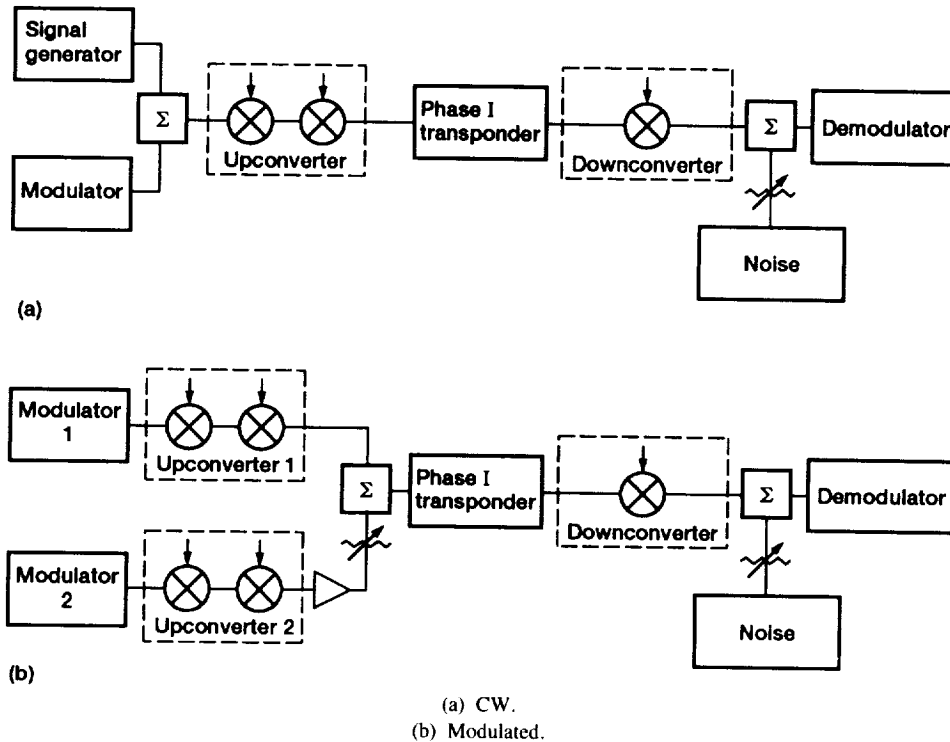


Figure 29.—Uplink interference test configurations.

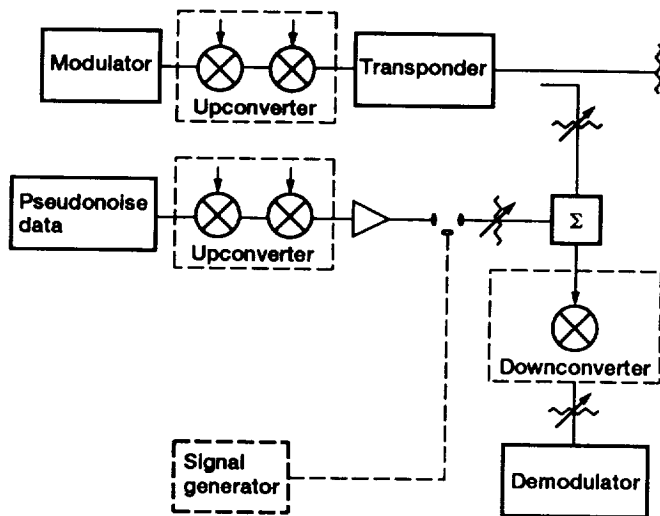


Figure 30.—Downlink interference test setup.

4.4.2 BER Test Results

The large number of BER results obtained as part of this testing have been summarized in tables 18 to 24. The E_b/N_0 degradation from the ideal SMSK curve at a BER of 10^{-6} is provided in the tables. The following sections summarize the various comparisons and effects of interference present in the system.

4.4.2.1 Comparison of CW Tone and Modulated Interference

The CW signal interferer and the modulated signal interferer can be compared for any particular frequency and power level. For the tests performed in phase I it was also dependent on the test configuration of the transponder. For identical test conditions (e.g., the downlink-TWT saturated condition at -10 dBc interferer level), it is apparent that the BER degraded in a similar fashion for both cases. As shown in figure 31, a comparison can be made between CW and modulated interferers. As expected in both cases, the best BER was obtained when the interferer was farthest from the center of the main data channel spectrum. The BER degraded rapidly as the interference approached the center of the band. In either case, with an interferer located in the center of the band, an additional 6 dB of E_b/N_0 would be required to maintain a BER of 10^{-6} . In other words, signal four times as strong as the original would be needed just to overcome the presence of this interferer. This is important to note because in real applications satellite downlink amplifiers normally operate at saturation. The margin simply would not be available to overcome such interference.

For the uplink cases the CW interferer had a more negative effect on the BER performance than the modulated interferer. At a power level of -5 dBc the uplink CW interferer was strong enough to keep the demodulator from locking (i.e., a 50-percent BER). Uplink modulated interferers, however, could be tested at -5 -dBc levels and in some cases at 0 dBc.

TABLE 18.—CONTINUOUS-WAVE UPLINK WITH
AUTOMATIC GAIN CONTROL
(a) Hughes TWT (saturation)

Frequency, GHz	Interferer power level, dBc				
	−10	−15	−20	−30	−40
	E_b/N_0 degradation from ideal at BER of 10^{-6} , dB				
F5-28.580	2.51	2.54	1.99	1.31	----
F6-28.635	----	2.92	2.93	1.38	1.17
F7-28.690	----	9.54	3.82	1.74	1.37
F8-28.745	----	----	9.13	1.98	1.28
F9-28.800	----	----	5.69	1.70	1.31
F10-28.855	----	40.51	4.23	1.24	1.07
F11-28.910	----	4.14	2.49	1.30	1.25
F12-28.965	5.30	2.90	2.58	1.25	----
F13-29.020	3.28	1.96	2.10	1.30	----

(b) TI GaAs FET (saturation)

Frequency, GHz	Interferer power level, dBc				
	−10	−15	−20	−30	−40
	E_b/N_0 degradation from ideal at BER of 10^{-6} , dB				
F5-28.580	2.02	1.54	1.17	1.03	----
F6-28.635	5.63	2.27	1.33	1.06	0.96
F7-28.690	----	6.30	2.26	1.10	.97
F8-28.745	----	----	6.47	1.28	1.05
F9-28.800	----	----	6.25	1.44	1.07
F10-28.855	----	65.32	3.17	1.18	.94
F11-28.910	13.17	3.29	1.58	.98	.95
F12-28.965	4.13	2.65	1.41	1.01	----
F13-29.020	1.88	1.31	1.24	.98	----

TABLE 19.—CONTINUOUS-WAVE
DOWNLINK WITHOUT AGC

Frequency, GHz	Interferer power level, dBc			
	−5	−10	−15	−25
	E_b/N_0 degradation from ideal at BER of 10^{-6} , dB			
F5-3.153	1.03	1.10	0.97	1.06
F6-2.208	3.40	1.83	1.29	1.08
F7-3.263	6.39	3.09	1.27	1.15
F8-3.318	----	6.21	2.68	1.27
F9-3.373	----	6.29	3.07	1.33
F10-3.428	10.61	4.07	2.24	1.22
F11-3.483	4.27	2.20	1.48	1.12
F12-3.538	2.42	1.41	1.18	1.15
F13-3.593	1.06	.96	1.08	1.22

TABLE 20.—MODULATED UPLINK FOR
HUGHES TWT WITH AGC
(a) Saturation operating point

Frequency, GHz	Interferer power level, dBc			
	-5	-10	-15	-20
	E_b/N_0 degradation from ideal at BER of 10^{-6} , dB			
F1-28.360	2.33	1.48	1.41	1.18
F2-28.415	4.81	2.15	1.43	1.13
F3-28.470	5.81	2.02	1.33	1.17
F4-28.525	2.72	1.02	1.21	1.27
F5-28.580	2.17	1.46	1.17	1.20
F6-28.635	3.93	1.81	1.57	1.29
F7-28.690	14.70	3.34	2.10	1.32
F8-28.745	41.10	5.05	2.66	1.41
F9-28.800	46.19	4.74	2.80	1.54
F10-28.855	33.54	3.57	2.31	1.33
F11-28.910	11.51	2.07	1.53	1.02
F12-28.965	2.55	1.39	1.20	.99
F13-29.020	1.97	1.20	1.32	1.10
F14-29.075	1.47	.98	1.17	1.01
F15-29.130	1.26	.96	1.18	1.00
F16-29.185	1.14	.95	1.05	1.00
F17-29.240	1.09	.91	1.21	1.03

(b) 1-dB-compression operating point

Frequency, GHz	Interferer power level, dBc					
	0	-5	-10	-15	-20	-30
	E_b/N_0 degradation from ideal at BER of 10^{-6} , dB					
F6-28.635	8.13	3.39	2.08	1.58	1.65	----
F7-28.690	----	----	----	----	----	----
F8-28.745	----	----	----	----	----	----
F9-28.800	----	14.50	4.70	2.84	1.98	0.87
F10-28.855	----	----	----	----	----	----
F11-28.910	----	----	----	----	----	----
F12-28.965	6.89	2.65	1.69	----	----	----

TABLE 21.—MODULATED UPLINK FOR
HUGHES TWT WITHOUT AGC
(a) Saturation operating point

Frequency, GHz	Interferer power level, dBc				
	-5	-10	-15	-20	-30
	E_b/N_0 degradation from ideal at BER of 10^{-6} , dB				
F1-28.360	7.24	3.09	1.50	1.16	----
F2-28.415	9.01	3.46	1.60	1.11	----
F3-28.470	1.81	2.33	1.42	1.08	----
F4-28.525	4.18	1.70	1.44	.90	----
F5-28.580	2.90	1.60	1.37	.97	----
F6-28.635	4.88	1.84	1.58	1.02	----
F7-28.690	34.85	2.71	2.26	1.38	----
F8-28.745	60.24	4.60	3.14	1.69	0.92
F9-28.800	----	3.66	3.44	1.44	.89
F10-28.855	42.78	3.05	2.66	1.31	.93
F11-28.910	22.17	2.34	1.41	1.04	----
F12-28.965	3.28	1.79	1.39	1.19	----
F13-29.020	2.09	1.54	1.20	1.10	----
F14-29.075	2.14	1.45	1.21	1.17	----
F15-29.130	1.80	1.31	.93	1.22	----
F16-29.185	1.76	1.32	1.01	.96	----
F17-29.240	1.51	1.27	1.17	1.08	----

(b) 1-dB-compression operating point

Frequency, GHz	Interferer power level, dBc					
	0	-5	-10	-15	-20	-30
	E_b/N_0 degradation from ideal at BER of 10^{-6} , dB					
F6-28.635	8.34	3.27	1.89	1.88	1.57	----
F7-28.690	----	----	----	----	----	----
F8-28.745	----	----	----	----	----	----
F9-28.800	----	14.14	4.29	2.73	1.87	1.14
F10-28.855	----	----	----	----	----	----
F11-28.910	----	----	----	----	----	----
F12-28.965	4.84	2.44	1.81	1.65	1.45	----

TABLE 22.—MODULATED UPLINK FOR TI GaAs FET
WITH AGC

(a) Saturation operating point

Frequency, GHz	Interferer power level, dBc					
	0	-5	-10	-15	-20	-30
	E_b/N_0 degradation from ideal at BER of 10^{-6} , dB					
F1-28.360	----	1.45	0.94	0.78	----	----
F2-28.415	----	2.68	.92	.70	----	----
F3-28.470	----	2.33	----	----	0.76	----
F4-28.525	----	1.20	----	----	----	----
F5-28.580	----	1.11	.90	.74	----	----
F6-28.635	64.71	1.95	1.12	----	.82	----
F7-28.690	----	5.69	----	----	----	----
F8-28.745	----	29.04	3.18	1.93	----	----
F9-28.800	----	31.65	3.35	1.88	1.05	0.82
F10-28.855	----	13.99	2.71	1.64	----	----
F11-28.910	----	7.24	----	----	----	----
F12-28.965	30.01	1.87	.92	----	.78	----
F13-29.020	----	1.32	.78	.88	----	----
F14-29.075	----	.86	----	----	----	----
F15-29.130	----	.84	----	----	.69	----
F16-29.185	----	.82	.63	.79	----	----
F17-29.240	----	.72	.63	.74	----	----

(b) 1-dB-compression operating point

Frequency, GHz	Interferer power level, dBc				
	0	-5	-10	-20	-30
	E_b/N_0 degradation from ideal at BER of 10^{-6} , dB				
F6-28.635	21.76	1.93	1.12	0.73	----
F7-28.690	----	----	----	----	----
F8-28.745	----	----	----	----	----
F9-28.800	----	13.47	3.43	1.13	0.76
F10-28.855	----	----	----	----	----
F11-28.910	----	----	----	----	----
F12-28.965	15.79	1.63	.94	.71	----

TABLE 23.—MODULATED UPLINK FOR TI GaAs FET
WITHOUT AGC

(a) Saturation operating point

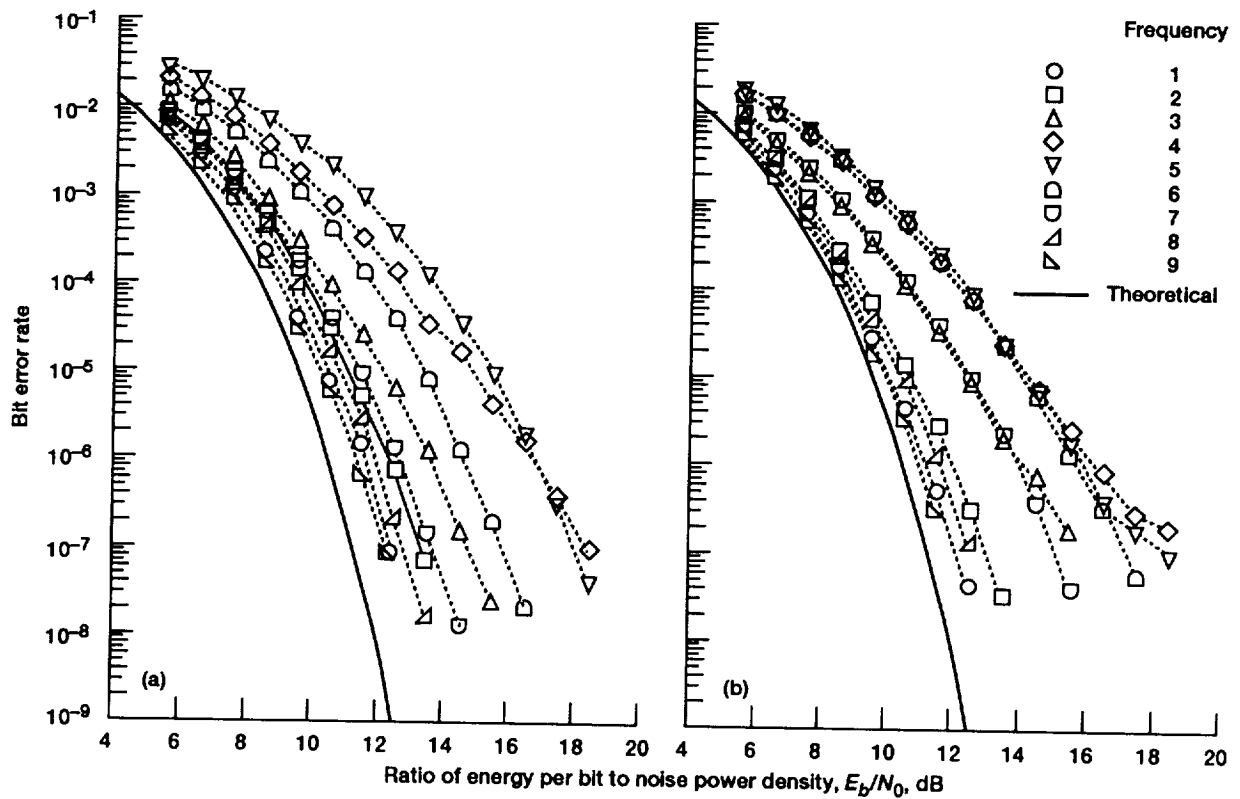
Frequency, GHz	Interferer power level, dBc					
	0	-5	-10	-15	-20	-30
	E_b/N_0 degradation from ideal at BER of 10^{-6} , dB					
F1-28.360	----	4.06	0.73	1.37	----	----
F2-28.415	----	4.41	.85	1.29	----	----
F3-28.470	----	3.09	----	----	0.88	----
F4-28.525	----	2.20	----	----	----	----
F5-28.580	----	1.98	.86	.92	----	----
F6-28.635	76.58	2.84	1.04	----	.78	----
F7-28.690	----	7.08	----	----	----	----
F8-28.745	----	40.28	3.35	1.85	----	----
F9-28.800	----	16.41	3.36	2.02	1.01	0.73
F10-28.855	----	11.23	2.83	1.71	----	----
F11-28.910	----	6.57	----	----	----	----
F12-28.965	35.85	2.67	1.00	----	.75	----
F13-29.020	----	1.69	.97	.92	----	----
F14-29.075	----	1.47	----	----	----	----
F15-29.130	----	1.22	----	----	.72	----
F16-29.185	----	1.20	.78	.79	----	----
F17-29.240	----	.88	.77	.80	----	----

(b) 1-dB-compression operating point

Frequency, GHz	Interferer power level, dBc				
	0	-5	-10	-20	-30
	E_b/N_0 degradation from ideal at BER of 10^{-6} , dB				
F6-28.635	26.92	1.90	1.17	0.69	----
F7-28.690	----	----	----	----	----
F8-28.745	----	----	----	----	----
F9-28.800	----	16.67	3.39	.34	0.54
F10-28.855	----	----	----	----	----
F11-28.910	----	----	----	----	----
F12-28.965	19.07	2.19	.96	.74	----

TABLE 24.—MODULATED DOWNLINK FOR
HUGHES TWT (SATURATION)

Frequency, GHz	Interferer power level, dBc				
	0	-5	-10	-15	-20
	E_b/N_0 degradation from ideal at BER of 10^{-6} , dB				
F1-2.933	----	0.85	0.83	0.77	----
F2-2.988	----	.82	.71	.77	----
F3-3.043	----	1.05	.71	.85	----
F4-3.098	1.26	.96	.68	.70	----
F5-3.153	2.66	1.28	1.14	.76	----
F6-3.208	19.15	3.29	1.90	.99	----
F7-3.263	----	10.75	3.98	1.59	----
F8-3.318	----	10.72	6.14	2.25	1.62
F9-3.373	----	----	5.72	2.50	1.80
F10-3.428	----	36.04	5.49	2.31	1.73
F11-3.483	----	13.78	3.94	1.69	----
F12-3.538	11.64	3.25	1.52	.98	----
F13-3.593	2.30	1.17	.89	.62	----
F14-3.648	1.26	1.11	.82	.69	----
F15-3.703	----	.78	.71	.73	----
F16-3.758	----	.99	.78	.76	----
F17-3.813	----	.88	.72	.74	----



(a) CW (TWT saturated).
(b) Modulated.

Figure 31.—Downlink interference at -10 dBc.

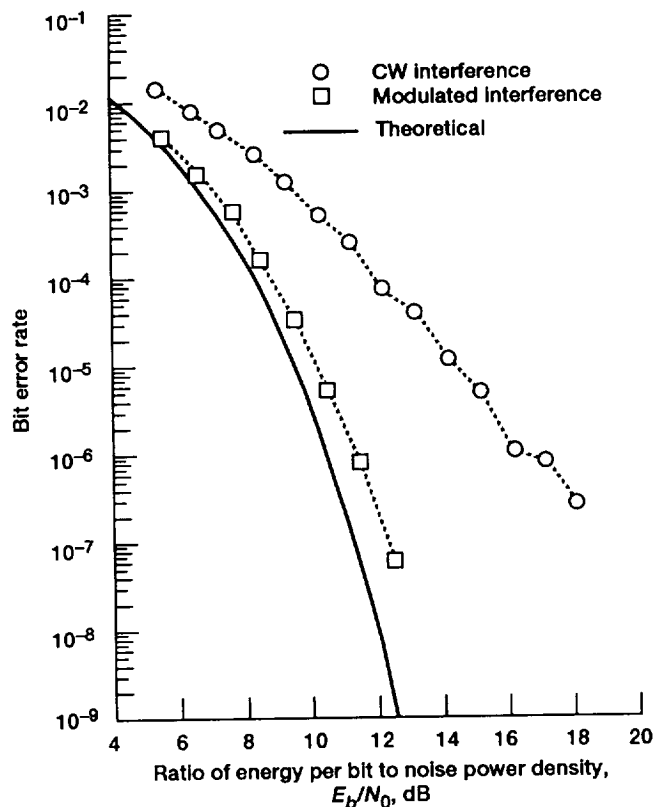


Figure 32.—Typical BER curves.

Several typical BER curves are shown in figure 32. In this case the interferer was located at band center, 28.8 GHz (cochannel test) with a power level of -20 dBc. The example illustrated here is for the TI GaAs FET at saturation, with AGC.

The CW interferer caused a 5.2-dB degradation in E_b/N_0 over the modulated interferer at a BER of 10^{-6} . This was the general trend for these tests. Large differences in the two types of interferer generally occurred only near the center of the band and at the higher power levels. Typically, as the interferer level was reduced, differences between the two types of interferers became less noticeable.

4.4.2.2 Performance as a Function of Frequency

The frequency settings tested in the system were stepped in 55-MHz increments across the test channel bandwidth. The CW interferer was tested for 9 frequencies; the modulated interferer, for 17 frequencies. As expected, the BER performance was dependent on the frequency of the interference. The BER curves of figure 31 also illustrate the BER performance as a function of frequency. The BER performance was similar for both types of interferer. As the interferer signal approached the center of the band, the BER degraded rapidly. When the interferer was located on the lower side of the test channel, the degradation was greater than when it was located on the

high side. The reason for this occurrence is that the SMSK signal carrier is offset from center by $-\frac{1}{4}$ of the data rate.

4.4.2.3 Comparison With and Without AGC

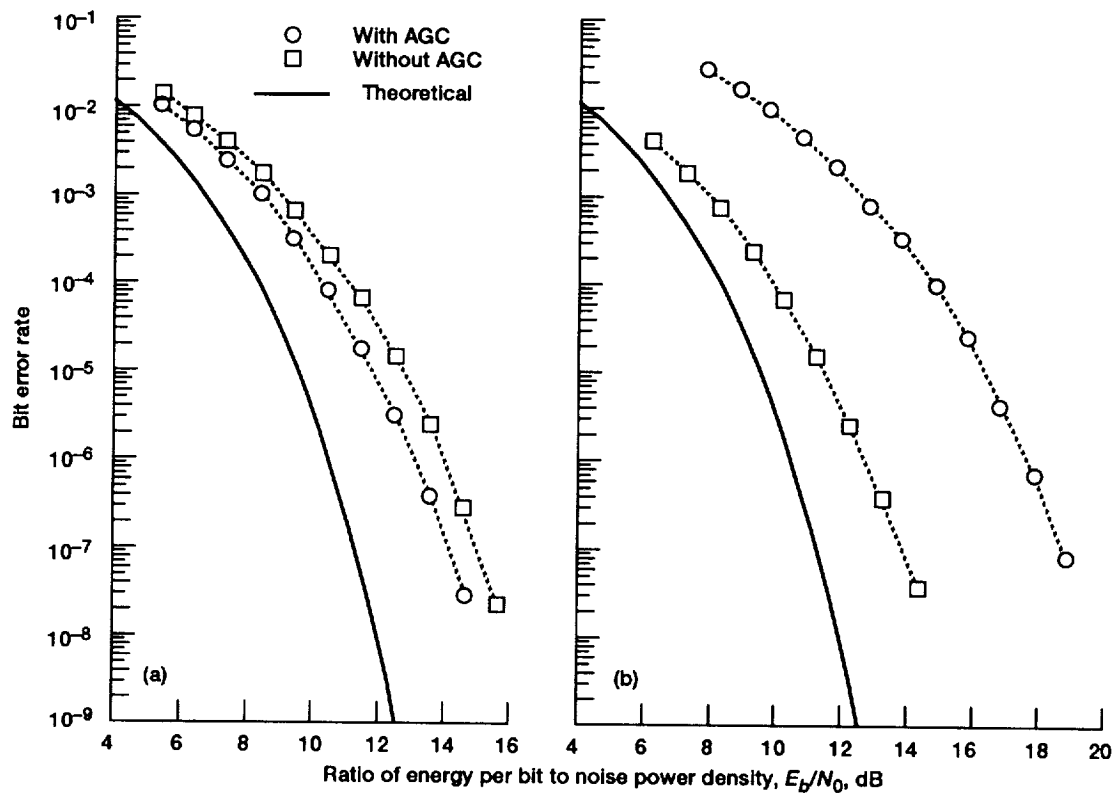
For a given interferer frequency and power level the AGC tended to improve the BER slightly at the lower interferer power levels and more at the higher power levels. This effect was more pronounced with the modulated interferer. As can be seen from the figure 33, for a CW interferer at frequency f_1 and -10 dBc the E_b/N_0 improvement with AGC at a BER of 10^{-6} was about 0.9 dB, but for the modulated interferer at f_1 and -5 dBc the E_b/N_0 improvement with AGC at a BER of 10^{-6} was roughly 4.5 dB.

4.4.2.4 Comparison of Uplink and Downlink Cases

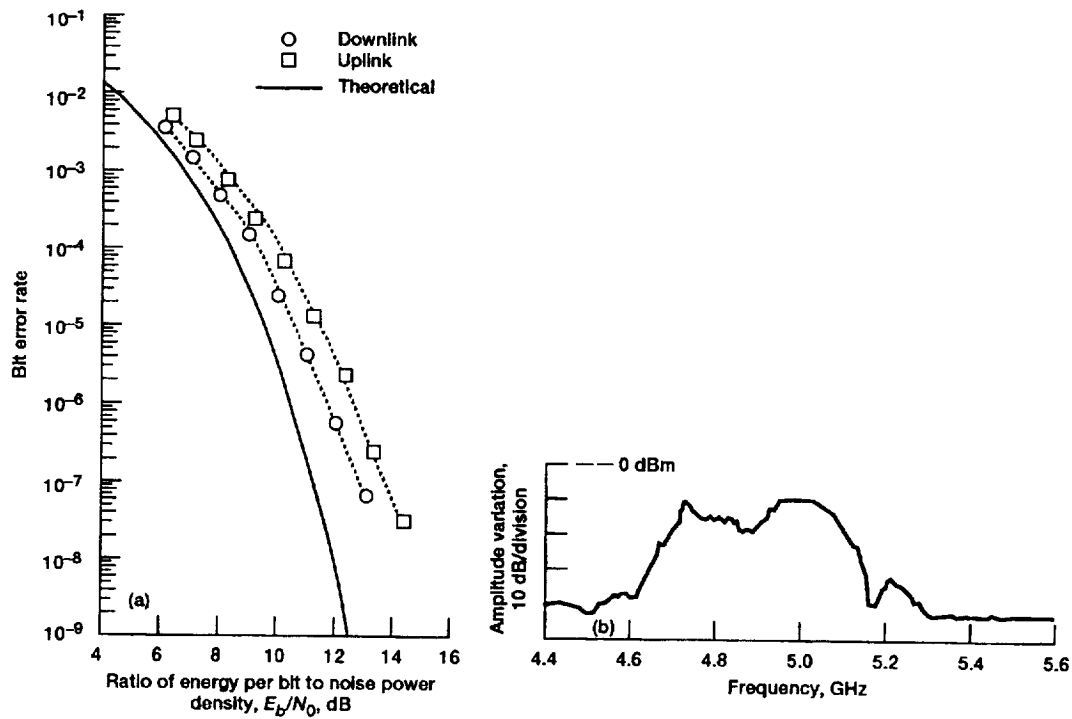
In figures 34 and 35 the modulated interference case at -5 dBc is shown for frequencies f_5 and f_{15} , respectively. Also shown in these figures are the receiver IF output spectra of each case, which clearly show the interference effect on the main data channel spectrum centered at 5.0 GHz. From the BER curves it is evident that the addition of the interferer (CW or modulated), when summed at the input to the transponder, required more signal energy for the uplink case than for the downlink case. This result is reasonable because intermodulation and other mixing effects, such as spurious responses, will be introduced into the system for uplink interference. Note that for most of the conditions tested the relative difference in required E_b/N_0 to maintain a BER of 10^{-6} was less than 1 dB between uplink and downlink curves. The differences between the uplink and downlink cases can be attributed to the interferer bypassing the transponder system in the downlink case. Any deviations or distortions that are present within the single channel, including nonlinearities, spurious responses, and amplitude fluctuations, are present only for the data channel. The degradation in BER will then mainly be attributed to the downlink interferer. The downlink interferer, whether CW or modulated, was summed with the data channel in the 20-GHz band. The downlink interference test thus realistically simulates a possible interference scenario for the 30/20-GHz communications satellite link.

4.4.3 Concluding Remarks—Interference Tests

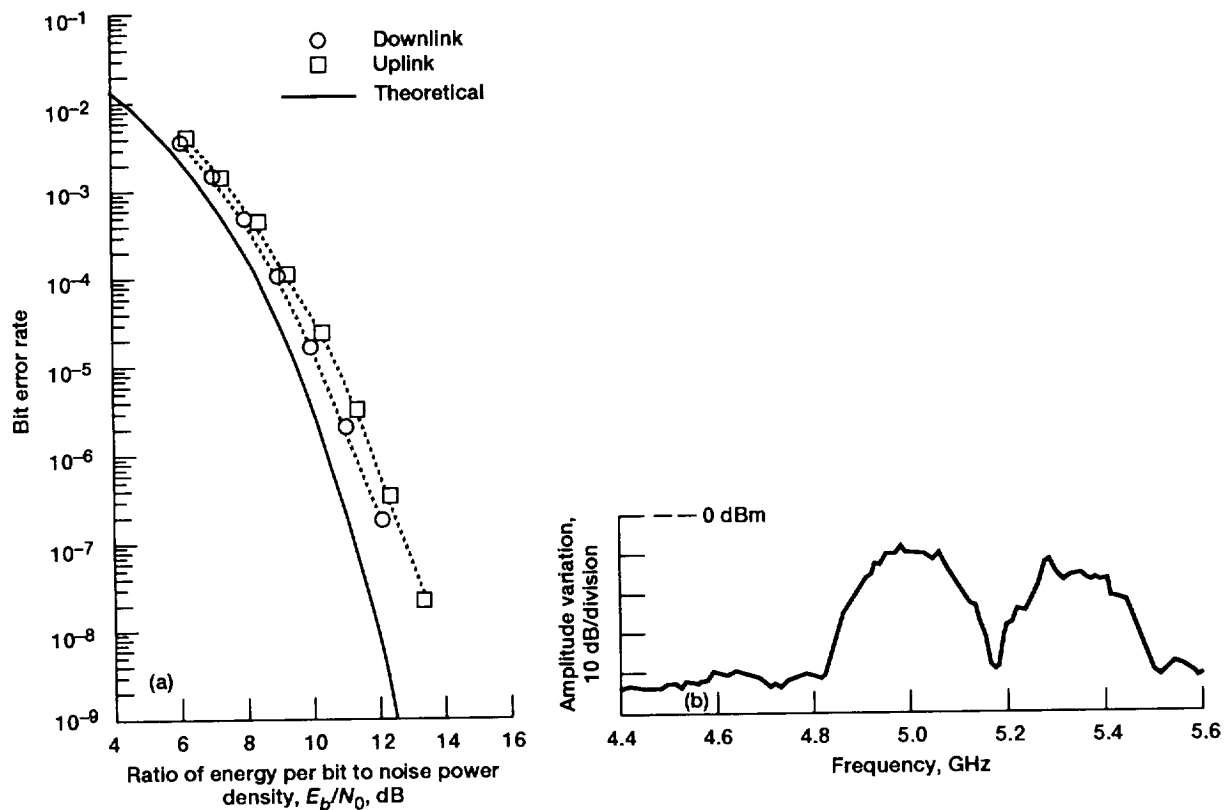
From these tests it is readily apparent that the presence of interferers, whether single-tone CW or modulated, has a pronounced effect on BER performance. The BER performance was similar for both types of interferer. As the interfering signal approached the center of the band, the BER degraded rapidly. When the interferer was located on the lower frequency side of the test channel, the degradation was greater than when it was located on the high side. This is a characteristic of the SMSK modulation used in these tests. For the uplink cases the CW interferer had a more negative effect on the BER performance than the modulated interferer. Large



(a) CW interference at level of -10 dBc.
 (b) Modulated interference at level of -5 dBc.
 Figure 33.—Uplink interference at frequency f_1 .



(a) BER performance.
 (b) Receiver IF output. Reference, 0 dBm.
 Figure 34.—Modulated uplink and downlink interference at frequency f_3 and interference level of -5 dBc.



(a) BER performance.
 (b) Receiver IF output. Reference, 0 dBm.
 Figure 35.—Modulated uplink and downlink interference at frequency f_{15} and interference level of -5 dBc.

differences in the two types of interferer generally occurred only near the center of the band and at the higher interferer power levels. Typically, as the interferer level was reduced, differences between the two types of interferer were less noticeable.

4.5 Matrix Switch Tests

The matrix switch is another key technology for communications satellites employing multiple-beam antennas and on-board switching. The matrix switch provides the dynamic interconnectivity on the spacecraft that will increase the system's efficiency and effectively reduce its cost. The phase I testing employed two matrix switches developed for the NASA Lewis 30/20-GHz POC Program. One was built by General Electric Company (GE), and the other by Ford Aerospace and Communications Corporation. The Ford matrix switch was used in most of the phase I testing, as was previously discussed in section 4.1, but the GE matrix switch was also tested. The phase I testing offered an opportunity to compare the two devices.

The requirements of a matrix switch are fast switching speeds, high isolation between crosspoints, and flat amplitude response within the passband. The signal degradation resulting from the transmission through the matrix switches—in particular, the performance variation of the phase I satellite simulator system as different matrix switch crosspoints are traversed—has been measured. Measurements of the BER were taken and evaluated for a number of active crosspoints. The test results are discussed in the following sections.

4.5.1 Matrix Switch Description

The POC matrix switches were designed to have 20 inputs and 20 outputs. In order to reduce the cost of these POC models, only a portion of the available crosspoints were populated with switching elements. The GE switch contained 61 active crosspoints; the Ford switch contained 65 active crosspoints.

Both contractors chose a coupled crossbar architecture for their POC models. Figure 36 shows the GE crossbar architecture. The input and output transmission lines are coupled to each other through a switching element. With the switch open the input and output lines are isolated. With the switch closed the input and output lines are connected with roughly 20 dB of insertion loss. The most significant differences

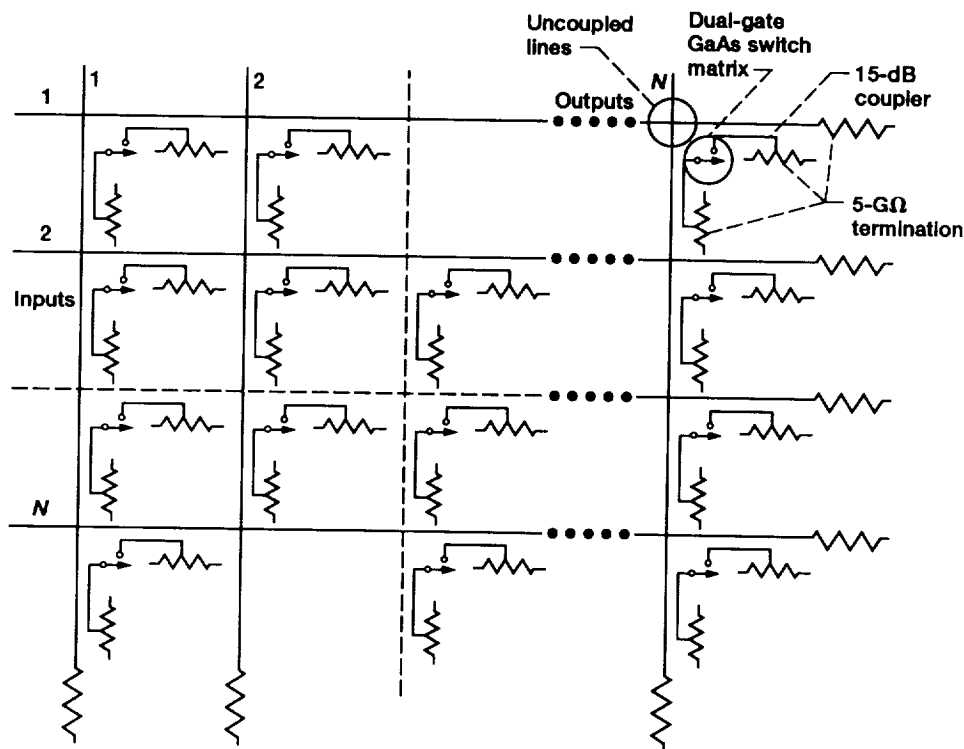


Figure 36.—GE coupled-crossbar architecture.

between the design approaches of the two contractors were the values of the coupling coefficients used in the coupled-crossbar designs and the packaging. For the GE switch the coupling coefficients were chosen to be 15 dB for all crosspoints; in the Ford switch the coupling coefficients were increased for crosspoints farther from the RF input to minimize the insertion loss variation between crosspoints.

The different packaging approaches are seen in figures 37 and 38. Figure 37(a) shows the distribution of crosspoints for the Ford switch. In the photograph of the Ford switch (fig. 37(b)) the arrangement of crosspoints in the top horizontal chassis can be seen. The GE switch crosspoint distribution (fig. 38(a)) contains five input columns, two of which are connected to all 20 outputs. In figure 38(b) several of these columns are visible. In both photographs the digital switch control units are visible as the vertical chassis at the rear of the RF switch chassis.

Block diagrams of the switch elements for the Ford and GE matrix switches are shown in figures 39(a) and 40 (a), respectively. Both contractors used a two-stage, dual-gate GaAs FET configuration with appropriate input, output, and interstage matching networks. Fast-switching bipolar transistors were used to drive the GaAs FET's. Photographs of the Ford and GE crosspoint modules are shown in the figures 39(b) and 40(b).

The greatest difficulty encountered by both contractors was the impedance matching problems occurring at the input and output of the switching elements. These mismatches resulted

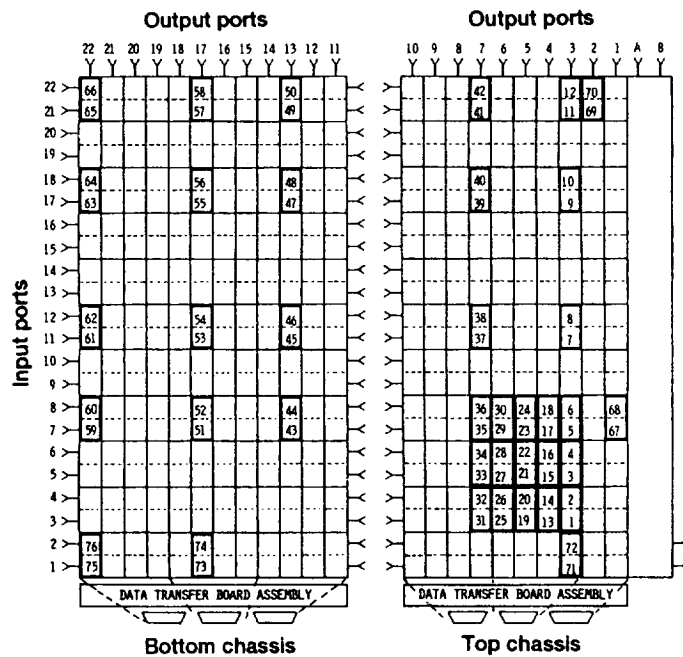
in large-amplitude ripple (versus frequency). GE's approach to this problem was to narrow the switch-operating bandwidth from the design goal of 2.5 GHz to the contract minimum of 1 GHz in order to improve the performance of the matching networks. In the Ford design the line lengths between the switching elements were varied to tune out the amplitude ripple while maintaining the 2.5-GHz bandwidth.

4.5.2 Matrix Switch CW Performance

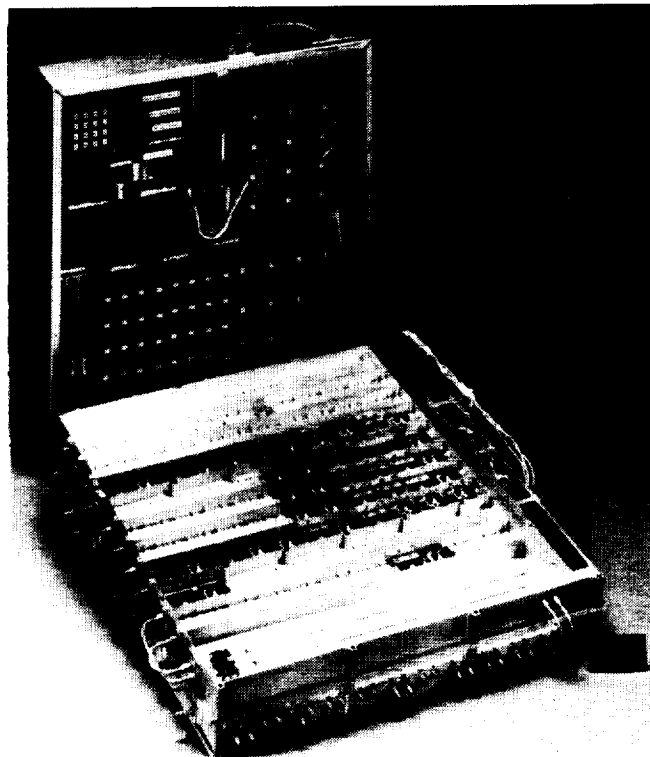
Both matrix switches were tested extensively at NASA Lewis. Among the more important parameters tested were bandwidth, insertion loss, bandpass amplitude ripple, input and output VSWR, isolation, and switching speed. These tests were conducted on all active crosspoints for both matrix switches; the results are summarized in table 25.

One of the critical performance parameters of a matrix switch is the isolation between input and output ports when the crosspoint is open. Poor isolation will degrade the system performance by introducing crosstalk interference between unconnected channels. Both POC model switches achieved isolation of over 50 dB.

The switching speed as measured at NASA Lewis determined the time required for an input RF signal to be switched from one port to another. This parameter determines the maximum reconfiguration rate of the matrix switch and thus drives many of the time-division multiple access (TDMA) operating parameters of a system employing this type of



(a)



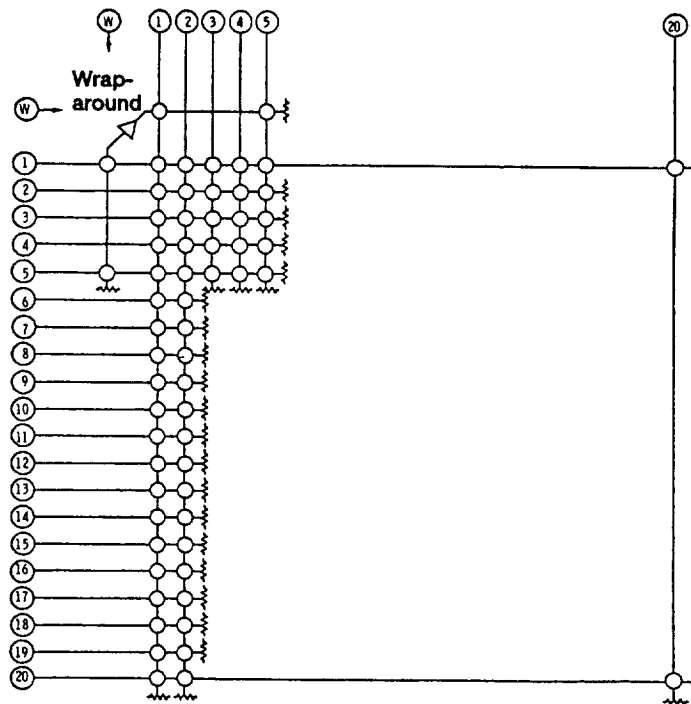
(b)

C-83-4607

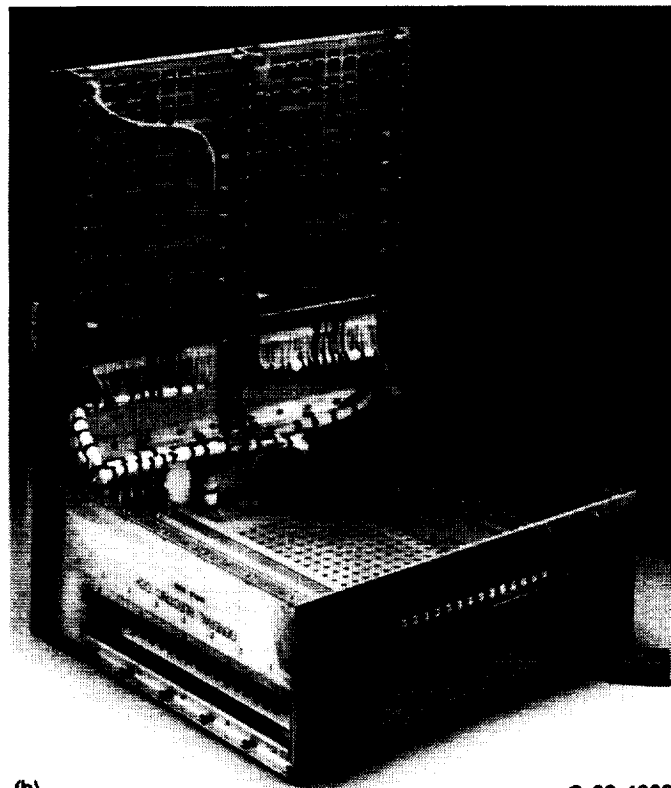
(a) Crosspoint distribution.

(b) Hardware.

Figure 37.—Ford POC matrix switch.



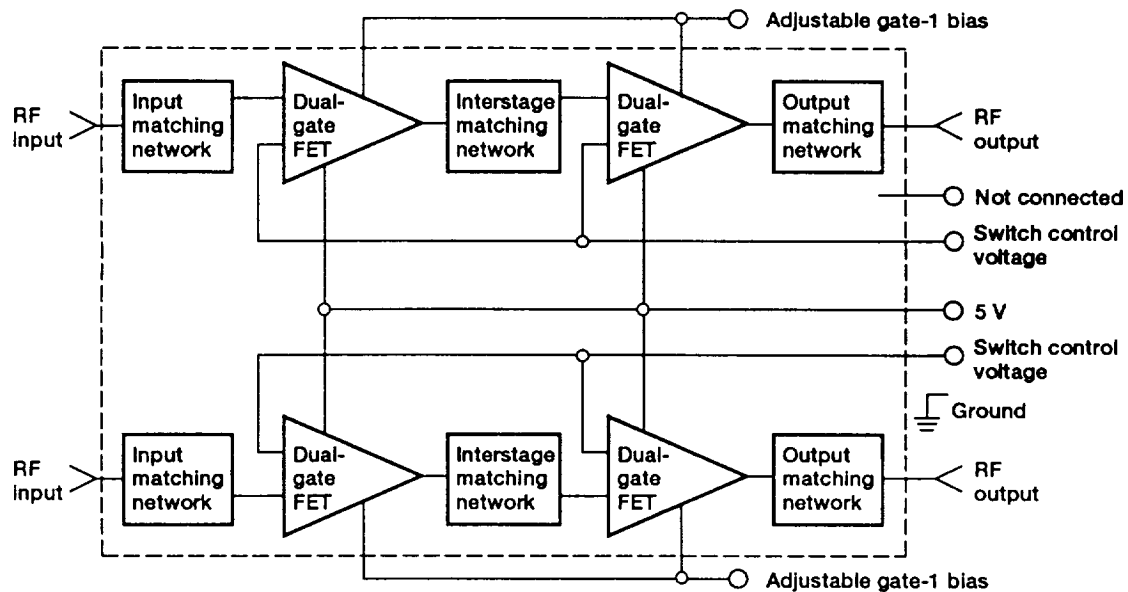
(a)



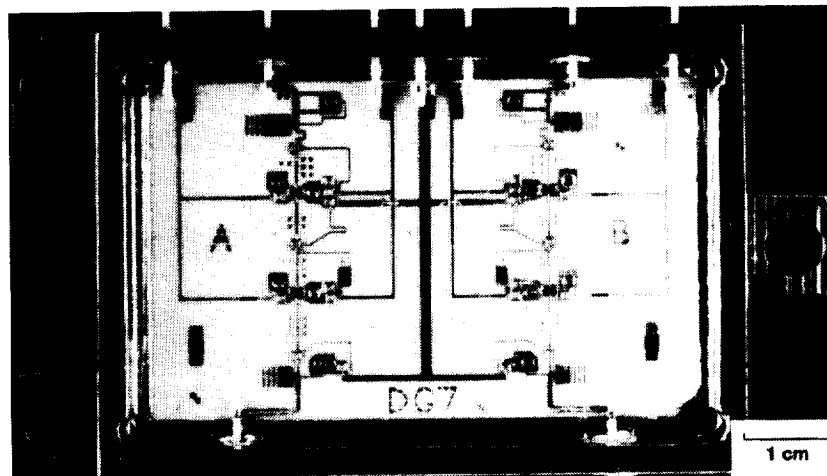
(b)

C-83-4606

(a) Crosspoint distribution.
(b) Hardware.
Figure 38.—GE POC matrix switch.



(a)



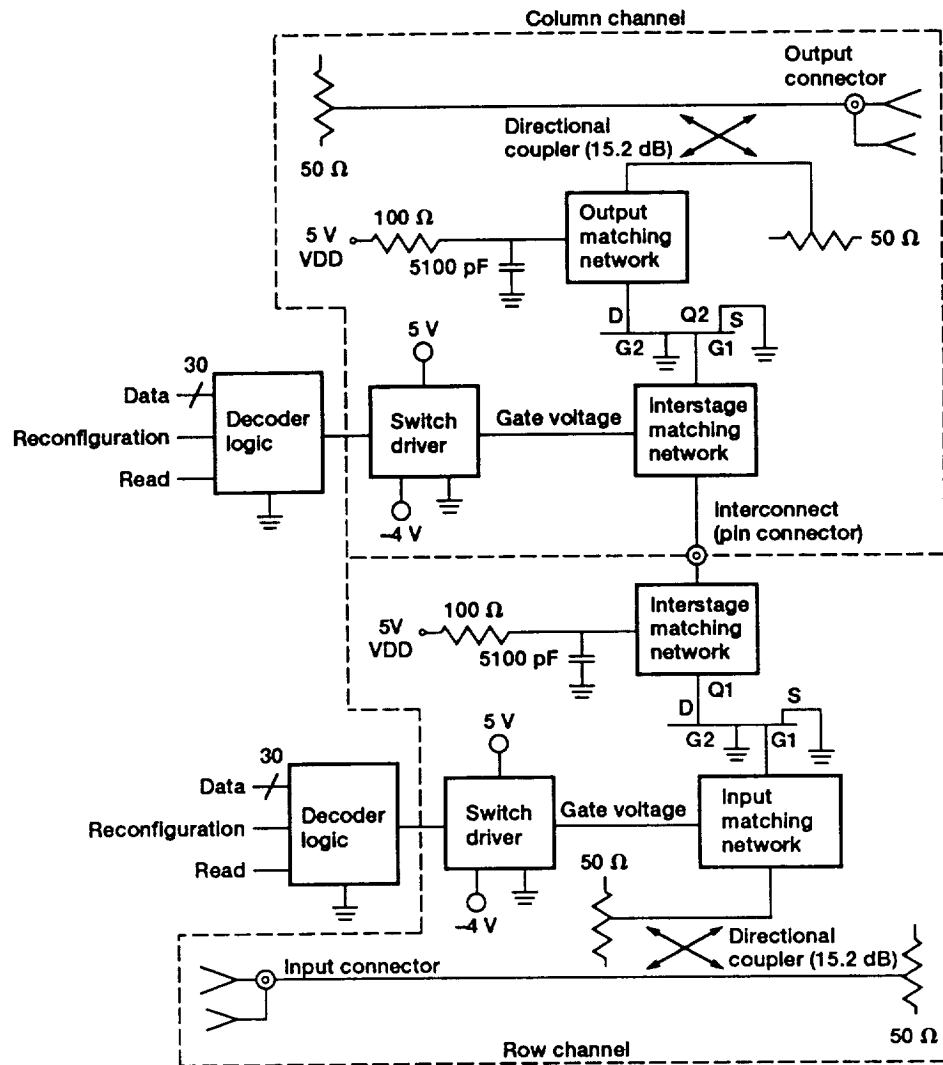
(b)

(a) Block diagram.

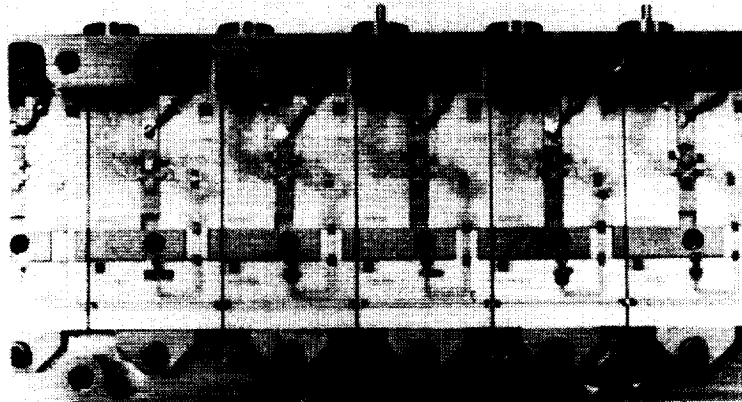
(b) Crosspoint pair.

Figure 39.—Ford crosspoint design.

ORIGINAL PAGE
BLACK AND WHITE PHOTOGRAPH



(a)



(b)

(a) Block diagram.
(b) Crosspoint module.

Figure 40.—GE crosspoint design.

TABLE 25.—SUMMARY OF CW PERFORMANCE FOR FORD AND GE POC MATRIX SWITCHES

Parameter	Contract goals	Ford		GE	
		Mean	Standard deviation	Mean	Standard deviation
3-dB bandwidth, GHz	2.5 (1.0 min.)	2.7	0.35	1.28	0.21
Insertion loss, dB	15 (18 max.)	20.7	7.62	18.0	4.06
Bandpass ripple, dB	1.0	5.6	1.4	2.23	1.45
Input VSWR	1.2:1 (1.5 max.)	1.82:1	0.30:1	1.30:1	0.09:1
Output VSWR	1.2:1	1.70:1	0.26:1	1.40:1	0.12:1
Isolation, dB	40	54.0	5.7	58.0	5.7
Switching speed, ns	10	15.6	10.9	32.2	3.6
Number of active crosspoints		65		57	
Design center frequency, GHz		4.75		6.5	

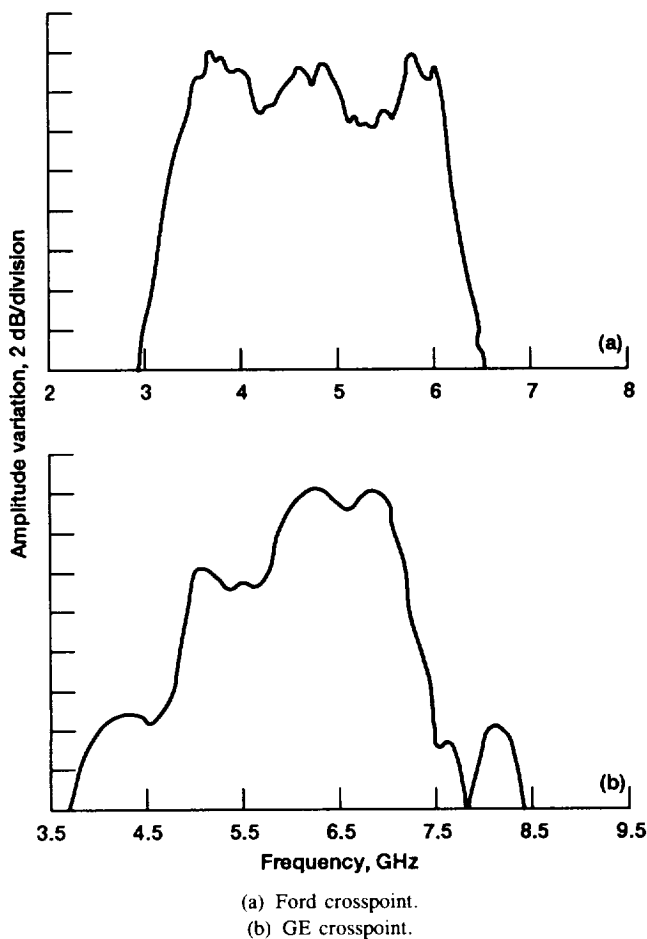


Figure 41.—Typical frequency response.

device. Good performance was achieved by both switches, with a 15.6-ns average speed for the Ford switch and a 32.2-ns average for the GE switch.

The frequency response has proved to be a major contributor to the degradation of the signals transmitted through the phase I simulator system, as well as through its components. As was

discussed previously, impedance-matching problems contributed to significant amplitude ripple for both matrix switches. In-band ripple for the GE switch averaged less than half that for the Ford switch but at the expense of reduce bandwidth. Table 25 shows the mean in-band ripples measured at NASA Lewis as 5.6 dB for the Ford switch and 2.23 dB for the GE matrix switch. Frequency response plots for the typical Ford and GE crosspoints are shown in figure 41. The general shape of the GE switch response varied much less than that of the Ford switch response.

4.5.3 BER Test Results

The matrix switch was tested in a static mode (no dynamic switching during the BER measurement) by using one system simulator ground terminal. For the Ford switch 17 crosspoints were tested with the HPA in saturation and at 1-dB compression, and 5 crosspoints were tested in the linear region. Twelve GE switch crosspoints were tested at each of the HPA operating points.

Matrix switch performance can be evaluated by transmitting signals through the system first with the component in place and then with the component bypassed. Alternatively, component performance can be compared by direct substitution into the system. With the availability of two different matrix switch models, both methods of evaluation can be used. The amount of degradation introduced into the end-to-end system can be determined by using the bypass method. In the case of the matrix switches an equivalent amount of attenuation (about 20 dB) was added in place of the switches to maintain consistent power levels throughout the system and provide a valid comparison. In making a direct comparison of the performance of the two switches, one difference must be considered. As was shown in table 25, the switches were designed to operate in two frequency bands. The phase I system simulator operates over a satellite band of 3.7 to 6.2 GHz. The Ford switch has a design frequency band of 3.5 to 6.0 GHz, which nearly matches the entire satellite

simulator system operating band. This allowed testing in three different frequency bands, one at the lower end of the band (centered at 4.25 GHz), one at the center of the band (centered at 5.0 GHz), and one at the upper end of the band (centered at 5.725 GHz). These three bands have been designated as bands A, B, and C, respectively. Because of the presence of the other POC development components in the system, the overall frequency response without the matrix switch is far from ideal. The selection of these three test bands provides varying transmission characteristics against which the matrix switch test results can be viewed. In general, band B, which was near the band center of all of the major system components, exhibited the best overall transmission characteristics (in particular in having the flattest frequency response). The other two bands exhibited varying degrees of degraded transmission characteristics.

The GE switch matrix operates over a band of approximately 6 to 7 GHz, centered at 6.025 GHz. This offers only a narrow frequency band overlapping the upper end of the simulator system bandwidth and the lower end of the GE switch bandwidth in which the testing can take place. Because the bandwidth of the GE switch varies somewhat from crosspoint to crosspoint, the 12 crosspoints with the most frequency overlap were selected for these tests. The GE test band does not coincide with any of the Ford test bands.

BER measurement results for the GE matrix switch and for each of the three Ford switch test bands are summarized in table 26. The data clearly demonstrate the contribution of both switches to system amplitude ripple and data transmission quality degradation. By comparing the mean amplitude ripple with the measurements made with the matrix switch bypassed, the mean contribution of the matrix switches to the overall amplitude ripple of the system simulator can be seen for each frequency band and HPA operating point. The degradation of data transmission quality through the switch can be similarly determined.

For both switch matrices, operation of the HPA in saturation provided a hard-limiting effect that flattened the overall frequency response. The amplitude ripple increased as the HPA was backed off to the 1-dB-compression point and increased further in the linear region. Figure 42 gives a good example of this effect for one Ford crosspoint in frequency band C. The BER generally degraded as the amplitude ripple increased. Example of measured BER curves showing the degradation that occurred as the HPA was backed off are shown in figure 43 for both switches. For the Ford switch the results of the linear HPA tests deviated somewhat from those results, possibly because of the smaller number of crosspoints tested. Overall, operating the HPA in saturation significantly reduced the data degradation attributable to the matrix switches themselves.

In comparing the performance of the Ford and GE matrix switches, several points can be alluded to. When the HPA operated in saturation, the average E_b/N_0 required to maintain a BER of 10^{-6} was about the same. The

performance of the system deteriorated much more rapidly with the GE switch than with the Ford switch as the HPA was backed off. This was primarily due to the placement of the GE test band near the system component band edges as described earlier. Evidence of this is the increase of the amplitude ripple of the GE switch relative to the Ford switch as the HPA was backed off. The contribution to the system amplitude ripple, however, was considerably smaller for the GE switch, as would be expected considering its flatter frequency response. The clearest result to be seen from these data is the performance variation from crosspoint to crosspoint. The standard deviation of the E_b/N_0 data and the amplitude ripple data shows that the GE switch outperformed the Ford switch because of its much flatter frequency response. The range of highest-to-lowest E_b/N_0 underscores this point, as shown in the BER curves of figure 44. Even with the HPA at saturation the range and standard deviation were several times higher for the Ford switch than for the GE switch. These results indicate the relative importance of frequency response in the design of future switch matrix subsystems.

4.5.4 Concluding Remarks—Matrix Switch Tests

The Ford and GE matrix switches were fully evaluated in the phase I testing. The data presented indicate that, although the matrix switch may meet many desirable specifications, such as isolation and switching speed, the forward transmission characteristics of the switch had a significant effect on the data transmission quality. In particular, the frequency response in terms of amplitude ripple and variation from crosspoint to crosspoint had a measurable effect on the quality of the SMSK-modulated signals transmitted through the phase I system.

The presence of a hard limiter after the matrix switch was shown to reduce the degrading effects of amplitude ripple. Recall though that hard limiting may introduce intermodulation distortion when several channels are simultaneously present. The Ford and GE matrix switches demonstrated the bandwidth-versus-amplitude-ripple tradeoff that occurs in the switch design. The BER data presented show how that tradeoff affected system performance. In particular, the BER performance varied greatly from crosspoint to crosspoint as the amplitude ripple became severe. The data from the GE switch indicated that for amplitude ripple averaging 2.2 dB, the E_b/N_0 required to maintain a BER of 10^{-6} varied about ± 0.6 dB even with no limiting. This indicates that 2-dB amplitude ripple within the passband might be a reasonable goal for future switch matrix designs.

NASA Lewis continues to develop technology in the matrix switch area for future NASA projects and commercial applications. Monolithic microwave integrated circuit (MMIC) approaches are now making a strong impact in the switching market. Reliability, lower cost, and size and power savings are some of the benefits to be gained by this approach. Predictions are that onboard switching may require a matrix switch with 100 inputs and 100 outputs. These large matrix

TABLE 26.—SUMMARY OF BER RESULTS FOR FORD AND GE POC MATRIX SWITCHES
(a) Ford

Frequency band	HPA operating point	Number of crosspoints tested	E_b/N_0 required for BER of 10^{-6}				Amplitude ripple for system (330-MHz bandwidth)	
			Mean	Standard deviation	High	Low	Mean	Standard deviation
A	Saturation	17	12.76	0.77	15.19	11.89	3.53	0.56
	Saturation (a)		11.41	----	-----	-----	1.26	----
	1-dB compression	17	13.83	1.30	15.95	11.91	2.67	.64
	1-dB compression (a)		11.75	----	-----	-----	1.70	----
	Linear	5	13.38	1.38	15.90	12.06	5.34	.59
	Linear (a)		12.13	----	-----	-----	2.34	----
B	Saturation	17	11.94	0.47	13.03	11.43	1.74	0.36
	Saturation (a)		11.33	----	-----	-----	1.30	----
	1-dB compression	17	12.11	.23	12.56	11.65	2.11	.53
	1-dB compression (a)		11.20	----	-----	-----	1.48	----
	Linear	5	12.45	.22	12.78	12.24	3.26	.96
	Linear (a)		11.40	----	-----	-----	1.72	----
C	Saturation	17	12.41	0.85	15.41	11.78	3.42	1.35
	Saturation (a)		11.67	----	-----	-----	2.02	----
	1-dB compression	17	14.31	1.00	17.25	13.00	7.01	1.48
	1-dB compression (a)		12.25	----	-----	-----	4.50	----
	Linear	5	12.60	.97	14.40	11.70	8.41	.80
	Linear (a)		13.04	----	-----	-----	5.32	----
A,B,C	Saturation	51	12.36	0.79	15.41	11.43	2.90	1.20
	Saturation (a)		11.47	----	-----	-----	1.53	----
	1-dB compression	51	13.42	1.35	17.25	11.65	3.93	2.40
	1-dB compression (a)		11.73	----	-----	-----	2.56	----
	Linear	15	12.81	1.06	15.90	11.70	5.67	2.26
	Linear (a)		12.19	----	-----	-----	3.29	----

(b) GE

HPA operating point	Number of crosspoints tested	E_b/N_0 required for BER of 10^{-6}				Amplitude ripple for system (330-MHz bandwidth)	
		Mean	Standard deviation	High	Low	Mean	Standard deviation
Saturation	12	12.33	0.10	12.50	12.13	2.91	0.09
Saturation (a)		11.74	----	-----	-----	3.02	----
1-dB compression	12	14.67	.33	14.97	13.81	6.32	.39
1-dB compression (a)		13.20	----	-----	-----	5.70	----
Linear	12	15.25	.36	15.87	14.63	7.46	.52
Linear (a)		13.29	----	-----	-----	6.66	----

^aBypassed.

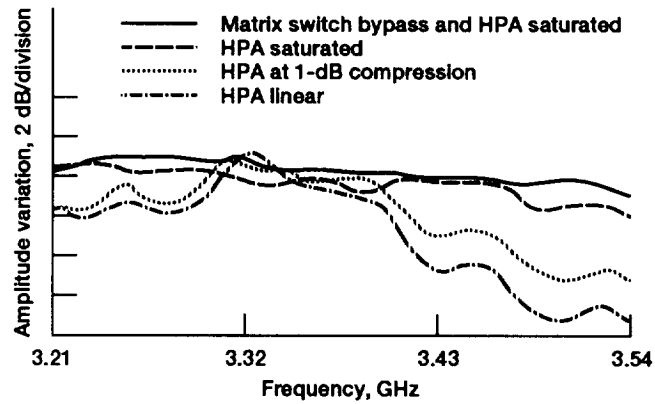
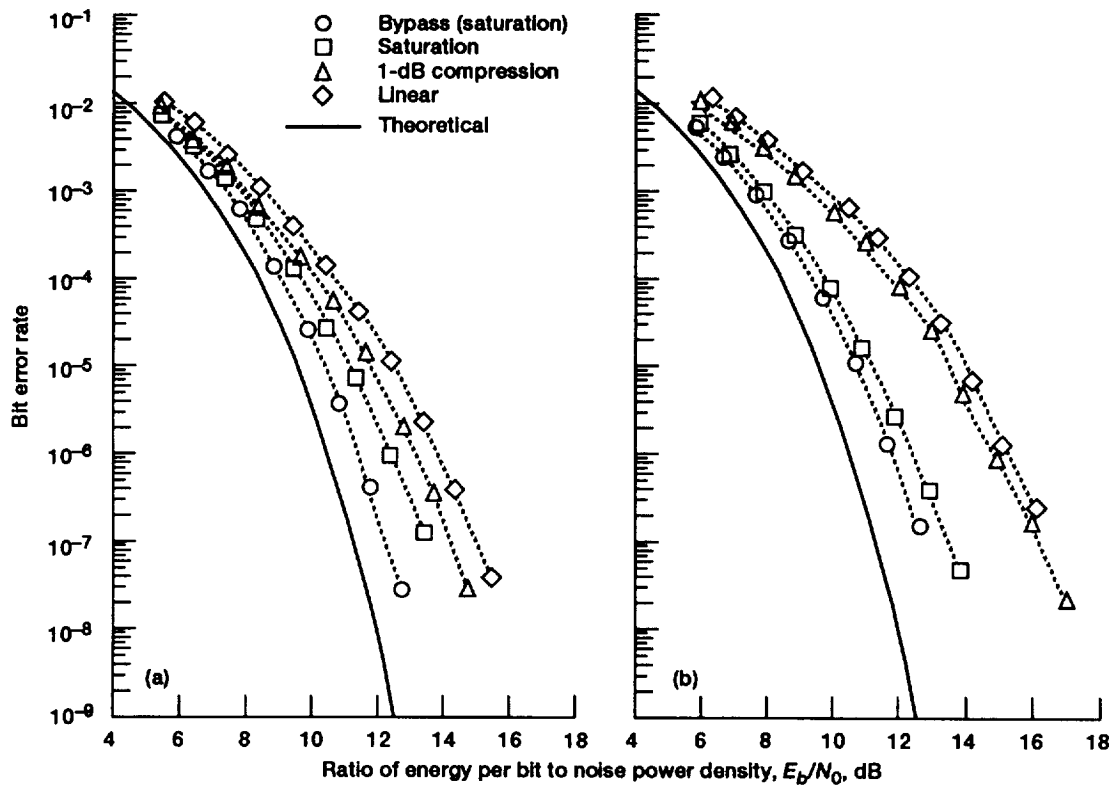


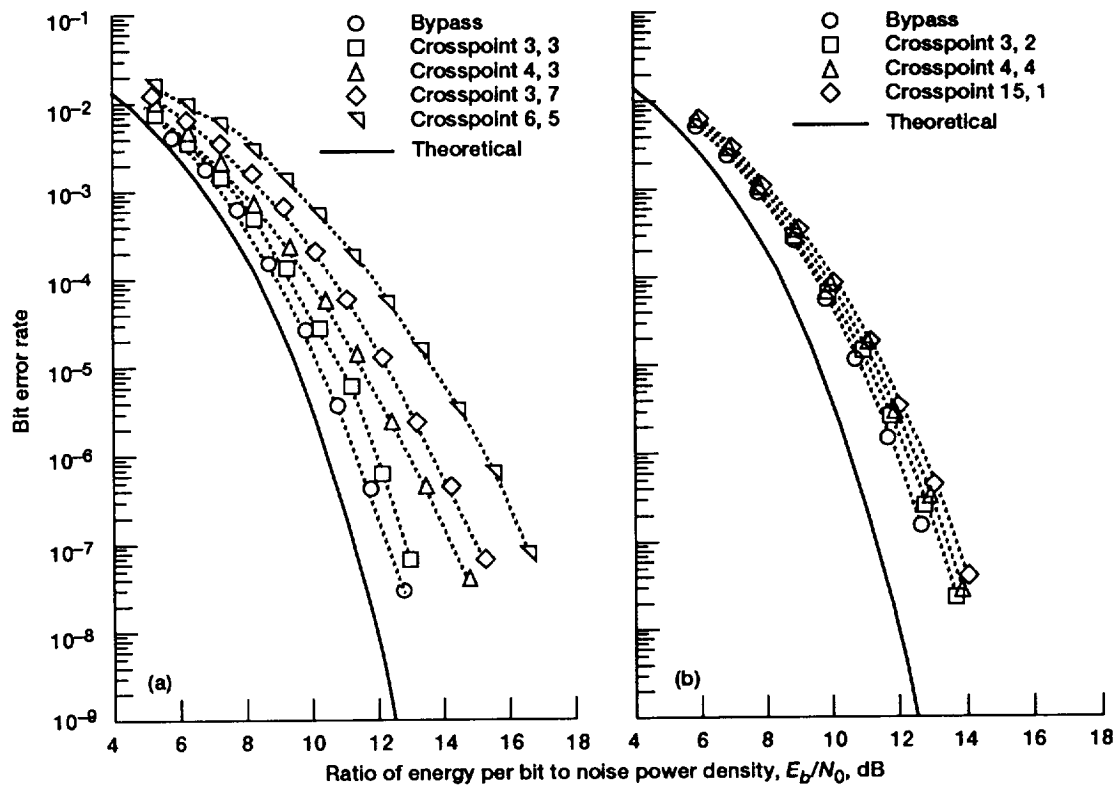
Figure 42.—System frequency response with Ford POC matrix switch (crosspoint 6,5) in test band C. Reference, -29.0 dBm.



(a) Ford crosspoint 7,6 (band A).

(b) GE crosspoint 5,2.

Figure 43.—Measured BER for two crosspoints at all HPA operating points.



(a) Several Ford crosspoints (band A).
(b) Several GE crosspoints.

Figure 44.—Measured BER for several crosspoints with HPA at saturation.

switch designs will need to focus not only on the stringent switching-speed and low-power-consumption requirements, but also on maintaining flat transmission response from crosspoint to crosspoint.

4.6 Amplitude Equalization Tests

For a digital communications link an amplitude response that is constant with frequency represents the ideal, distortionless case (ref. 14). For a satellite communications link the amplitude response is often distorted by atmospheric and propagation effects, such as scintillation, rain attenuation, and multipath fading. The cumulative effects of less-than-ideal responses of satellite transponder and Earth terminal hardware and antennas contribute additional distortion to the system's amplitude response. As shown in section 4.1 the system's amplitude response is among the most important RF parameters in terms of its effect on BER.

As part of the phase I testing, experiments were performed to quantify the effects of amplitude distortion on the BER of a satellite communications system. The SITE satellite

communications system simulator was used to simulate system amplitude distortion and the effectiveness of fixed IF amplitude equalization in improving degraded links. In one set of experiments a tunable IF equalizer was used to simulate some types of amplitude distortion found in real systems. The resulting BER degradations caused by the simulated distortions were measured. In a second set of experiments the equalizer was used to improve the amplitude response of several degraded channels of the system simulator, and the resulting BER improvement was measured.

The following sections describe the experiments performed and results obtained.

4.6.1 Amplitude Distortions in Satellite Communications Systems

The two major sources of amplitude distortion in satellite communications systems are propagation effects and hardware imperfections. The simulation of these distortions was based upon the characteristics of real systems to the extent possible given the limitations of the test hardware. Propagation effects were simulated by amplitude distortion induced by the tunable IF equalizer. The hardware imperfections were simulated both by equalizer-induced amplitude distortion and by real imperfect hardware in the SITE simulation system.

4.6.1.1 Satellite Link Propagation Effects

The propagation characteristics of the transmission path are important when considering the design and operation of a satellite communications system. Many factors have been cited as significant in space communications applications operating in the atmospheric windows up to 100 GHz. These include signal attenuation due to scattering or absorption, depolarization, scintillation or atmospheric multipath fading, and angle of arrival fluctuations (ref. 15). Multipath fading has been shown to cause distortions on terrestrial digital links. This effect is frequency selective across the channel bandwidth under operation. Previous research using beacons in the 30/20-GHz range has indicated that multipath effects are insignificant for wideband satellite communications systems operating at frequencies above 10 GHz, except at low elevation angles ($< 15^\circ$, ref. 16). However, it remains of interest to determine if such frequency-selective distortions have any pronounced effect on a digitally modulated signal transmitted through a simulated satellite channel.

It has been shown that the amplitude characteristic during a wideband multipath fading period is basically a notch (minimum) at a selected frequency (ref. 17). This minimum in the signal power is also accompanied by a maximum or minimum in group delay distortion. Because we are primarily interested in the amplitude characteristics, the delay distortion is not discussed any further. The amplitude characteristics that represent the propagation fading effects are primarily the notch and slope distortions. The amplitude distortions simulated by the IF equalizers in the induced-distortion experiments represent those propagation effects.

4.6.1.2 Satellite Link Hardware Imperfections

A satellite communications link contains a cascade of numerous components including both passive devices, such as filters, multiplexers, and antennas, and active devices, such as receivers, up/down converters, and power amplifiers. The SITE system contains several major contributors to amplitude distortion: satellite receiver, matrix switch, satellite HPA, and Earth terminal up/downconverters. These major components were built under POC technology development programs. Thus, their amplitude responses are somewhat more degraded than would be expected in an operational system. Additional elements, including filters, couplers, and driver amplifiers, contribute smaller amounts of degradation.

The amplitude distortions that result from the various system components, when combined, yield a wide variety of system distortion shapes. However, these shapes are mainly a combination of three basic distortions: ripple, parabolic, and slope. The ripple distortions originate mostly from filter and matching network circuits and especially from mismatches between adjacent components. Parabolic distortion results from filters and other band-limiting components. Amplitude slope can be produced by any component and usually occurs when the component is being operated near its design band edge.

The induced-distortion experiments, in addition to simulating propagation effects, also simulated the three basic hardware-induced distortions just described. The IF equalization tests took advantage of the degraded amplitude responses resulting from the POC components in the SITE system. Thus, the general problem of hardware-induced amplitude distortion was investigated in the two experiments described next.

4.6.2 Induced-Distortion Tests

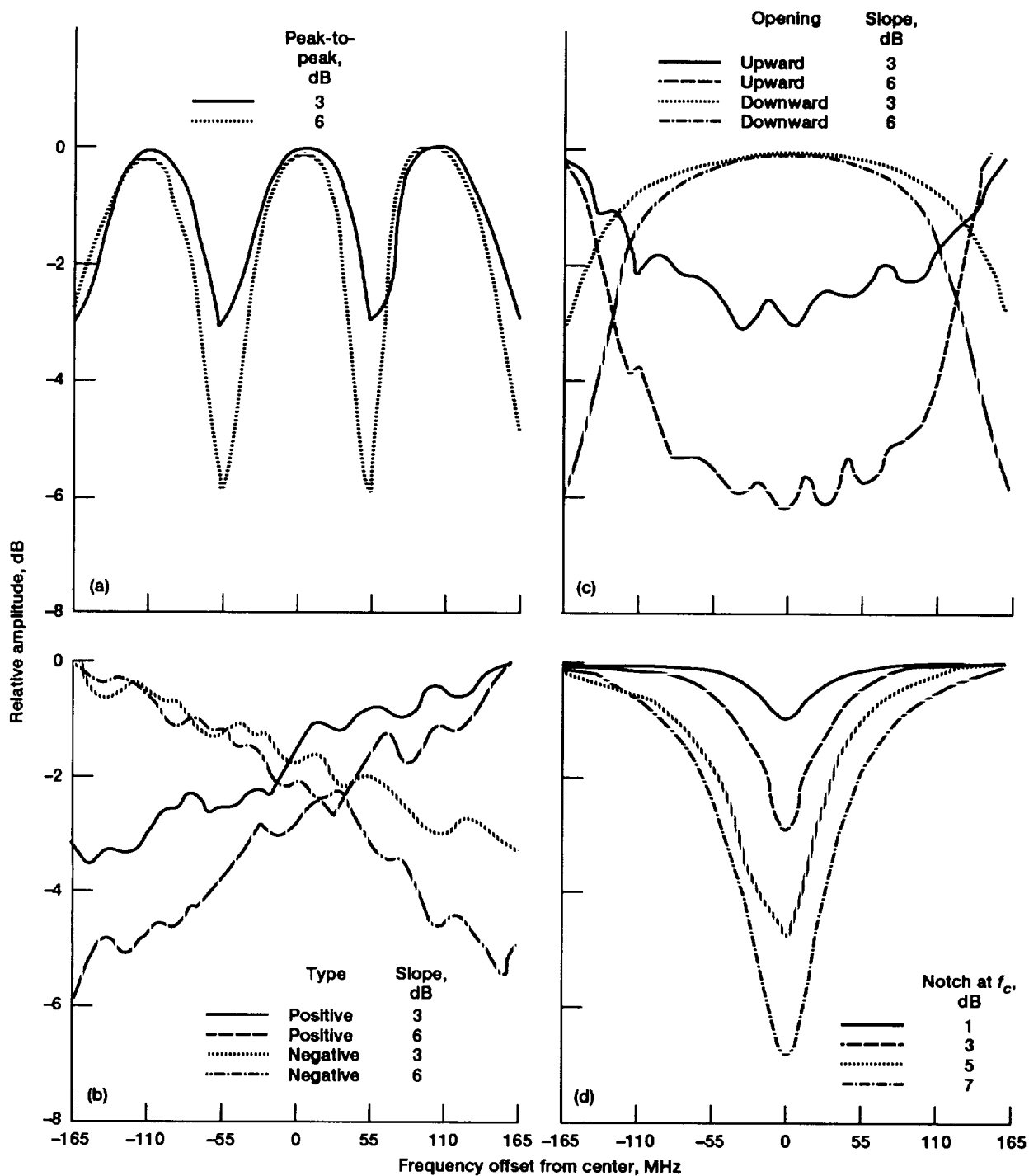
4.6.2.1 Test Description

The induced-distortion tests attempted to simulate some of the amplitude distortions resulting from propagation effects and hardware imperfections. A variety of amplitude distortions were deliberately induced by an adjustable IF equalizer to simulate a distorted satellite channel.

The IF equalizer used to simulate amplitude distortions is a 10-section mechanically tunable filter device built by Innowave, Inc. Each equalizer section is a resonator with two adjustments that allow both the center frequency and the attenuation of the resonator to be varied. A single resonator can be tuned to produce an amplitude notch at a desired frequency and depth, or the resonators can be used in combination to produce desired shapes across a passband of 3.2 to 3.55 GHz.

The equalizer was adjusted while viewing its amplitude response on a network analyzer. Examples of the resulting amplitude responses, as plotted from the network analyzer, are shown in figure 45. Four types of distortion were induced: ripple, slope, parabolic, and notch. The ripple distortions were obtained by adjusting several of the equalizer's resonators at equal intervals across the passband. For the three-ripple case (fig. 45(a)) four resonators were tuned to give three positive peaks (at f_0 and $f_0 \pm 110$ MHz) and four negative peaks (at $f_0 \pm 55$ MHz and $f_0 \pm 165$ MHz). Ripples with two, four, and five positive peaks were similarly obtained. Positive and negative slopes (fig. 45(b)) were obtained by tuning a combination of resonators across the band to give either a rising or falling slope. Parabolic distortions are shown in figure 45(c). The upward-opening parabola required a number of resonators tuned in combination; the downward-opening parabola required resonators placed at each end of the band. For all of these cases the amount of distortion, as measured by the difference between the highest and lowest in-band amplitudes, was varied as shown in table 27. The magnitude of each distortion was increased until the equalizer tunability limit was reached. In some cases adding additional distortion produced a negligible increase in BER degradation or caused a complete loss of demodulator lock (i.e., 50-percent BER), in which case no further increase in distortion was attempted.

The notch distortions were generally the easiest to obtain, because they usually required only one or two resonators to be tuned. An example of notch distortions is shown in figure 45(d). The first set of notch tests involved moving a 6-dB notch across the passband from 3.21 to 3.54 GHz. A second set of tests involved placing a notch of varying depth



- (a) Three ripple.
 (b) Positive and negative slope.
 (c) Parabolic.
 (d) Notch.

Figure 45.—Measured amplitude responses for induced distortions.

TABLE 27.—TEST RESULTS FOR INDUCED DISTORTION

Type of distortion	Magnitude of distortion dB	BER degradation at BER of 10^{-6} , dB	Type of distortion	Magnitude of distortion, dB	BER degradation at BER of 10^{-6} , dB
None	---	0.81	Notch (3.265 GHz)	6	1.02
Two ripple	3	2.24	Notch (3.298 GHz)	↓	1.97
	6	4.33	Notch (3.320 GHz)		3.02
Three ripple	1	1.21	Notch (3.353 GHz)		3.09
	2	1.64	Notch (3.375 GHz)		2.86
	3	2.13	Notch (3.408 GHz)		4.60
	4	3.28	Notch (3.430 GHz)		4.81
	5	6.15	Notch (3.463 GHz)		2.51
	6	8.11	Notch (3.485 GHz)		1.62
Four ripple	3	2.24	Notch (3.518 GHz)		1.18
			Notch (3.540 GHz)		.95
Five ripple	3	2.17	Notch (3.320 GHz)	1	0.89
				2	1.05
				3	1.64
				4	1.77
				5	2.33
				6	3.02
Positive slope	3	0.89	Notch (3.375 GHz)	7	3.55
	4	.90		8	5.25
	5	.86		12	9.71
	6	1.04	Notch (3.430 GHz)	1	1.11
	7	.93		2	1.48
	8	1.45		3	1.92
Negative slope	12	1.86		4	2.43
	15	3.14		5	2.10
				6	2.86
Upward parabola	3	1.25		7	3.88
	4	.93		8	5.29
	6	.88		10	5.19
Downward parabola	3	0.74	Notch (3.430 GHz)	1	1.53
	4	.82		2	1.86
	6	.88		3	2.69
	8	.92		4	3.18
Notch (3.210 GHz)	6	1.13		5	3.96
	6	1.00		6	4.81
Notch (3.243 GHz)	6	1.13		7	5.27
	6	1.00		8	6.76

at a fixed frequency. This was done at three frequencies: the band center ($f_0 = 3.375$ GHz) and $f_0 \pm (1/4)R$ (± 55 MHz) corresponding to 3.32 and 3.43 GHz, respectively, where R is the data rate above and below the center frequency of the modulated spectrum. An example of how the SMSK spectrum is distorted by a notch is shown in figure 46 for a 10-dB notch at the band center frequency.

After the desired distortion pattern had been obtained, the equalizer was connected to the test system as shown in figure 47 (flow path a), simulating an amplitude-distorted satellite channel. A BER curve was measured for each of 66 distortions. The results of these measurements are given in table 27 and are discussed here.

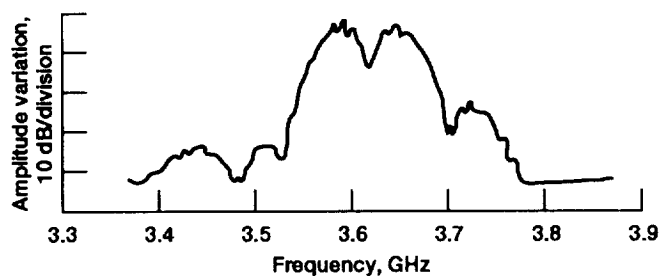


Figure 46.—Example of SMSK spectrum distorted by 10-dB notch at band center frequency. Reference, 0 dBm.

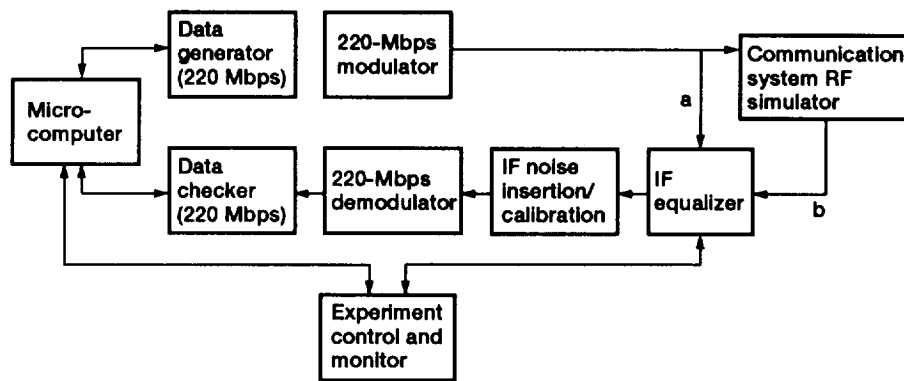


Figure 47.—Block diagram of BER measurement setup. With the simulator bypassed (flow path a), the equalizer induced an amplitude distortion. In equalization tests (flow path b) the IF equalizer is used to flatten the amplitude distortions caused by the RF simulator.

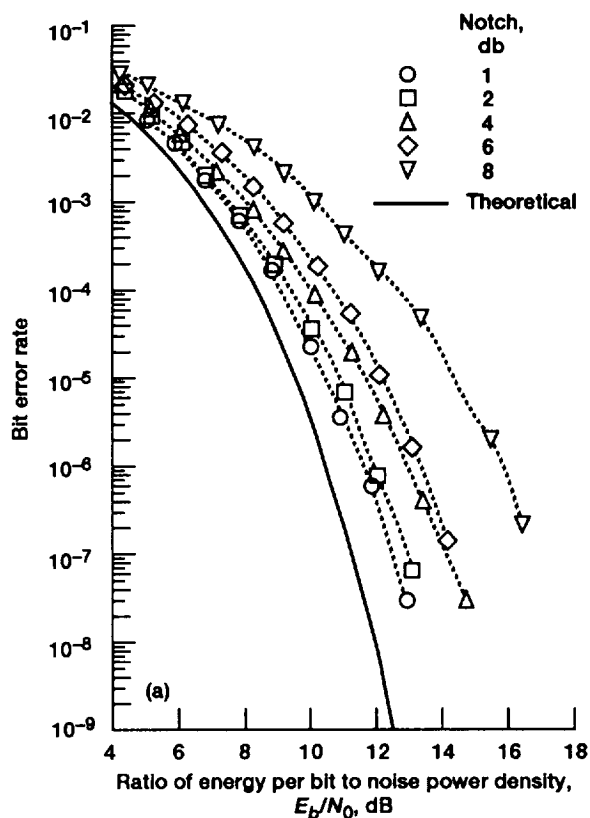


Figure 48.—BER curves for 6-dB notch at 3.375 GHz.

4.6.2.2 Results of Induced-Distortion Tests

The induced-distortion tests resulted in 66 measured BER-versus- E_b/N_0 curves. An example of these curves is shown in figure 48. In this example an amplitude notch of varying depth was induced at the center of the test band (3.375 GHz). The BER curves measured for each of several notch depths were plotted. Using a BER of 10^{-6} as a reference, the BER degradation measured for each of the 66 induced distortions

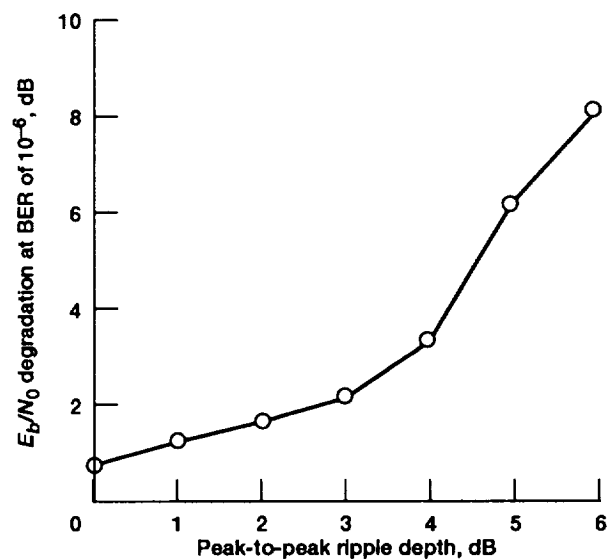


Figure 49.—BER degradation as a function of ripple depth for induced three-ripple amplitude distortion.

is listed in table 27. The first entry in the table represents the distortionless case, where the BER degradation of 0.81 dB resulted from modem implementation losses. The results for each type of induced distortion are discussed here.

Several variations of amplitude ripple were induced and are referred to by the number of positive amplitude peaks occurring in the band. Thus, the two-ripple case had two positive peaks, the three-ripple case had three positive peaks, etc. For the three-ripple case the amount of ripple was varied from 1 to 6 dB. The resulting BER degradation is plotted in figure 49 as a function of peak-to-peak ripple depth. Slight degradation occurred until the ripple depth reached 4 dB, at which time the BER degradation began to increase rapidly. For the two-, four-, and five-ripple cases, measurements made for a 3-dB ripple showed a degradation like that for the three-ripple case. A measurement made for the two-ripple case at 6-dB depth, however, showed significantly less degradation than that for

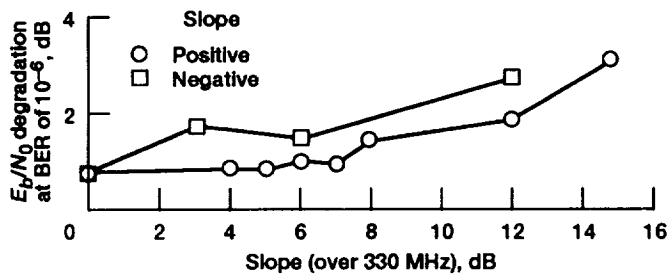


Figure 50.—BER degradation as a function of amplitude slope for induced positive and negative slope amplitude distortion.

the three-ripple case at 6 dB. We believe that this is due to the location of the negative-amplitude peaks at $f_0 \pm (1/4) R$ (± 55 MHz) from the center frequency. These two frequencies are significant for SMSK modulation. The carrier f_c is located at $f_0 - (1/4) R$ and there are no data transitions, corresponding to transmission of a sequence of consecutive 1's or 0's. Transmission of a 1-0-1-0... data sequence results in the instantaneous frequency $f_0 + (1/4) R$ (ref. 14). Thus, the three-ripple case affected both the carrier tracking and the phase transitions.

The BER degradation measured for amplitude slope is plotted in figure 50. Very little degradation due to either positive or negative slope was observed. For the positive slope virtually no additional degradation (relative to the distortionless case) occurred until an 8-dB slope was induced. Even for a 15-dB slope the additional degradation was only 2 dB. The degradation due to a negative slope was 0.5 to 0.9 dB greater than that for a positive slope but still relatively minor relative to other distortion types.

Parabolic distortions produced even less degradation than the amplitude slope distortions. Figure 51 shows that the BER degradation due to parabolic slope was practically negligible. This is a significant result because channel filtering in a system often degrades BER by a parabolic response that results in distortion at the band edges. For SMSK, very little signal power resides at the band edges, because nearly all the power is concentrated in the main spectral lobe. This most probably accounts for the negligible degradation caused by parabolic distortion. This result also is similar to results found for SMSK group delay distortion at the band edges in a previous study (ref. 4), where it was found that group delay distortions at the band edges do not affect the BER for an SMSK satellite channel.

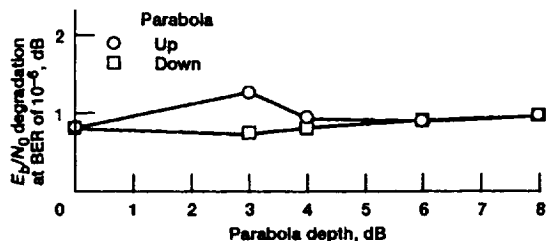


Figure 51.—BER degradation as a function of parabola depth for induced parabolic amplitude distortion.

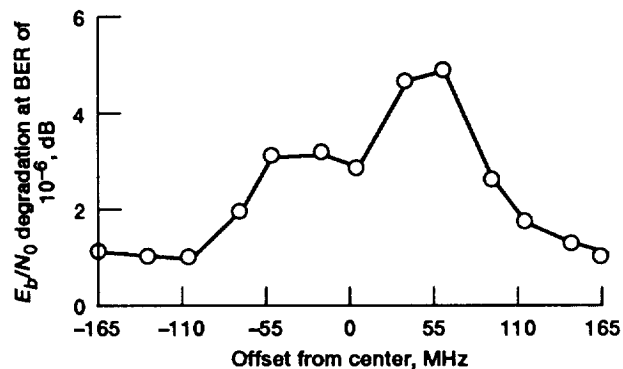


Figure 52.—BER degradation as function of frequency offset from center for 6-dB notch.

The most interesting results were produced by the induced amplitude notch distortions. In the first set of notch tests a 6-dB notch was induced at a number of frequencies across the band, from 3.21 to 3.54 GHz. The 330-MHz test bandwidth corresponds to the bandwidth of the main spectral lobe for 220-Mbps SMSK. Figure 52 shows the BER degradation resulting from a 6-dB notch as a function of frequency offset from f_0 . Degradation caused by notches near the band edges was negligible. As notches were moved toward the center of the band the degradation increased, peaking at approximately $f_0 \pm 55$ MHz, corresponding to the $\pm 1/4 R$ frequencies. The degradation for a 6-dB notch was about 3 dB at -55 MHz and 5 dB at 55 MHz, indicating that detection of the 1-0-1-0... phase transitions is particularly sensitive to this type of distortion. In contrast, the group delay distortions (ref. 20) produced much more BER degradation at -55 MHz.

In the second set of notch tests, notches of varying depth were induced at three frequencies of interest: 3.32, 3.375, and 3.43 GHz, corresponding to $f_0 - 55$ MHz, f_0 , and $f_0 + 55$ MHz, respectively. These results are plotted in figure 53. For the $f_0 - 55$ MHz and f_0 notches the additional BER degradation relative to the distortionless case was small, less than 1.5 dB, up to a notch depth of 5 dB. For deeper notches the degradation increased more rapidly, at a rate of 1 dB of degradation per decibel of notch depth. For the $f_0 + 55$ MHz notch the degradation was 1 to 2 dB greater than at the other two frequencies for corresponding notch depths. This again indicates the greater sensitivity to amplitude distortion at $f_0 + 55$ MHz.

In summary, the induced-amplitude-distortion experiments indicated that BER degradation is dependent on both the type of distortion and its location in frequency with respect to the modulated spectrum. The slope and parabolic distortions contributed negligible degradation. The ripple distortions, which represent the most common type of distortion attributable to system hardware, caused significant distortion when the peak-to-peak ripple became greater than 3 dB. Degradation was most severe when the negative ripple peaks occurred at $\pm (1/4) R$ from the center frequency. Notch distortion, which represents multipath propagation effects, create degradation

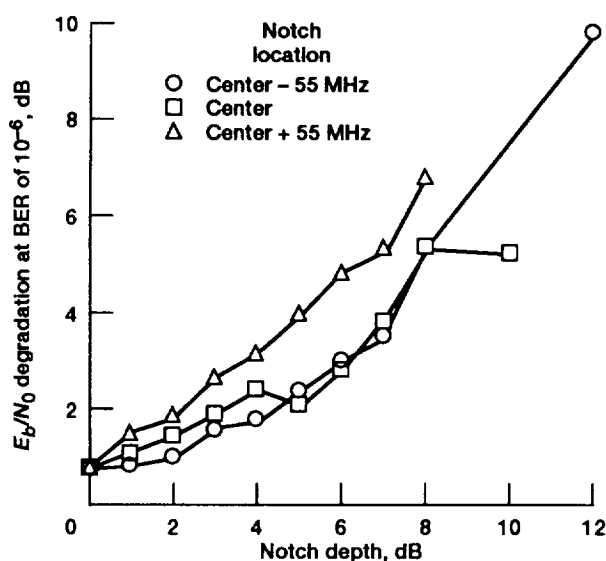


Figure 53.—BER degradation as function of notch depth for induced notch distortion.

that is also a function of relative frequency. Notches approaching the center of the spectrum create more degradation than those at the band edges. For the SMSK modulation notches at the frequency $f_0 + (1/4) R$ caused the greatest distortion per decibel of notch depth.

4.6.3 Link Equalization Tests

4.6.3.1 Test Description

The SITE communications system simulator provided the opportunity to test the effectiveness of fixed IF amplitude equalization in improving the BER performance of a satellite

channel. As applied to a real system this procedure assumes that there are constant-amplitude distortions resulting from system hardware which can be improved permanently by using a fixed-amplitude equalizer.

Channels suitable for equalization experiments were chosen from the baseline configurations. In selecting six channels for testing the frequency band used remained constant (band C). The TWT was operated in the low- and medium-power modes at the 1-dB-compression and linear operating points, and five matrix switch crosspoints were used.

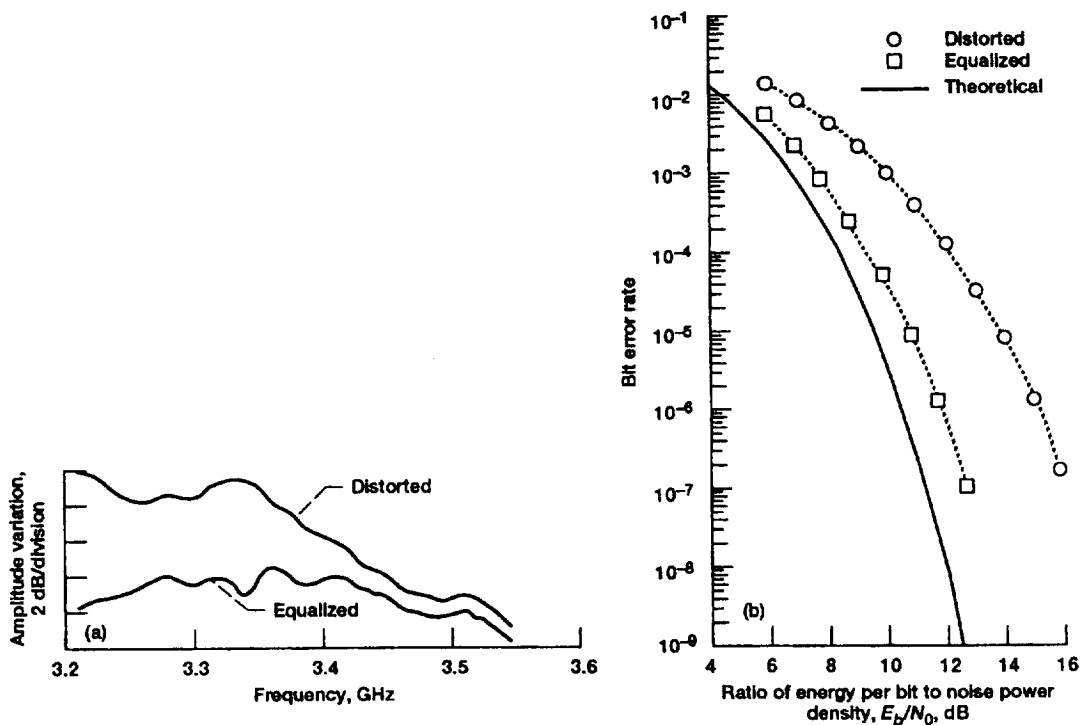
Seven equalization tests were performed using these six channel parameter combinations. In each case a swept CW amplitude measurement was made over the link from the Earth terminal transmitter IF to the Earth terminal receiver IF (or from the modulator output to the demodulator input). In this way the distorted amplitude response seen by the SMSK demodulator was measured. A BER measurement was performed on the unequalized link. The IF equalizer was adjusted to flatten the amplitude response of the distorted channel to the extent possible and inserted in front of the SMSK demodulator, as shown in figure 47 (flow path b). The swept CW and BER measurements were repeated on the equalized channel to complete the test. For one of the six channel parameter combinations, two equalization tests were performed: a partial equalization to observe incremental BER improvement, and then further equalization to obtain the best possible amplitude response and BER improvement.

4.6.3.2 Results of Link Equalization Tests

The results of the seven link equalization tests are summarized in table 28. Examples of plotted link equalization results are shown in figures 54 and 55. In figure 54(a) the

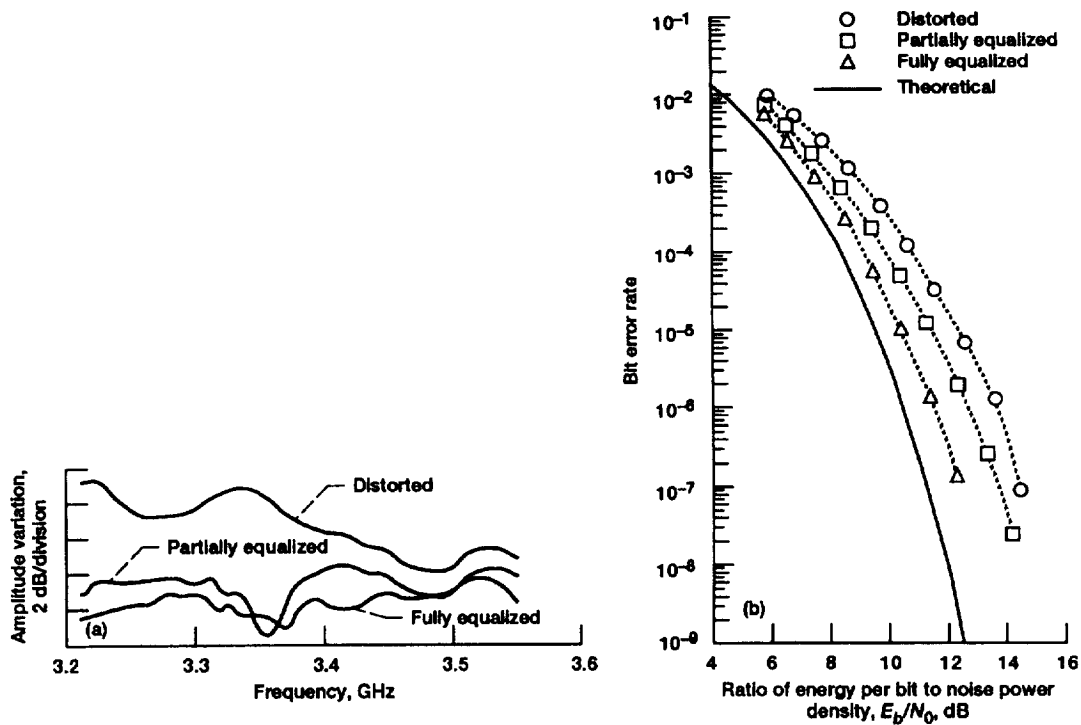
TABLE 28.—TEST RESULTS FOR LINK EQUALIZATION

Description of channel amplitude distortion	Channel configuration	Reference figure	Peak-to-peak amplitude distortion, dB		BER degradation of 10^{-6} , dB		BER improvement due to equalization, dB
			Before equalization	After equalization	Before equalization	After equalization	
5-dB linear drop (3.34 to 3.48 GHz)	Medium mode; linear crosspoint 3,3	55	5.0	1.7	2.9	1.0	1.9
2.7-dB linear rise (3.24 to 3.34 GHz)	Low-mode; linear crosspoint 4,3	53	8.0	4.0	4.7	1.3	3.4
8-dB linear drop (3.34 to 3.54 GHz); nearly flat (3.21 to 3.32 GHz)	Medium mode; 1-dB crosspoint 4,3	56	6.0	4.0	4.0	.9	3.1
6-dB linear drop (3.32 to 3.47 GHz); nearly flat (3.21 to 3.32 GHz)	Low mode; linear crosspoint 5,5	57	4.0	2.0	1.5	1.0	.5
3-dB ripple; peaks at 3.34 GHz and 3.42 GHz	Medium mode; 1-dB crosspoint 6,6	58	4.0	2.0	1.8	1.8	0
2- to 3-dB ripples; peaks at 3.34, 3.42, and 3.52	Low mode; linear crosspoint 6,3	54	5.0	3.5	3.3	2.2	1.1
5-dB linear drop (3.32 to 3.47 GHz); 2-dB valley (3.21 to 3.32 GHz)	Low mode; linear crosspoint 6,3	54	5.0	3.0	3.3	1.1	2.2



(a) Distorted and equalized amplitude responses.
(b) Distorted and equalized BER curves.

Figure 54.—Example of link equalization test results for TWT low mode, linear operating point, crosspoint 4,3, and reference, -28.0 dBm.



(a) Distorted, partially equalized, and fully equalized amplitude responses.
(b) Distorted, partially equalized, and fully equalized BER curves.

Figure 55.—Example of link equalization test results for TWT low mode, linear operating point, crosspoint 6,3, and reference, -28.0 dBm.

swept CW amplitude response before and after equalization is plotted for the channel configured with the transponder TWT operated linearly in the low-power mode and using matrix switch crosspoint 4,3. The equalizer significantly improved amplitude response. The BER performance, plotted in figure 54(b), shows 3.4 dB of improvement (at a BER of 10^{-6}) due to equalization. In figure 55(a), with the TWT operated linearly in the low-power mode and using matrix switch crosspoint 6,3, two levels of equalization were attempted. The first equalization attempt improved the original response but added a 3-dB notch at 3.35 GHz. In the final equalization the notch was essentially removed. The resulting BER curves (fig. 55(b)) show that the partial equalization resulted in a 1.1-dB improvement in BER performance (at a BER of 10^{-6}) and that the final equalization attempt yielded an additional 1.1 dB of improvement. The amplitude responses before and after equalization for the remaining four equalization tests are plotted in figure 56.

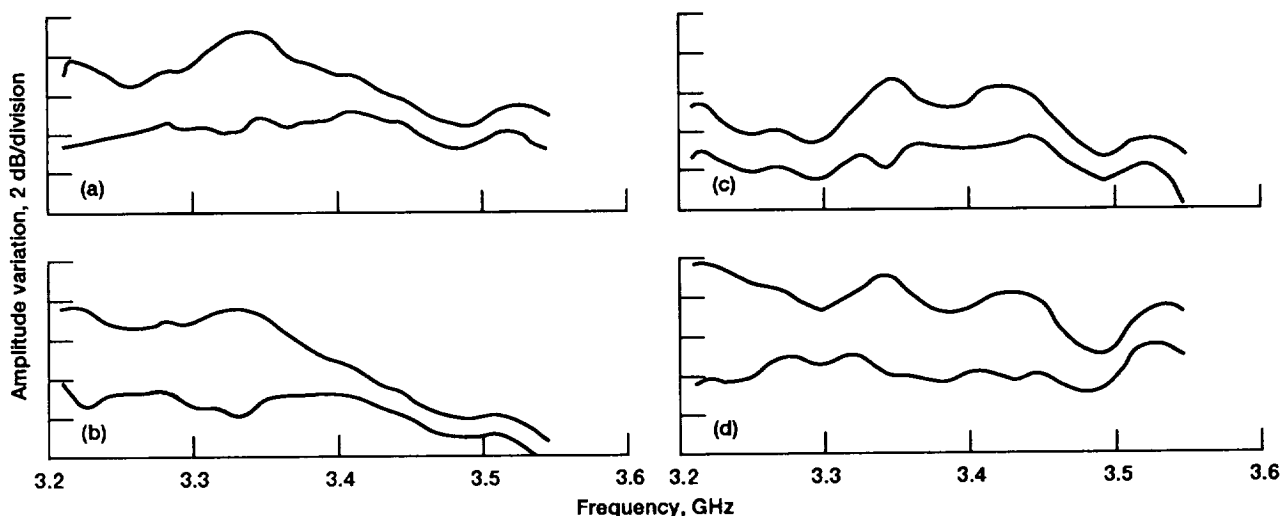
Improved BER performance was observed in six of the seven equalization tests. The improvement ranged from 0.5 to 3.4 dB and was proportional to the amount of distortion in the unequalized channel. In the one test in which no improvement was obtained, the equalization applied resulted in only a modest improvement in amplitude response, reducing the depth of a three-ripple response by about 1 dB. The induced-distortion tests for the three-ripple case predicted only a modest improvement in BER for this case. The measured results showed an identical BER performance before and after equalization.

4.6.4 Concluding Remarks—Amplitude Equalization Tests

The results of the induced-distortion tests indicate that the BER degradations resulting from amplitude distortions are related to the type of distortion and its location in frequency relative to the modulated spectrum. Distortions occurring at the band edges were negligible, as were pure slope and parabolic distortions. Distortions occurring toward the center of the modulated spectrum caused degradation that was proportional to the magnitude of the amplitude distortion.

Of particular importance was the result that notch distortions significantly affected the BER when they occurred at frequencies corresponding to $f_0 \pm (1/4) R$. For SMSK modulation these two frequencies correspond to the instantaneous frequencies occurring during alternating bit sequences (1-0-1-0. . . at $f_0 + (1/4) R$) or consecutive bit sequences (0-0-0. . . or 1-1-1. . . at $f_0 - (1/4) R$). For other modulation schemes the sensitivity to notch distortions will depend on the structure of the modulated spectrum, particularly the instantaneous frequencies occurring during the transition of bits or groups of bits.

Multipath propagation effects generally manifested themselves in frequency-selective notches, such as those simulated in the induced-distortion tests. The tests results show that, depending on the frequency of the notch relative to the modulated spectrum, notches greater than 6 dB in depth can cause severe BER degradation. Each 1-dB increase in notch depth above 6 dB caused approximately 1 dB of additional BER degradation.



(a) Medium mode; linear operating point; crosspoint 3,3; reference, -32.0 dBm.
 (b) Medium mode; 1-dB-compression operating point; crosspoint 4,3; reference, -30.0 dBm.
 (c) Low mode; linear operating point; crosspoint 5,5; reference, -30.0 dBm.
 (d) Medium mode; 1-dB-compression operating point; crosspoint 6,6; reference, -32.0 dBm.

Figure 56.—Link equalization test results for distorted and equalized amplitude responses of Hughes TWT.

The hardware portion of a satellite link will contribute amplitude distortion to the channel. The induced-distortion tests and the link equalization tests have shown that some amount of amplitude distortion is tolerable without seriously degrading the BER. Ripples up to 2 dB in depth contribute no more than 1 dB of BER degradation. For SMSK modulation, distortions occurring near the band edges can be ignored.

The link equalization tests demonstrated that significant improvement in BER can be obtained in degraded channels through equalization. For fixed-amplitude distortions resulting from hardware imperfections, a fixed equalizer placed in the Earth terminal IF path or in the satellite transponder itself can restore the BER performance to a level approaching the undistorted case. For time-varying distortions due to atmospheric effects, adaptive equalization could be employed to obtain similar BER improvement.

5.0 Conclusions

All of the stated objectives of the SITE phase I testing have been successfully achieved. Many radiofrequency distortions in a component or system can affect the bit error rate to some extent. The data that are presented in this report encompass a variety of testing procedures relative to the Ka-band satellite communications system simulator developed at the NASA Lewis Research Center. However, many of the results presented herein can be useful and valuable to those involved in similar applications and research areas. Where pertinent conclusions could be reached from the test results, we have attempted to do so. In areas where no clear conclusion could be made, the data have simply been presented for reference purposes.

The SITE Project is presently into phase II testing. The primary objective of phase II is the development of a two-channel transponder, complete with network control, rain fade and power augmentation, range delay simulation, and dynamic satellite switching capability. Continuous data transmission, which was the basis of phase I, and burst data transmission of SMSK-modulated signals will also be compared. The results obtained from phase II should help resolve more key questions surrounding these various aspects of satellite communications research.

Acknowledgments

The successful first phase of the SITE Project was the result of a coordinated effort involving approximately 25 persons over the course of several years. The authors gratefully acknowledge these engineers and technicians for their contributions: James W. Bagwell, Regis F. Leonard, Joseph L. Harrold, and Godfrey Anzic for providing project management and initial system level design; Martin J. Conroy, Dale E. Pope, and Alan L. Saunders for design of the RF subsystems; James M. Budinger, Monty Andro, William D. Ivancic, Mary Jo Shalkhauser, and Lawrence A. Nagy for design of the digital

subsystems; Ihor Kramarchuk, Edward J. Petrik, and Elaine S. Daugherty for design and development of the experiment control and monitor systems; Donald P. Ohlemacher and Robert M. Brej for hardware buildup and integration and collection of test data; James S. Svoboda for collection of test data; Norman S. Melnyk, Gerald P. Buchar, and John Calderon for buildup of digital subsystems; and Gerald J. Chomos and Carol A. Vidoli for review and coordination of the final report.

Lewis Research Center
National Aeronautics and Space Administration
Cleveland, Ohio, October 29, 1991

Appendix A

Complete Results of RF and BER Baseline Measurements

Tables 29 and 30 summarize the RF and BER test results for each of the baseline measurement configurations. An explanation of the transponder baseline settings is given in section 4.1. The measurement methods used for each test are explained in appendix B. The data are organized into 12 subtables, each consisting of the data for a given HPA or HPA operating mode (TI GaAs FET, Hughes TWT low mode, Hughes TWT medium mode, and Hughes TWT high mode) at one of three amplifier operating points (linear, 1-dB compression, and saturation). The combinations of these system parameters (four HPA's times three operating points) were tested for three frequency bands (bands A, B, and C). Seventeen matrix switch crosspoints were tested at the 1-dB-compression and saturation operating points, and five matrix switch crosspoints were tested at the linear operating point. The resulting total number of baseline system configurations tested was 468. The method of data presentation for each test is described briefly here.

Amplitude Variation

A swept CW spectrum analyzer plot was made for each of the 468 baseline test configurations. For each plot the highest and lowest amplitude points within the 330-MHz test bandwidth were identified. The amplitude variation for each system configuration was determined by calculating the difference between these two points. This difference, measured in decibels, is recorded in the table for each case.

Group Delay Variation

As with the amplitude variation tests a group delay measurement was made for each system configuration, resulting in 468 tests. The group delay was measured at 10-MHz intervals, and the difference was automatically calculated between the highest and lowest group delay within the

330-MHz bandwidth. This result is listed in the tables as the group delay variation, measured in nanoseconds.

Third-Order Intermodulation

Third-order intermodulation distortion measurements were made only for matrix switch crosspoint 7,6. No measurements were made for the TI GaAs FET at the linear operating point. The result was 33 third-order intermodulation measurements. The results of these tests are given in the tables as the difference (in decibels) at the system output between the lowest amplitude fundamental signal and the highest amplitude third-order intermodulation product.

AM-PM Conversion

The AM-PM conversion coefficient was measured for each system configuration with the exception of the TI GaAs FET at the linear operating point, resulting in 453 tests. The output was a conversion coefficient in degrees per decibel. These data are listed in the tables.

Output Carrier-to-Noise Ratio

The C/N (in decibels) was directly measured at the system output. These data are listed in the tables. This measurement

was made for each system configuration with the exception of the TI GaAs FET at the linear operating point. Also, the data for eight crosspoints with the TWT in the medium mode at the saturated operating point have been lost. Data are reported for 445 C/N tests.

E_b/N_0 at BER of 10^{-6}

For each system configuration a complete BER-versus- E_b/N_0 curve was measured. In order to quantify the BER performance for each case tested, a "desirable" BER was chosen against which all BER curves could be compared. The method of comparison was to determine the E_b/N_0 corresponding to a BER of 10^{-6} , normalize this number by subtracting the E_b/N_0 at a BER of 10^{-6} for the theoretical SMSK curve, and use the resulting number as a figure of merit for the system tested. This number represents the E_b/N_0 degradation, or the additional amount of E_b/N_0 that the system requires in order to obtain a BER of 10^{-6} when compared with an ideal system. In this way the BER performances of the different system configurations were compared. The data tables list the E_b/N_0 degradation (in decibels) for 468 system configurations.

TABLE 29.—PHASE I SINGLE-CHANNEL RF AND BER RESULTS FOR HUGHES TWT
(a) Low mode at linear operating point

Band	Matrix switch crosspoint	Amplitude variation	Group delay variation	Third-order intermodulation	AM-PM conversion	Output C/N ratio	E_b/N_0 at BER of 10^{-6}
A	3,3	1.96	1.66	----	1.50	22.53	0.69
	4,5	1.64	1.64	----	1.23	23.25	.93
	5,6	2.30	1.56	----	1.16	22.98	1.51
	6,7	2.22	1.34	----	1.15	23.19	.70
	7,6	2.34	.99	25.1	.70	20.81	1.64
	Mean	2.09	1.44	----	1.15	22.55	1.09
	Standard deviation	0.29	0.28	----	0.29	1.01	0.45
B	3,3	2.60	1.80	----	1.59	22.88	0.95
	4,5	3.52	2.02	----	1.04	19.48	1.62
	5,6	4.64	2.57	----	1.58	21.90	1.00
	6,7	3.04	1.66	----	1.46	21.35	1.27
	7,6	3.54	1.24	23.0	.78	21.09	1.43
	Mean	3.47	1.86	----	1.29	21.34	1.25
	Standard deviation	0.76	0.49	----	0.36	1.25	0.28
C	3,3	8.86	4.02	----	4.39	26.10	5.62
	4,5	10.48	9.97	----	3.80	23.14	4.97
	5,6	9.38	7.84	----	3.92	23.14	5.21
	6,7	9.30	5.45	----	4.17	25.26	5.55
	7,6	8.84	8.70	28.9	3.47	21.14	4.36
	Mean	9.37	7.20	----	3.95	23.76	5.14
	Standard deviation	0.67	2.42	----	0.35	1.96	0.51
All bands	Mean	4.98	3.50	25.67	2.13	22.55	2.50
	Standard deviation	3.32	3.02	2.99	1.37	1.70	1.98

TABLE 29.—Continued.
(b) Low mode at 1-dB-compression operating point

Band	Matrix switch crosspoint	Amplitude variation	Group delay variation	Third-order intermodulation	AM-PM conversion	Output C/N ratio	E_b/N_0 at BER of 10^{-6}
A	3,3	1.70	2.04	----	3.11	16.88	0.74
	4,3	3.12	1.72	----	3.23	15.00	.85
	5,3	2.82	1.81	----	3.49	16.80	.88
	6,3	1.76	1.80	----	3.57	17.15	.83
	3,5	2.06	2.44	----	2.87	18.33	.96
	4,5	1.44	2.39	----	2.70	17.76	.85
	5,5	2.50	1.99	----	3.73	17.40	1.05
	6,5	1.82	1.96	----	2.66	13.89	1.05
	3,6	1.72	2.31	----	2.66	17.38	1.22
	4,6	1.72	2.34	----	2.34	16.22	1.27
	5,6	1.82	2.22	----	3.34	17.32	1.24
	6,6	1.92	3.43	----	2.34	15.82	1.07
	3,7	2.50	2.17	----	2.59	16.32	.83
	4,7	1.92	3.76	----	2.75	14.49	.77
	5,7	2.32	2.40	----	3.33	15.75	1.03
	6,7	1.94	2.26	----	3.50	17.66	.71
	7,6	1.90	1.86	16.6	3.03	14.93	1.45
	Mean	2.06	2.29	----	3.01	16.42	0.99
	Standard deviation	0.45	0.55	----	0.44	1.27	0.21
B	3,3	1.24	1.86	----	3.61	13.38	0.99
	4,3	2.92	2.73	----	2.51	15.27	1.39
	5,3	2.52	2.96	----	4.03	17.55	1.11
	6,3	2.82	3.25	----	4.01	17.33	.79
	3,5	2.56	2.00	----	3.54	16.32	1.08
	4,5	3.46	2.38	----	2.75	15.21	1.53
	5,5	2.70	1.97	----	2.23	15.30	1.13
	6,5	3.44	2.09	----	2.35	16.45	.90
	3,6	2.06	1.95	----	4.37	14.53	1.01
	4,6	2.32	2.04	----	3.74	12.30	1.23
	5,6	4.18	2.19	----	4.60	17.36	1.00
	6,6	2.90	1.95	----	3.10	15.63	.80
	3,7	2.90	2.15	----	4.54	15.69	.91
	4,7	2.72	2.50	----	3.31	15.42	.81
	5,7	4.70	2.18	----	3.39	17.76	.91
	6,7	2.70	1.90	----	4.15	17.06	1.15
	7,6	2.48	2.00	13.7	3.28	13.97	1.49
	Mean	2.86	2.24	----	3.50	15.68	1.07
	Standard deviation	0.78	0.40	----	0.74	1.54	0.23
C	3,3	4.56	2.86	----	3.23	17.72	2.39
	4,3	11.52	4.08	----	2.14	15.18	10.40
	5,3	7.88	2.78	----	2.67	16.63	4.07
	6,3	7.16	3.10	----	2.92	16.56	5.37
	3,5	5.62	2.34	----	2.49	17.30	2.23
	4,5	8.46	3.37	----	2.17	16.94	2.87
	5,5	7.80	3.81	----	1.37	16.10	3.35
	6,5	7.14	4.03	----	1.14	14.13	3.98
	3,6	5.04	2.41	----	2.63	17.12	2.23
	4,6	5.50	2.56	----	2.86	17.40	2.41
	5,6	6.80	2.68	----	1.41	16.98	3.35
	6,6	8.14	3.05	----	1.00	12.74	4.89
	3,7	6.56	2.16	----	.97	16.02	3.01
	4,7	7.62	3.62	----	1.97	15.69	3.43
	5,7	6.96	4.04	----	1.72	15.68	3.65
	6,7	5.60	3.32	----	3.54	15.97	2.90
	7,6	7.58	3.71	9.7	5.19	16.02	3.22
	Mean	7.06	3.17	----	2.32	16.13	3.75
	Standard deviation	1.62	0.64	----	1.08	1.25	1.93
All bands	Mean	4.00	2.57	----	2.94	16.08	1.94
	Standard deviation	2.45	0.68	----	0.92	1.36	1.70

TABLE 29.—Continued
(c) Low mode at saturation operating point

Band	Matrix switch crosspoint	Amplitude variation	Group delay variation	Third-order intermodulation	AM-PM conversion	Output C/N ratio	E_b/N_0 at BER of 10^{-6}
A	3,3	1.72	7.37	----	5.24	16.20	0.88
	4,3	1.04	6.19	----	5.16	15.74	.80
	5,3	1.44	6.95	----	4.16	15.85	.96
	6,3	1.92	6.58	----	4.73	15.10	.99
	3,5	1.92	6.26	----	3.60	14.87	.89
	4,5	1.80	6.70	----	4.85	15.03	.97
	5,5	1.52	6.55	----	6.22	15.46	.98
	6,5	1.82	6.54	----	4.73	13.56	.98
	3,6	2.00	6.41	----	3.53	14.78	1.02
	4,6	1.98	6.93	----	4.26	14.13	1.10
	5,6	1.76	11.46	----	4.81	14.74	1.14
	6,6	1.92	6.59	----	4.26	14.09	1.06
	3,7	2.16	6.59	----	4.89	14.14	.92
	4,7	1.70	6.65	----	5.18	13.36	.90
	5,7	2.18	6.85	----	5.06	14.76	.99
	6,7	1.98	6.89	----	4.85	14.66	.90
	7,6	1.40	7.98	6.6	5.23	15.15	1.21
	Mean Standard deviation	1.78 0.29	7.03 1.22	---- ----	4.75 0.65	14.80 0.78	0.98 0.10
B	3,3	0.90	4.21	----	3.48	13.94	0.85
	4,3	2.16	3.80	----	2.52	11.46	.94
	5,3	1.12	3.98	----	3.67	14.26	.97
	6,3	1.14	3.89	----	4.27	14.34	.79
	3,5	.98	4.34	----	3.69	14.61	.97
	4,5	2.28	3.84	----	4.54	13.80	1.02
	5,5	1.44	4.86	----	3.16	13.78	1.01
	6,5	2.52	4.85	----	5.51	12.84	.83
	3,6	1.08	4.98	----	4.30	14.43	.89
	4,6	.90	4.03	----	4.28	13.38	.89
	5,6	1.74	4.10	----	3.42	14.42	.93
	6,6	1.54	4.24	----	5.36	14.28	.80
	3,7	1.18	4.09	----	3.89	14.29	.88
	4,7	1.28	4.14	----	4.20	14.30	.78
	5,7	2.00	4.35	----	5.04	14.39	.92
	6,7	1.08	4.06	----	5.98	12.60	.84
	7,6	1.44	4.48	8.3	2.86	14.10	.97
	Mean Standard deviation	1.46 0.51	4.25 0.36	---- ----	4.13 0.95	13.84 0.83	0.90 0.08
C	3,3	2.76	4.97	----	1.21	14.80	2.03
	4,3	11.26	24.87	----	2.16	14.96	7.09
	5,3	6.42	9.74	----	2.24	15.19	2.67
	6,3	4.90	6.90	----	3.96	14.42	3.62
	3,5	3.70	5.96	----	3.50	14.76	1.95
	4,5	7.08	11.47	----	5.09	15.14	2.16
	5,5	6.88	11.79	----	2.96	14.52	2.36
	6,5	7.74	11.52	----	5.56	14.18	3.49
	3,6	3.14	5.48	----	3.78	14.97	1.77
	4,6	4.08	6.52	----	4.29	14.98	1.77
	5,6	5.48	7.45	----	4.31	15.65	2.65
	6,6	7.08	10.73	----	6.22	13.22	4.31
	3,7	5.56	5.72	----	3.74	15.59	2.37
	4,7	5.08	8.51	----	2.71	15.18	2.62
	5,7	5.58	5.75	----	3.10	15.46	2.95
	6,7	3.68	4.71	----	3.46	15.32	2.37
	7,6	6.74	9.90	9.1	5.23	13.37	2.37
	Mean Standard deviation	5.72 2.07	8.94 4.79	---- ----	3.74 1.31	14.81 0.69	2.86 1.29
All bands	Mean Standard deviation	2.98 2.30	6.74 3.41	---- ----	4.20 1.07	14.48 0.88	1.58 1.17

TABLE 29.—Continued.
(d) Medium mode at linear operating point

Band	Matrix switch crosspoint	Amplitude variation	Group delay variation	Third-order intermodulation	AM-PM conversion	Output C/N ratio	E_b/N_0 at BER of 10^{-6}
A	3,3	2.98	1.82	----	1.44	21.96	2.28
	4,5	2.86	1.59	----	1.72	22.73	2.96
	5,6	3.50	1.89	----	1.40	22.42	3.55
	6,7	3.04	1.67	----	1.48	22.59	2.00
	7,6	3.84	2.20	20.8	.68	20.58	1.95
	Mean	3.24	1.83	----	1.35	22.06	2.55
	Standard deviation	0.41	0.24	----	0.89	0.87	0.69
B	3,3	2.06	1.59	----	0.99	23.19	2.03
	4,5	3.68	1.82	----	.47	18.90	2.73
	5,6	4.10	2.54	----	1.00	21.52	1.83
	6,7	3.00	1.59	----	.98	20.64	2.63
	7,6	3.38	1.62	26.1	.44	21.33	1.72
	Mean	3.24	1.83	----	0.78	21.12	2.18
	Standard deviation	0.78	0.41	----	0.29	1.55	0.46
C	3,3	8.00	4.24	----	4.18	25.49	6.63
	4,5	9.68	9.14	----	3.79	22.91	6.19
	5,6	8.52	6.62	----	3.81	22.91	6.88
	6,7	8.30	5.14	----	4.01	24.98	6.70
	7,6	7.86	8.51	20.9	3.40	21.09	4.35
	Mean	8.47	6.73	----	3.84	23.48	6.15
	Standard deviation	0.72	2.10	----	0.29	1.78	1.04
All bands	Mean	4.99	3.47	22.60	1.99	22.22	3.63
	Standard deviation	2.62	2.65	3.03	1.41	1.68	1.98

TABLE 29.—Continued.
(c) Medium mode at 1-dB-compression operating point

Band	Matrix switch crosspoint	Amplitude variation	Group delay variation	Third-order intermodulation	AM-PM conversion	Output C/N ratio	E_b/N_0 at BER of 10^{-6}
A	3,3	4.00	1.55	----	4.16	16.64	1.07
	4,3	6.46	1.96	----	3.43	16.01	1.34
	5,3	5.72	2.37	----	3.86	17.49	1.25
	6,3	4.30	1.72	----	4.17	16.36	1.23
	3,5	3.28	1.63	----	3.37	17.10	1.27
	4,5	4.26	1.69	----	3.43	17.40	1.31
	5,5	5.58	3.14	----	4.85	17.90	1.50
	6,5	3.76	1.81	----	1.89	15.81	1.62
	3,6	3.34	1.74	----	3.12	17.63	1.52
	4,6	3.70	1.77	----	2.90	16.62	1.80
	5,6	4.48	1.53	----	3.55	17.31	1.59
	6,6	3.82	1.61	----	3.05	16.22	1.32
	3,7	3.76	1.61	----	3.54	15.22	1.34
	4,7	4.76	1.35	----	2.72	14.55	1.44
	5,7	4.02	1.58	----	3.99	16.55	1.42
	6,7	4.12	1.75	----	4.55	17.58	1.08
	7,6	5.02	1.72	14.5	4.25	16.76	1.84
	Mean	4.38	1.80	----	3.58	16.66	1.41
	Standard deviation	0.88	0.41	----	0.73	0.91	0.22
B	3,3	1.68	1.49	----	3.92	16.64	1.18
	4,3	3.14	2.19	----	2.80	16.08	1.67
	5,3	2.50	1.63	----	3.09	15.88	1.42
	6,3	1.56	1.41	----	5.06	15.60	.98
	3,5	1.96	1.63	----	4.42	16.82	1.33
	4,5	3.22	1.82	----	3.75	15.26	1.71
	5,5	2.76	1.56	----	4.12	15.54	1.32
	6,5	2.14	1.46	----	3.24	14.42	1.31
	3,6	1.58	2.22	----	4.68	17.01	1.37
	4,6	1.96	2.17	----	4.73	16.78	1.39
	5,6	2.52	3.29	----	4.71	16.08	1.13
	6,6	1.88	2.72	----	3.83	16.07	.99
	3,7	1.94	2.86	----	3.90	16.95	1.24
	4,7	2.32	2.16	----	3.96	15.94	1.05
	5,7	3.66	5.85	----	5.78	17.33	1.14
	6,7	2.24	3.60	----	4.66	16.77	1.24
	7,6	3.08	1.84	12.3	4.51	15.64	1.46
	Mean	2.36	2.35	----	4.19	16.17	1.27
	Standard deviation	0.63	1.11	----	0.75	0.75	0.21
C	3,3	5.02	4.43	----	0.94	18.47	3.64
	4,3	11.08	7.13	----	.57	15.39	12.19
	5,3	7.68	9.37	----	2.00	17.42	6.33
	6,3	7.40	20.40	----	2.55	14.59	7.51
	3,5	5.46	5.89	----	1.20	16.86	3.39
	4,5	8.02	8.85	----	3.29	16.33	4.92
	5,5	6.90	8.19	----	2.25	16.13	4.75
	6,5	6.32	6.99	----	.91	12.56	5.72
	3,6	5.26	5.22	----	.94	17.43	3.76
	4,6	5.42	6.04	----	4.98	17.39	3.82
	5,6	6.80	7.03	----	2.35	16.36	5.42
	6,6	7.80	8.02	----	1.70	14.34	8.57
	3,7	6.10	5.62	----	2.42	16.98	5.41
	4,7	7.26	8.10	----	3.52	17.34	5.51
	5,7	6.72	6.65	----	1.89	16.25	6.37
	6,7	6.08	5.76	----	.64	18.06	5.43
	7,6	6.78	1.38	10.8	5.26	16.17	3.72
	Mean	6.83	7.36	----	2.20	16.36	5.67
	Standard deviation	1.43	3.85	----	1.40	1.48	2.19
All bands	Mean	4.52	3.83	----	3.32	16.39	2.79
	Standard deviation	2.11	3.40	----	1.30	1.09	2.41

TABLE 29.—Continued.
(f) Medium mode at saturation operating point

Band	Matrix switch crosspoint	Amplitude variation	Group delay variation	Third-order intermodulation	AM-PM conversion	Output C/N ratio	E_b/N_0 at BER of 10^{-6}
A	3,3	2.92	2.68	----	3.67	10.66	0.87
	4,3	2.44	2.59	----	4.24	10.81	1.05
	5,3	2.50	2.20	----	5.32	10.57	1.10
	6,3	3.12	2.05	----	4.34	11.35	1.00
	3,5	2.92	2.48	----	3.97	11.25	1.00
	4,5	2.72	2.86	----	2.61	10.23	1.01
	5,5	2.10	2.32	----	5.17	10.02	1.17
	6,5	3.16	2.25	----	3.90	11.62	1.19
	3,6	2.76	2.38	----	3.43	10.51	1.07
	4,6	2.88	2.43	----	3.53	11.12	1.26
	5,6	2.48	2.63	----	4.24	11.34	1.35
	6,6	2.94	2.28	----	3.52	11.23	1.02
	3,7	3.70	2.31	----	3.16	9.54	.95
	4,7	3.12	2.50	----	4.14	10.81	1.16
	5,7	3.40	2.51	----	4.47	10.00	.98
	6,7	2.98	2.53	----	3.68	11.02	.86
	7,6	2.90	2.44	8.4	4.93	14.84	1.28
	Mean	2.88	2.44	----	4.02	11.00	1.08
	Standard deviation	0.38	0.20	----	0.71	1.14	0.14
B	3,3	1.98	2.64	----	3.41	14.60	0.77
	4,3	1.96	1.89	----	4.08	14.37	1.36
	5,3	2.18	2.38	----	1.90	14.26	.99
	6,3	2.16	2.25	----	4.17	14.25	.83
	3,5	1.90	1.86	----	3.40	13.84	.85
	4,5	1.38	3.20	----	4.79	14.47	1.05
	5,5	3.20	2.75	----	4.68	14.41	1.13
	6,5	2.86	2.09	----	5.92	13.63	.97
	3,6	2.20	2.66	----	4.23	14.32	.80
	4,6	2.04	2.95	----	4.19	14.62	.76
	5,6	2.60	2.59	----	4.55	14.23	.78
	6,6	2.26	1.69	----	6.08	14.58	.71
	3,7	2.26	2.08	----	5.16	14.00	.78
	4,7	2.20	2.17	----	4.92	14.61	1.18
	5,7	2.82	2.16	----	4.70	14.08	.89
	6,7	1.20	2.25	----	4.22	13.64	.79
	7,6	1.72	3.56	5.9	.77	13.44	.93
	Mean	2.17	2.42	----	4.19	14.20	.92
	Standard deviation	0.51	0.50	----	1.30	0.37	0.18
C	3,3	1.22	4.35	----	0.64	14.37	2.18
	4,3	6.48	3.26	----	.83	15.08	5.22
	5,3	2.96	3.53	----	.98	14.70	2.13
	6,3	1.22	3.69	----	2.19	13.92	3.03
	3,5	1.20	3.53	----	1.91	13.53	1.88
	4,5	1.22	3.62	----	2.02	14.10	1.79
	5,5	1.20	3.56	----	1.14	14.48	2.01
	6,5	1.14	2.94	----	4.02	14.60	3.05
	3,6	1.16	4.17	----	2.02	----	1.80
	4,6	1.78	3.78	----	3.40	----	1.65
	5,6	2.38	3.27	----	2.97	----	1.78
	6,6	4.12	2.86	----	3.31	----	2.99
	3,7	2.54	3.23	----	2.89	----	1.97
	4,7	3.48	4.14	----	3.28	----	1.93
	5,7	2.62	3.39	----	2.34	----	2.05
	6,7	1.66	3.83	----	1.31	----	2.05
	7,6	3.06	2.96	1.5	5.36	14.94	1.98
	Mean	2.32	3.54	----	2.39	14.41	2.32
	Standard deviation	1.43	0.43	----	1.26	0.50	0.87
All bands	Mean	2.46	2.80	----	3.53	12.98	1.44
	Standard deviation	0.94	0.66	----	1.37	1.80	0.81

TABLE 29.—Continued.
(g) High mode at linear operating point

Band	Matrix switch crosspoint	Amplitude variation	Group delay variation	Third-order intermodulation	AM-PM conversion	Output C/N ratio	E_b/N_0 at BER of 10^{-6}
A	3,3	4.84	2.22	----	0.90	22.23	1.56
	4,5	5.14	1.84	----	.84	22.82	2.06
	5,6	5.58	2.12	----	1.18	22.38	5.40
	6,7	4.76	2.85	----	1.04	22.04	2.10
	7,6	6.38	2.25	22.4	.46	21.12	3.29
	Mean	5.34	2.26	----	0.88	22.12	2.80
	Standard deviation	0.66	0.37	----	0.27	0.63	1.38
B	3,3	2.40	2.32	----	0.46	22.35	1.77
	4,5	2.94	2.22	----	.45	18.88	2.27
	5,6	5.14	2.74	----	.94	21.36	1.74
	6,7	2.82	2.41	----	.80	20.84	1.82
	7,6	3.02	2.66	27.4	.38	20.75	2.13
	Mean	3.26	2.47	----	0.61	20.84	1.95
	Standard deviation	1.08	0.22	----	0.25	1.26	0.24
C	3,3	8.04	3.00	----	4.25	25.77	1.20
	4,5	9.66	5.40	----	3.65	23.42	2.02
	5,6	8.40	3.55	----	3.83	23.42	1.32
	6,7	8.74	3.21	----	4.02	24.47	2.06
	7,6	7.22	9.67	24.0	3.31	21.55	3.90
	Mean	8.41	4.97	----	3.81	23.73	2.10
	Standard deviation	0.90	2.80	----	0.36	1.55	1.08
All bands	Mean	5.67	3.23	24.6	1.77	22.23	2.28
	Standard deviation	2.34	1.98	2.55	1.53	1.66	1.02

TABLE 29.—Continued.
(h) High mode at 1-dB-compression operating point

Band	Matrix switch crosspoint	Amplitude variation	Group delay variation	Third-order intermodulation	AM-PM conversion	Output C/N ratio	E_b/N_0 at BER of 10^{-6}
A	3,3	1.92	4.46	----	2.63	17.30	2.68
	4,3	3.40	7.33	----	1.78	15.31	5.36
	5,3	2.96	5.67	----	3.02	17.01	4.15
	6,3	2.04	5.10	----	2.06	16.10	3.99
	3,5	2.50	4.13	----	1.83	18.03	3.23
	4,5	1.84	4.28	----	2.85	16.54	3.91
	5,5	2.86	2.90	----	2.43	17.28	4.86
	6,5	2.24	5.44	----	1.18	15.70	5.95
	3,6	2.32	4.15	----	1.08	14.70	4.17
	4,6	2.26	3.98	----	1.09	16.28	4.89
	5,6	2.22	4.22	----	2.40	16.78	1.50
	6,6	2.44	4.53	----	1.64	15.74	2.49
	3,7	2.78	3.71	----	2.45	15.88	1.63
	4,7	2.44	4.89	----	1.96	15.16	2.23
	5,7	2.24	3.93	----	2.36	15.42	2.23
	6,7	2.18	3.78	----	2.89	18.01	1.40
	7,6	2.70	5.27	15.7	3.34	14.97	2.63
	Mean	2.43	4.57	----	2.18	16.25	3.37
	Standard deviation	0.40	1.00	----	0.68	1.03	1.41
B	3,3	1.50	3.16	----	4.32	17.62	1.26
	4,3	2.32	2.26	----	2.76	16.22	1.67
	5,3	2.32	2.09	----	3.45	16.93	1.25
	6,3	1.94	3.17	----	3.75	17.35	1.14
	3,5	1.62	3.09	----	3.22	14.69	1.76
	4,5	2.42	2.90	----	2.89	15.85	1.65
	5,5	2.66	2.51	----	2.60	15.95	1.51
	6,5	2.10	2.35	----	1.69	14.27	1.51
	3,6	1.24	3.04	----	3.74	17.92	1.62
	4,6	1.60	2.78	----	3.71	16.55	2.05
	5,6	3.04	2.76	----	4.05	16.76	1.89
	6,6	1.98	2.71	----	3.13	16.31	1.83
	3,7	2.14	2.74	----	3.58	17.60	1.52
	4,7	1.96	2.80	----	2.82	15.02	1.81
	5,7	3.22	2.47	----	4.13	17.93	1.52
	6,7	1.44	3.29	----	2.91	17.40	1.64
	7,6	2.44	1.87	13.4	3.32	15.72	1.56
	Mean	2.11	2.71	----	3.30	16.48	1.60
	Standard deviation	0.55	0.40	----	0.66	1.12	0.24
C	3,3	5.78	4.33	----	2.20	18.84	3.07
	4,3	11.88	7.47	----	2.51	15.44	7.40
	5,3	8.02	5.86	----	1.92	16.91	4.21
	6,3	7.62	1.83	----	2.50	16.70	4.82
	3,5	5.72	4.82	----	1.62	16.95	2.49
	4,5	8.24	6.13	----	1.49	15.46	3.58
	5,5	7.32	5.41	----	1.95	16.38	3.12
	6,5	6.70	4.82	----	.55	14.04	3.57
	3,6	5.68	4.33	----	2.08	17.78	3.01
	4,6	5.44	4.59	----	3.66	16.53	2.91
	5,6	6.78	5.37	----	.45	16.48	3.69
	6,6	7.54	5.88	----	.93	14.64	5.27
	3,7	6.08	3.91	----	1.29	15.29	3.12
	4,7	7.16	5.17	----	2.32	17.23	3.71
	5,7	6.42	4.62	----	1.76	16.30	4.53
	6,7	5.84	4.53	----	1.61	17.84	4.14
	7,6	7.00	5.64	12.1	5.15	16.16	3.03
	Mean	7.01	4.98	----	2.00	16.43	3.86
	Standard deviation	1.52	1.18	----	1.12	1.20	1.18
All bands	Mean	3.85	4.09	----	2.49	16.38	2.94
	Standard deviation	2.45	1.35	----	1.01	1.10	1.44

TABLE 29.—Concluded.
(i) High mode at saturated operating point

Band	Matrix switch crosspoint	Amplitude variation	Group delay variation	Third-order intermodulation	AM-PM conversion	Output C/N ratio	E_b/N_0 at BER of 10^{-6}
A	3,3	3.30	4.57	----	4.42	14.99	1.39
	4,3	5.22	6.11	----	5.53	14.00	4.70
	5,3	4.16	5.65	----	5.89	14.27	2.47
	6,3	3.46	5.13	----	4.32	14.46	2.06
	3,5	2.96	5.77	----	4.91	12.80	1.53
	4,5	3.08	3.58	----	4.60	14.75	1.67
	5,5	3.76	3.94	----	5.10	15.04	2.61
	6,5	4.04	1.83	----	5.95	15.13	3.06
	3,6	2.94	1.84	----	5.61	15.00	1.85
	4,6	3.18	1.84	----	3.64	14.58	2.12
	5,6	3.20	1.84	----	5.26	12.87	1.88
	6,6	3.46	5.03	----	4.24	14.18	2.14
	3,7	3.46	6.09	----	5.10	14.18	2.36
	4,7	4.10	7.93	----	4.35	11.68	2.93
	5,7	3.32	14.64	----	5.17	14.14	2.12
	6,7	3.04	9.97	----	5.29	14.23	1.39
	7,6	3.44	3.62	8.7	4.07	14.01	1.91
	Mean	3.54	5.26	----	4.91	14.14	2.25
	Standard deviation	0.58	3.30	----	0.67	0.92	0.80
B	3,3	1.38	5.26	----	1.71	11.24	1.06
	4,3	2.72	3.35	----	2.44	11.60	2.53
	5,3	1.64	4.28	----	3.60	10.51	1.49
	6,3	1.58	4.72	----	3.16	11.93	1.26
	3,5	1.52	5.02	----	3.52	11.52	1.35
	4,5	2.22	5.23	----	3.62	11.18	1.89
	5,5	2.18	4.50	----	5.12	10.73	2.03
	6,5	1.56	4.40	----	5.35	10.50	2.34
	3,6	1.52	3.81	----	2.96	11.74	1.04
	4,6	1.42	4.07	----	4.28	12.66	1.21
	5,6	1.70	2.94	----	4.59	12.24	1.30
	6,6	1.36	3.77	----	4.35	12.00	1.11
	3,7	1.62	3.14	----	5.69	10.88	1.09
	4,7	2.18	3.33	----	5.36	10.98	1.71
	5,7	1.64	2.61	----	3.64	12.51	1.11
	6,7	1.44	4.26	----	5.18	12.36	.93
	7,6	1.90	3.27	7.4	2.83	13.60	1.01
	Mean	1.74	4.00	----	3.96	11.66	1.44
	Standard deviation	0.38	0.81	----	1.15	0.85	0.49
C	3,3	1.76	5.33	----	3.82	13.90	1.78
	4,3	7.26	5.54	----	1.05	13.89	5.19
	5,3	3.44	4.02	----	2.53	14.51	1.96
	6,3	2.96	4.10	----	1.71	14.47	1.57
	3,5	2.18	3.93	----	2.11	13.40	1.53
	4,5	4.24	3.73	----	2.66	13.23	1.36
	5,5	3.96	3.65	----	2.59	14.80	1.59
	6,5	4.84	4.10	----	.57	15.79	2.80
	3,6	1.64	3.64	----	2.67	13.03	1.40
	4,6	2.20	3.96	----	2.66	14.59	1.28
	5,6	2.50	3.54	----	.90	14.62	1.33
	6,6	4.36	3.41	----	3.49	14.86	2.52
	3,7	3.24	3.48	----	1.62	14.02	1.61
	4,7	3.92	3.89	----	1.68	14.93	1.41
	5,7	3.10	3.67	----	3.54	15.53	1.89
	6,7	2.24	4.44	----	2.52	13.58	1.81
	7,6	4.24	3.20	-0.9	5.35	15.24	1.67
	Mean	3.42	3.98	----	2.44	14.38	1.90
	Standard deviation	1.39	0.63	----	1.19	0.80	0.95
All bands	Mean	2.90	4.41	----	3.77	13.39	1.87
	Standard deviation	1.21	2.04	----	1.44	1.50	0.82

TABLE 30.—PHASE I SINGLE-CHANNEL RADIOFREQUENCY AND BIT-ERROR-RATE RESULTS FOR TI GaAs FET
(a) Linear operating point

Band	Matrix switch crosspoint	Amplitude variation	Group delay variation	Third-order intermodulation	AM-PM conversion	Output C/N ratio	E_b/N_0 at BER of 10^{-6}
A	3,3	2.16	1.76	----	----	----	0.88
	4,5	2.30	1.59	----	----	----	1.06
	5,6	3.20	1.92	----	----	----	1.61
	6,7	2.52	1.56	----	----	----	.92
	7,6	2.80	1.98	----	----	----	1.58
	Mean Standard deviation	2.60 0.42	1.76 0.19	---- ----	---- ----	---- ----	1.21 0.36
B	3,3	2.94	1.57	----	----	----	0.88
	4,5	2.20	1.60	----	----	----	1.21
	5,6	6.60	3.78	----	----	----	1.03
	6,7	4.10	1.71	----	----	----	.84
	7,6	3.22	1.57	----	----	----	1.07
	Mean Standard deviation	3.81 1.70	2.05 0.97	---- ----	---- ----	---- ----	1.01 0.15
C	3,3	8.72	5.24	----	----	----	4.72
	4,5	10.36	12.00	----	----	----	3.78
	5,6	9.34	8.79	----	----	----	4.15
	6,7	9.04	6.70	----	----	----	4.27
	7,6	8.68	11.59	----	----	----	3.54
	Mean Standard deviation	9.23 0.69	8.86 2.96	---- ----	---- ----	---- ----	4.09 0.46
All bands	Mean Standard deviation	5.21 3.15	4.22 3.79	---- ----	---- ----	---- ----	2.10 1.49

TABLE 30.—Continued.
(b) 1-dB-compression operating point

Band	Matrix switch crosspoint	Amplitude variation	Group delay variation	Third-order intermodulation	AM-PM conversion	Output C/N ratio	E_b/N_0 at BER of 10^{-6}
A	3,3	0.80	1.31	----	4.87	18.37	0.87
	4,3	3.68	1.00	----	5.83	16.89	.89
	5,3	2.48	1.30	----	2.98	18.31	1.05
	6,3	1.20	1.21	----	2.97	17.76	.99
	3,5	1.24	1.29	----	3.46	18.00	1.01
	4,5	1.20	1.16	----	3.63	18.67	1.07
	5,5	2.68	1.31	----	4.41	18.22	1.17
	6,5	1.38	1.09	----	4.10	15.03	1.13
	3,6	1.30	1.17	----	3.28	18.23	1.24
	4,6	1.22	1.23	----	4.04	18.00	1.30
	5,6	1.48	1.55	----	4.76	18.46	1.37
	6,6	1.20	1.15	----	3.79	17.39	1.20
	3,7	1.40	1.37	----	3.58	17.04	.91
	4,7	1.56	1.20	----	3.50	17.10	.92
	5,7	1.20	1.52	----	4.27	17.95	1.20
	6,7	1.04	1.48	----	2.97	17.50	.84
	7,6	2.04	.97	12.3	3.53	17.58	1.31
	Mean	1.59	1.25	----	3.88	17.68	1.08
	Standard deviation	0.73	0.17	----	0.77	0.86	0.17
B	3,3	1.76	1.00	----	1.35	19.63	0.94
	4,3	2.52	1.71	----	2.40	16.93	1.08
	5,3	3.32	1.37	----	3.96	17.42	1.00
	6,3	3.44	1.61	----	4.36	17.49	.80
	3,5	2.08	1.77	----	3.73	18.50	.87
	4,5	1.68	1.95	----	3.29	14.31	1.05
	5,5	4.44	1.82	----	3.54	18.31	.93
	6,5	4.18	1.90	----	3.85	15.40	.89
	3,6	2.02	1.73	----	2.34	19.41	.82
	4,6	2.32	1.79	----	4.87	18.94	.91
	5,6	4.18	1.95	----	4.58	19.06	.90
	6,6	3.32	1.98	----	4.45	18.13	.74
	3,7	3.34	1.69	----	4.23	18.99	.80
	4,7	3.10	1.80	----	3.85	18.24	.75
	5,7	4.48	1.87	----	4.77	19.28	.92
	6,7	2.18	1.76	----	4.48	18.34	.76
	7,6	2.28	1.15	12.2	2.80	18.85	1.00
	Mean	2.98	1.70	----	3.71	18.07	0.89
	Standard deviation	0.95	0.28	----	0.99	1.43	0.10
C	3,3	7.10	3.23	----	2.86	21.95	3.35
	4,3	12.74	4.47	----	2.80	17.17	6.51
	5,3	9.54	3.77	----	3.33	20.35	3.86
	6,3	7.84	3.30	----	1.96	19.02	4.37
	3,5	6.86	3.28	----	2.42	21.61	2.22
	4,5	9.10	3.80	----	1.77	19.80	2.96
	5,5	8.64	3.67	----	1.97	19.38	2.48
	6,5	7.44	3.51	----	1.50	16.11	2.90
	3,6	6.46	3.31	----	1.13	20.53	2.79
	4,6	7.04	3.19	----	1.89	19.44	2.35
	5,6	7.98	3.51	----	2.51	20.40	3.46
	6,6	8.30	4.16	----	1.88	17.82	4.20
	3,7	6.78	2.81	----	2.65	19.73	2.82
	4,7	9.50	4.45	----	1.69	18.88	3.08
	5,7	7.74	3.33	----	.96	19.06	3.53
	6,7	7.44	3.19	----	1.60	20.87	3.41
	7,6	7.48	3.07	13.7	1.75	18.62	2.82
	Mean	8.12	3.53	----	2.04	19.46	3.36
	Standard deviation	1.51	0.47	----	0.64	1.51	1.01
All bands	Mean	4.23	2.16	----	3.21	18.40	1.78
	Standard deviation	3.04	1.05	----	1.16	1.49	1.27

TABLE 30.—Concluded.
(c) Saturated operating point

Band	Matrix switch crosspoint	Amplitude variation	Group delay variation	Third-order intermodulation	AM-PM conversion	Output C/N ratio	E_b/N_0 at BER of 10^{-6}
A	3,3	1.38	2.95	----	4.83	18.12	0.57
	4,3	2.04	2.66	----	5.25	17.24	.97
	5,3	1.12	2.50	----	4.41	17.34	1.07
	6,3	1.28	3.32	----	4.73	18.23	.87
	3,5	1.52	2.93	----	3.98	17.42	.61
	4,5	1.36	3.77	----	4.24	17.86	.88
	5,5	1.30	1.81	----	4.65	17.98	1.23
	6,5	1.40	2.97	----	4.06	18.02	1.08
	3,6	1.50	3.33	----	4.41	18.00	.87
	4,6	1.36	3.08	----	3.02	17.44	.99
	5,6	1.30	2.98	----	3.98	18.04	1.03
	6,6	1.36	2.53	----	3.48	17.60	1.05
	3,7	1.72	2.83	----	4.84	18.01	.86
	4,7	.98	2.54	----	4.37	17.56	1.00
	5,7	1.52	2.98	----	5.12	17.28	.89
	6,7	1.48	3.34	----	5.32	18.34	.49
	7,6	1.14	2.87	8.0	5.49	18.07	1.24
B	Mean	1.42	2.91	----	4.48	17.80	0.92
	Standard deviation	0.26	0.44	----	0.66	0.36	0.21
	3,3	1.34	3.21	----	3.11	18.27	0.75
	4,3	.98	2.78	----	3.97	17.39	.71
	5,3	1.70	3.57	----	1.86	17.48	.94
	6,3	1.58	3.69	----	4.10	18.17	.73
	3,5	1.24	3.02	----	4.22	16.95	.84
	4,5	1.02	1.25	----	4.37	17.66	.91
	5,5	1.76	3.62	----	4.02	17.78	1.05
	6,5	2.10	3.11	----	5.96	17.71	.82
	3,6	1.50	3.00	----	3.85	17.96	.75
	4,6	1.36	3.03	----	3.79	17.54	.82
	5,6	1.72	3.12	----	3.69	17.41	.90
	6,6	1.66	2.91	----	5.12	17.84	.75
	3,7	1.56	2.64	----	4.37	17.03	.74
	4,7	1.44	2.57	----	4.98	18.04	.77
	5,7	1.82	3.69	----	3.98	17.19	.97
	6,7	1.34	3.03	----	4.33	17.26	.75
	7,6	1.06	3.10	8.0	.72	18.04	.91
C	Mean	1.48	3.02	----	3.91	17.63	0.83
	Standard deviation	0.30	0.57	----	1.19	0.40	0.10
	3,3	1.64	4.91	----	4.22	18.90	1.87
	4,3	6.72	4.33	----	4.02	18.62	3.73
	5,3	3.60	5.14	----	3.86	18.45	2.13
	6,3	2.88	4.95	----	3.85	16.50	2.38
	3,5	2.36	4.24	----	3.80	16.71	1.59
	4,5	3.04	4.05	----	1.59	17.41	1.59
	5,5	3.18	4.14	----	2.55	18.48	1.59
	6,5	3.12	3.54	----	2.62	19.22	1.98
	3,6	2.08	4.16	----	4.04	18.92	1.62
	4,6	2.46	4.16	----	1.72	17.75	1.46
	5,6	2.44	4.65	----	3.60	18.68	1.78
	6,6	3.06	4.21	----	2.49	18.32	2.41
	3,7	2.22	4.40	----	1.97	17.97	1.77
	4,7	3.12	4.62	----	3.08	19.13	1.42
	5,7	2.42	4.39	----	2.13	19.23	1.78
	6,7	1.74	4.58	----	4.13	19.66	2.06
	7,6	3.00	3.43	2.8	1.91	17.72	1.65
All bands	Mean	2.89	4.34	----	3.03	18.33	1.93
	Standard deviation	1.13	0.45	----	0.95	0.89	0.55
All bands	Mean	1.93	3.42	----	3.81	17.92	1.23
	Standard deviation	0.96	0.82	----	1.12	0.66	0.61

Appendix B

RF Measurement Methods

The large number of RF measurements required dictated that the tests be computer automated as much as possible. All the test procedures were therefore converted to a form that allowed computer control programs to be developed. The programs significantly reduced the amount of time required to perform the measurements. In addition, greater measurement accuracy was achieved and clear graphical outputs were produced. In this appendix the method of performing each RF measurement and the functions of the control program are briefly reviewed.

Amplitude Variation Measurements

The amplitude variation measurement setup is shown in figure 57. It consists of a synthesized signal generator, a spectrum analyzer, and a graphics plotter under the control of an HP 9825B computer/controller. The control program slowly swept the synthesizer from 3.2 to 3.55 GHz in 0.3-MHz increments. The spectrum analyzer was set to a display band width of 3.21 to 3.54 GHz and a resolution bandwidth of 3 MHz. Other spectrum analyzer settings are shown in figure 58, which is a typical output plot. This plot was produced on the graphics plotter under computer control. Note that two spectrum analyzer markers have been set; the frequency and amplitude differences between the two markers are available from the control program output. The amplitude difference was the primary output of the amplitude variation measurement.

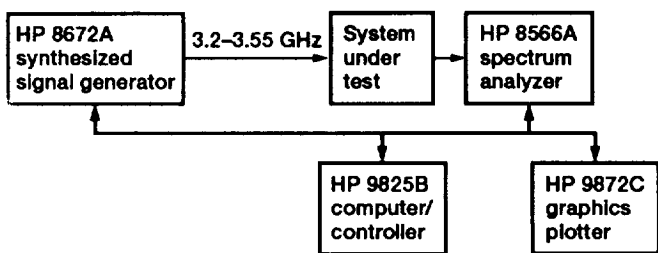


Figure 57.—Test setup for amplitude variation measurements.

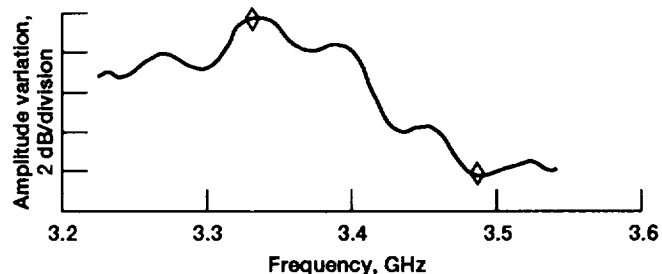


Figure 58.—Example of amplitude variation measurement result. Reference, -26.0 dBm.

Group Delay Measurements

The group delay measurement method is described in detail in reference 18. The test setup used is shown in figure 59. An amplitude-modulated test signal is transmitted through the system under test. The output envelope was detected and compared with the input modulating signal. The phase shift between the two signals can be mathematically related to the group delay induced by the system under test by the following equation:

$$\text{Group delay} = \frac{\text{Envelope phase shift}}{\text{Modulating frequency}}$$

For a modulating frequency of 2.778 MHz a measured envelope phase shift of 1° corresponds directly to a group delay of 1 ns.

Under the control of an HP 9845B computer the synthesized signal generator was stepped through a set of frequencies from 3.21 to 3.54 GHz in 10-MHz increments. The group delay was measured at each frequency by a vector voltmeter. The output of the vector voltmeter was accessed by the control program through a digital multimeter. In order to measure the group delay of the test system without including the group delay of the measurement system, a calibration had to be performed with the test system removed from the test setup, as shown in figure 59. The data set from the calibration was stored and the values were subtracted, point by point, from the data taken on the test system, resulting in a corrected data set that reflected only the group delay contribution of the test system.

A typical output of a group delay measurement is shown in figure 60. The last column of the table (fig. 60(a)) gives the final corrected measurement values. The computer program also determined the maximum variation in group

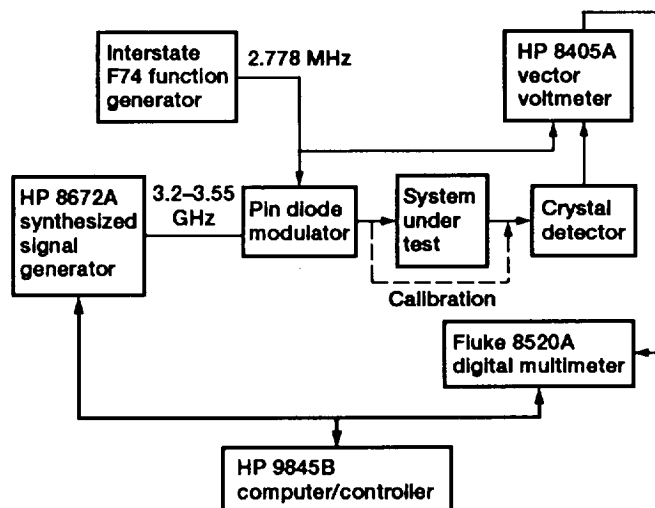


Figure 59.—Test setup for group delay variation measurements.

delay by subtracting the minimum measured group delay from the maximum. This result, the primary output goal of this measurement, appears at the lower left corner of the table. The computer program also plotted the measured group delay versus frequency, as shown in figure 60(b).

Frequency, GHz	Calibration, ns	Group delay, ^a ns	
		Uncorrected	Corrected
3.210	81.58	-20.15	101.72
3.220	81.92	-20.13	102.05
3.230	82.27	-19.99	102.26
3.240	81.80	-20.09	101.89
3.250	81.50	-20.23	101.73
3.260	82.00	-20.13	102.13
3.270	82.32	-19.98	102.30
3.280	81.75	-20.22	101.97
3.290	81.49	-20.15	101.63
3.300	82.07	-19.90	101.97
3.310	82.38	-20.26	102.64
3.320	81.71	-20.75	102.46
3.330	81.40	-21.25	102.65
3.340	82.01	-21.34	103.35
3.350	82.17	-20.83	103.00
3.360	81.54	-20.65	102.20
3.370	81.47	-20.95	102.41
3.380	82.16	-21.27	103.43
3.390	82.09	-22.12	104.21
3.400	81.33	-22.80	104.13
3.410	81.44	-22.55	104.00
3.420	82.15	-22.20	104.36
3.430	82.05	-22.17	104.22
3.440	81.29	-22.79	104.09
3.450	81.55	-23.55	105.09
3.460	82.21	-24.17	106.38
3.470	81.79	-24.59	106.38
3.480	81.14	-24.87	106.01
3.490	81.63	-25.16	106.80
3.500	82.34	-25.54	107.89
3.510	81.90	-25.99	107.88
3.520	81.22	-26.69	107.92
3.530	81.55	-27.42	108.98
3.540	82.17	-28.25	110.42

^aVariation, 8.79 ns.

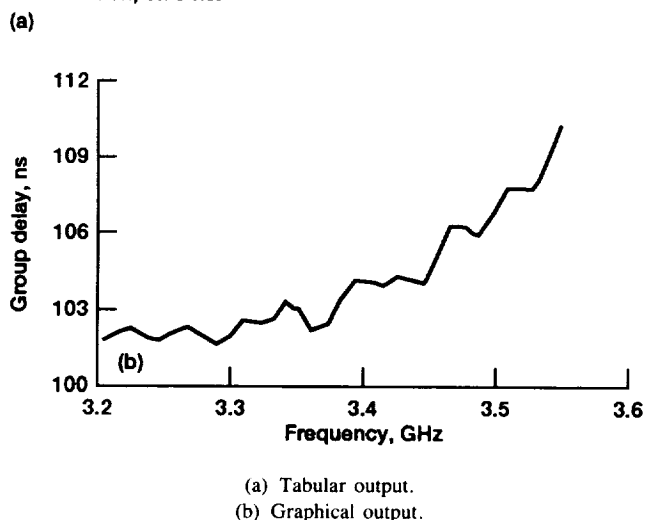


Figure 60.—Example of group delay variation measurements for TI GaAs FET linear band C; crosspoint 5,6.

Third-Order Intermodulation Distortion Measurements

The third-order intermodulation distortion measurement measured the level of the third-order intermodulation product produced by the system under tests resulting from the input of two CW signals. The amplitude of the third-order product was expressed relative to the amplitude of the fundamental signals in decibels below the carrier. Figure 61 shows the setup used for this test. Two synthesized signal generator outputs, spaced at 25 and -25 MHz from the test band center, were combined. The combined signal power was set equal to the normal system input power, and the signals were viewed on the spectrum analyzer and adjusted so that they were of equal amplitude. The signals were then transmitted through the test system, and the output was connected to the spectrum analyzer. The control program instructed the spectrum analyzer to find and measure the two highest output signals. The program then computed the frequency of all intermodulation products that would appear within a 500-MHz band centered at the test band center. The spectrum analyzer then found and measured each intermodulation product. The results were printed as shown in figure 62(a). The level of each intermodulation product was calculated relative to the lowest of the two fundamental signals. All of the intermodulation products were plotted as shown in figure 62(b).

AM-PM Conversion Coefficient Measurements

The technique used to measure the AM-PM conversion coefficient was derived from a technique used to measure the AM-PM conversion of traveling-wave tubes (ref. 19). This was found to be the only technique applicable to the phase I single-channel system. By using the same test setup as for the third-order intermodulation measurements (fig. 63), the AM-PM coefficients were determined by measuring the relative output levels of two signals plus a third-order intermodulation product. The output signals were the result of two input signals separated in frequency by 25 MHz and in amplitude by 30 dB. The AM-PM conversion coefficients K_p (in degrees per decibel) were calculated from the following

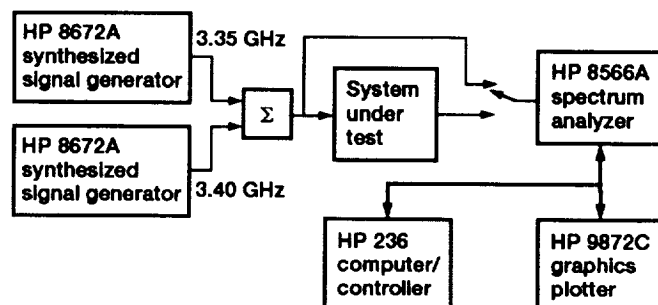
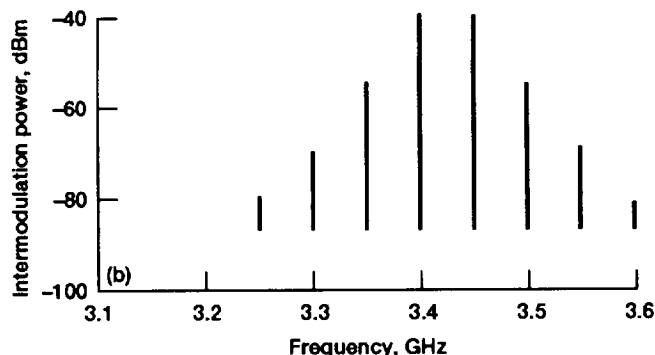


Figure 61.—Test setup for third-order intermodulation and AM-PM conversion variation measurements.

First input signal: 3.3991 GHz, -40.9 dBm
Second input signal: 3.4493 GHz, -40.1 dBm

Order	Frequency, GHz	Power, dBm	Decibels below primary signal, dBc
3	3.3489	-55.4	14.5
3	3.4995	-54.9	14
5	3.2987	-69.9	29
5	3.5497	-69.5	28.6
7	3.2485	-80.6	39.7
7	3.5999	-81.7	40.8

(a)



(a) Tabular output.
(b) Graphical output.

Figure 62.—Example of third-order intermodulation variation measurements for Hughes TWT medium mode, band A.

formulas (ref. 19):

$$K_p = 13.193 \left[S_1^2 - \left(\frac{1 + S_1^2 - S_2^2}{2} \right)^2 \right]^{1/2}$$

$$S_1 = 10^{\left(\frac{\Delta_{in} - \Delta_{out(2)}}{20} \right)}$$

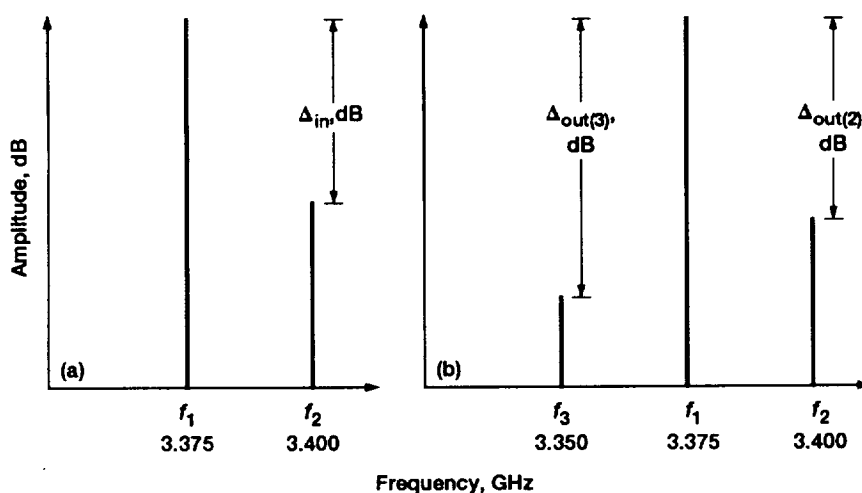
$$S_2 = 10^{\left(\frac{\Delta_{in} - \Delta_{out(1)}}{20} \right)}$$

where Δ_{in} and Δ_{out} are defined in figure 63.

Under the control of a computer program the spectrum analyzer measured the relative levels of the two input signals and the three output signals. The program then performed the preceding calculations and printed the resulting AM-PM conversion coefficient.

Output Carrier-to-Noise Ratio Measurements

The test setup for the output C/N measurements is shown in figure 64. An input CW signal was set at the band center frequency. The output of the system under test was connected to the spectrum analyzer. Under the control of a computer program the spectrum analyzer measured the amplitude and frequency of the output CW signal. Then the noise power per hertz was measured at 20 frequency intervals across the test band. No measurement was made within 20 MHz of the test signal in order to avoid including part of the CW signal power in the noise measurement. These 20 noise measurements were averaged and multiplied by the test bandwidth (330 MHz) to obtain the total noise power in the test band. The control program then calculated the ratio of carrier (CW signal) power to noise power and printed the result as the output C/N .



(a) Input signals.
(b) Output signals.

Figure 63.—AM-PM conversion coefficient measurement definitions.

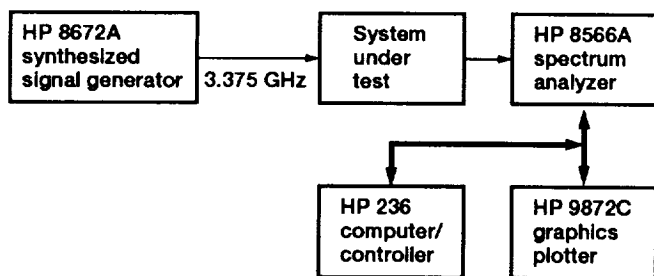


Figure 64.—Test setup for output carrier-to-noise ratio variation measurements.

Appendix C

BER Measurement Methods

The system used for measuring the bit error rate in these tests was built at NASA Lewis as a part of phase I of the SITE Project. The hardware and methods used to obtain a BER measurement are described briefly here. Any further information or detailed discussions on this subject can be found in references 7, 8, 20, and 21.

The phase I BER measurement system consisted of five main subsystems:

- (1) Data generator/data checker
- (2) Data processor
- (3) SMSK modem
- (4) Noise generation unit
- (5) EC&M

Figure 65 shows a block diagram of the BER measurement system hardware.

Data Generator/Data Checker

The data generator/data checker (DG/DC) test set was an operationally independent subsystem that compared closed-

loop reference data within the data checker with the received data bits. This feature enabled any data checker to operate with any data generator regardless of physical distance or signal delay. The data generator first created a reproducible digital bit pattern and then inserted an encoded control word as part of the transmitted bit stream. For the phase I tests all digital data were sent at an information rate of 220 Mbps. From the control word the data checker derived enough information about the original bit pattern to recreate the data transmitted by the data generator. The recreated data could then be compared with the received data to check for individual bit errors.

Data Processor

The data processor performed functions similar to a TDMA controller in a satellite-switched TDMA Earth terminal. The data processor formatted and routed digital user data, generated the necessary modem control signals and maintained the system timing. The data processor also scrambled and descrambled baseband data between the DG/DC subsystem and the modem to achieve adequate transition density within the data bits for demodulator synchronization. Parallel-to-serial (P/S) and serial-to-parallel (S/P) converters were employed to create serial data to the SMSK modem subsystem.

SMSK Modem

The modems used for the phase I experiments were 220-Mbps SMSK versions built by Motorola's Government Electronics Group. These SMSK modems have proven to be very reliable in high-data-rate systems. SMSK is theoretically equivalent to BPSK or QPSK in BER-versus- E_b/N_0 performance. TDMA transmission through a satellite requires the use of modulation schemes that are bandwidth and power efficient. SMSK is spectrally efficient for two reasons. One is that the main lobe of the spectrum contains 99 percent of the data energy; the SMSK main lobe is 50 percent wider than

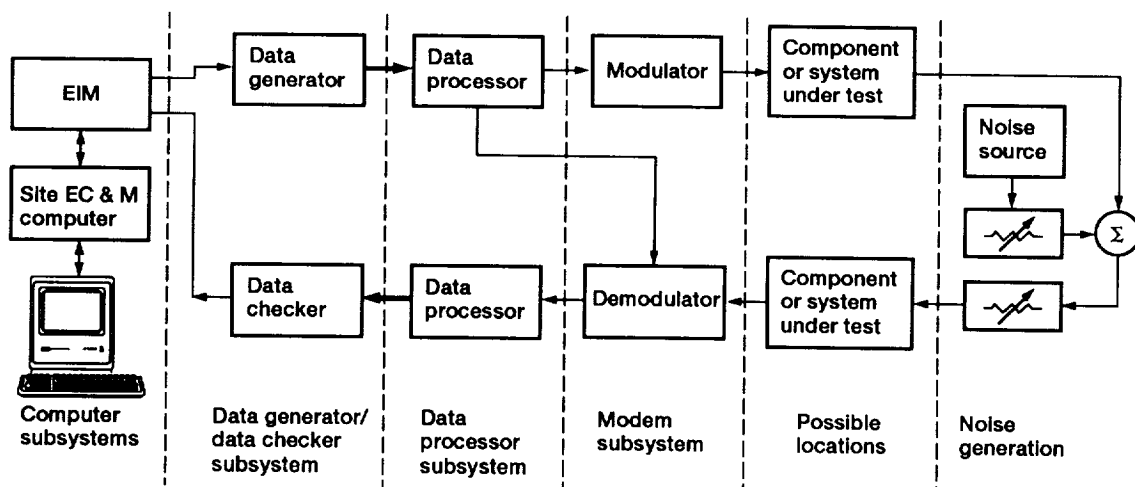


Figure 65.—Block diagram of BER measurement system hardware.

that in QPSK but is 25 percent narrower than that in BPSK. The out-of-band (side lobe) energy is significantly less than that in either BPSK or QPSK; thus, SMSK is more robust when encountering adjacent channel interference. SMSK is known as constant-envelope modulation and therefore can be used with nonlinear amplification without the chance of increasing out-band spectral energy. This is important because high-power amplifiers, such as TWTA's, are most efficient when operated near saturation.

The 220-Mbps modulator (fig. 66) was basically a BPSK modulator with a carrier frequency offset from center by one-quarter of the data rate (i.e., $f_c = f_0 - 1/4 R$). A bandpass conversion filter, consisting of a quadrature hybrid and a power summer followed by a two-pole Butterworth bandpass filter, realized the SMSK-modulated signal.

The basic structure of the 220-Mbps demodulator (fig. 67) was essentially the reverse of the modulator structure. It consisted of an input-bandpass-matched filter, followed by a coherent demodulator and then a low-pass filter to eliminate

the double frequency components at the mixer output. Automatic gain control circuitry was provided to allow for burst-to-burst baseband signal variation over a 20-dB dynamic range.

Carrier synchronization was implemented by a Costas loop, which derived a filtered phase error signal that was used to correct the phase of the 3.3-GHz VCO. Injection locking of an unmodulated carrier was performed to remove phase ambiguity (presence of stable lock points at 0° and 180°) in the carrier acquisition loop. This unmodulated carrier is sent as a portion of the preamble in a TDMA system. Bit timing was accomplished by transition tracking, which measured the timing error between the local clock and the measured transition times of the demodulated baseband data and used this error to pull the local clock into synchronization. This method of bit synchronization can be subject to lockup caused by a long sequence of ones or zeroes. It is therefore important to provide adequate transition density in the TDMA data burst in order to avoid this problem. A unique word detector was used to signal the beginning of the data words in the TDMA frame.

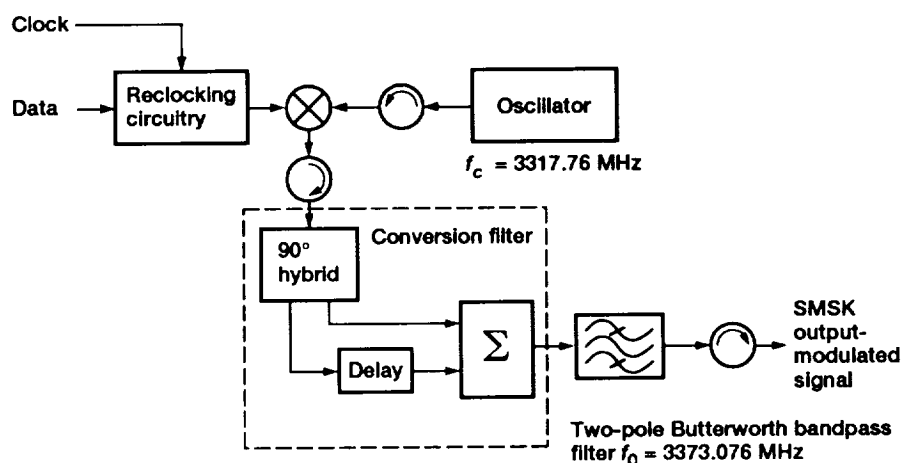


Figure 66.—Block diagram of 220-Mbps modulator.

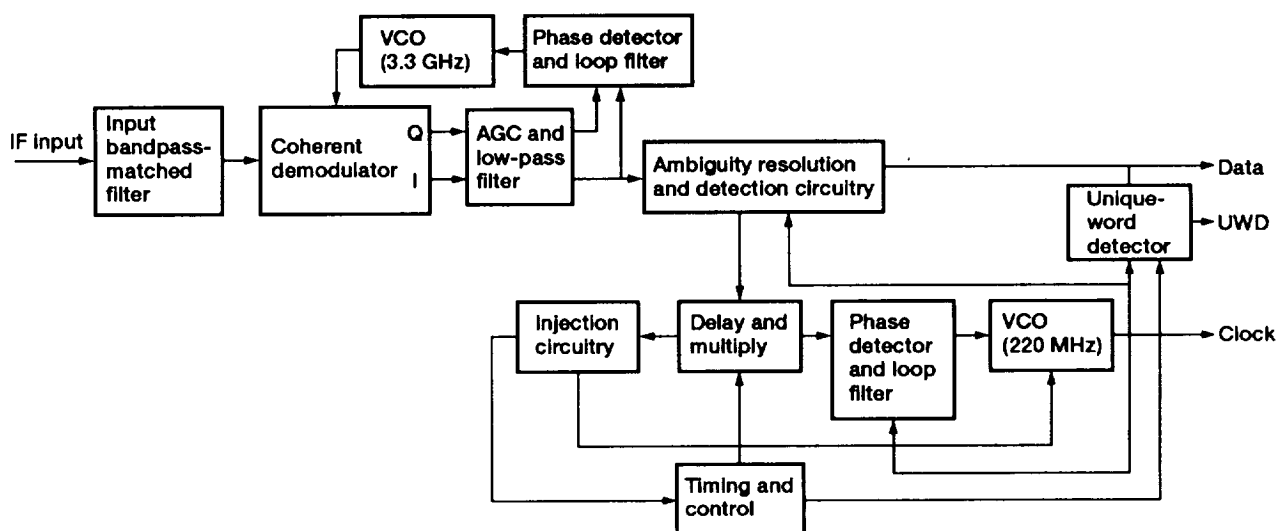


Figure 67.—Block diagram of 220-Mbps demodulator.

Noise Generation Unit

In order to control the signal-to-noise ratio S/N , a noise generation unit was built and added to the phase I digital Earth terminal. A block diagram is shown in figure 68. White noise power was generated by a solid-state noise source and regulated by a step attenuator. The noise and test signals were combined by using a power summer and adjusted to a constant power level with a second step attenuator. By selectively adjusting the attenuation settings in the noise generation unit, a range of S/N values were obtained, while maintaining a constant IF power level. The variation of the S/N allowed the user to vary the number of errors introduced by noise in the system and thus change the BER performance. The noise generation unit was bandlimited for the 220-Mbps data rate by a 330-MHz-wide bandpass filter centered at 3.373 GHz. The noise generation unit was calibrated by measuring the modulated signal power and the noise power generated from the noise unit. These measurements were used to determine two similar parameters, energy per bit E_b and noise power density N_0 . The E_b/N_0 values were used as the control variables during a given BER test. These values were based on the data rate employed and were calculated by using the expression

$$E_b/N_0(\text{dB}) = (P_s - P_n) + N_{bw} - R$$

where

P_s measured signal power, dB

P_n measured noise power, dB

N_{bw} noise bandwidth of calibration filter, dB Hz

R data rate, dB Hz

The noise was assumed to be additive white Gaussian; this assumption allowed the theoretical probability of error to be

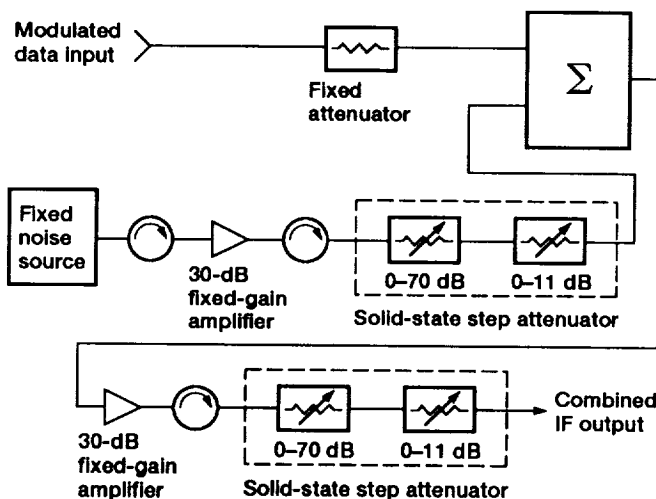


Figure 68.—Block diagram of noise generation unit.

defined as

$$\text{BER} = 1/2 \operatorname{erfc} (E_b/N_0)^{1/2}$$

This quantity served as the ideal limit in the case of a perfect demodulator. The BER performance of the back-to-back modulator-demodulator test is shown in figure 69.

Experiment Control and Monitor

An EC&M computer was employed to measure the numerous RF responses as well as the BER. It served as the controller and data processor throughout the phase I testing. Another computer, the EC&M interface microcomputer (EIM) controlled the BER data acquisition and provided the control interface to the data generator/data checker subsystem, as shown in figure 65.

A number of software routines were developed to automate the tests required by the SITE test engineers. The BER measurement software employed three control programs to complete a BER test. A menu-driven setup program began the test. In this program all necessary test instrument information, such as device type, address, and settings, was compiled and placed in the proper test sequence. The second program executed the sequence of actions required to perform the test. The validity of the measured data was also checked, and the test

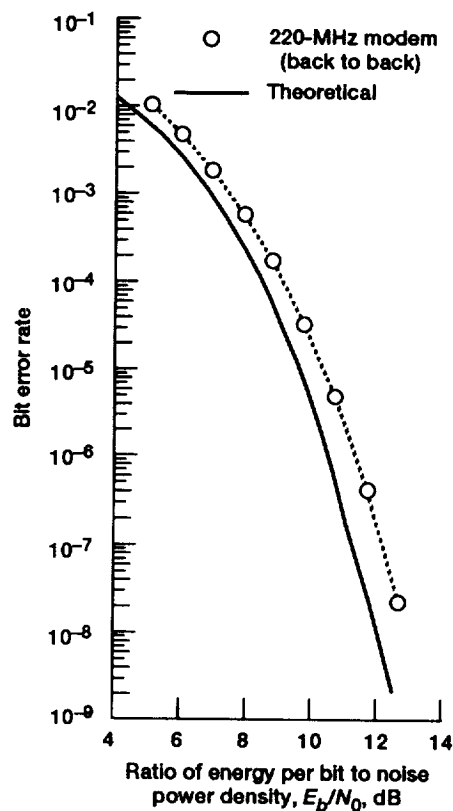


Figure 69.—Performance of back-to-back modems.

status was updated and displayed for use by the test engineer. The third phase was the data-processing phase. The data file created in the first two phases could then be printed directly or processed further to yield the test data in a desirable format.

The BER was usually measured over the range 10^{-2} to 10^{-8} . The lower figure was chosen as a goal for the overall system performance, and a BER test would normally run until at least one data point approached or exceeded this limit. For example, if the test device or system was required to operate

at a BER of 10^{-6} , one final data point would be taken at a BER less than 10^{-6} . A linear interpolation would then be done between the last and next-to-last data points to determine the E_b/N_0 required for a BER of 10^{-6} . An algorithm was employed to minimize the measurement time required to obtain a BER-versus- E_b/N_0 curve. The algorithm yielded a average measurement time of 35 minutes to produce a complete curve (BER measured over 10^{-2} to 10^{-8}) with an error bound of 0.1 and a probability of 0.9.

References

1. Kerczewski, R.J.: The Bit-Error Rate Performance of a Satellite Microwave Matrix Switch. 12th International Communications Satellite Systems Conference, AIAA, New York, 1988, pp. 403-414. (Also, NASA TM-100285, AIAA Paper 88-0826.)
2. Saunders, A.L.: 20 × 20 High Speed Microwave Switches. NASA TM-83775, 1984.
3. Shalkhauser, K.A.; Nagy, L. A.; and Svoboda, J. S.: Rain-Fade Simulation and Power Augmentation for Satellite Communication Systems. NASA TM-103134, 1990.
4. Kerczewski, R.J.: A Study of the Effect of Group Delay Distortion on an MSK Satellite Communications Channel. NASA TM-89835, 1987.
5. Matthews, I.: Technique Simplifies AM-to-PM Measurements. *Microwaves RF*, vol. 23, no. 8, Aug. 1984, pp. 108-110,112.
6. Sklar, B.: *Digital Communications Fundamentals and Applications*. Prentice Hall, 1988.
7. Shalkhauser, M.J.W.; and Budinger, J.M.: Digitally Modulated Bit Error Rate Measurement System for Microwave Component Evaluation. NASA TP-2912, 1989.
8. Kerczewski, R.J.; Daugherty, E. S.; and Kramarchuk, I.: Automated Measurement of the Bit-Error Rate as a Function of Signal-to-Noise Ratio for Microwave Communications Systems. NASA TM-89898, 1987.
9. Weinberg, A.: The Effects of Transponder Imperfections on the Error Probability Performance of a Satellite Communication System. *IEEE Trans. Commun.* COM-28, no. 6, June 1980, pp. 858-872.
10. Conroy, M.J.; and Kerczewski, R. J.: Testing of 30 GHz Low Noise Receivers. Eleventh AIAA Communications Satellite Systems Conference, AIAA, 1986, pp. 326-340. (Also, NASA TM-87171.)
11. Steffek, L.S.; and Smith, D.W.: The 30 GHz Communications Satellite Low Noise Receiver. (LNR-400, LNR Communications Inc.; NASA Contract NAS3-22494), NASA CR-168254, 1983.
12. Dewland, J.F.; and Goldman, H.: The 30 GHz Low Noise Receiver for Satellite Communications. NASA CR-168184, 1983.
13. Watkins, E.T.; and Schellenberg, J.M.: Hybrid Microwave Integrated Circuit Ka-Band Low Noise Receiver. NASA Contract NAS5-26731, Final Report.
14. Ziemer, R.E.; and Tranter, W.H.: *Principles of Communications*. 2nd ed., Houghton-Mifflin, 1985.
15. Ippolito, L.J.: Radio Propagation for Space Communications Systems. *Proc. IEEE*, vol. 69, no. 6, June 1981, pp.697-727.
16. Cox, D.C.; Arnold, H.W.; and Leck, R.P.: Phase and Amplitude Dispersion for Earth-Satellite Propagation in the 20- to 30-GHz Frequency Range. *IEEE Trans. Anten. Propagat.*, vol. AP-28, no. 3, May 1980, pp. 359-366.
17. Rummier, W.D.; Coutts, R.P.; Liniger, M.: Microwave Digital Radio. 3. Multipath Fading Channel Models for Microwave Digital Radio. *IEEE Communications Mag.*, vol.24, no. 11, Nov. 1986, pp. 30-42.
18. Swept-Frequency Group Delay Measurements. Application Note 77-4, Hewlett-Packard, 1968.
19. Laico, J.P.; McDowell, H.L.; and Moster, C.R.: A Medium Power Traveling-Wave Tube for 6,000-Mc Radio Relay. *Bell Syst. Tech. J.*, vol. 35, no. 6, Nov. 1956, pp. 1285-1346.
20. Shalkhauser, K.A.; and Fujikawa, G.: Bit-Error-Rate Testing of High Power 30-GHz Traveling Wave Tubes for Ground Terminal Applications. NASA TP-2635, 1986.
21. Shalkhauser, M.J.W.: Design and Implementation of a Microcomputer-Based User Interface Controller for Bursted Data Communications Satellite Ground Terminals. NASA TM-101375, 1988.

Bibliography

- A 30/20 GHz Low Data Rate Ground Terminal Design Study. NASA CR-177221, 1983.
- Cory, B.J.: Spacecraft IF Switch Matrix for Wideband Service Applications in 30/20 GHz Communication Satellite Systems. NASA CR-168089, 1982.
- Fujikawa, G.: Characterization of Two MMIC GaAs Switch Matrices at Microwave Frequencies. NASA TM-102449, 1990.
- Fujikawa, G.; and Kerczewski, R.J.: Performance of a Ka-Band Satellite System Under Variable Transmitted Signal Power Conditions. NASA TM-88984, 1987.
- Gagliardi, R.M.: *Satellite Communications*. 2nd Ed. Van Nostrand Reinhold, New York, 1991.
- Giger, A.J.; and Barnett, W.T.: Effects of Multipath Propagation on Digital Radio. *IEEE Trans. Commun.*, vol. COM-29, no. 9, Sept. 1981, pp. 1345-1352.
- Ho, P.T.; Coban, E.; and Pelose, J.: Spacecraft IF Switch Matrix for Wideband Service Applications in 30/20 GHz. NASA CR-168175, 1983.
- Hughes TWT and TWTA Handbook. Hughes Electron Dynamics Division, Hughes Aircraft Co.
- Kerczewski, R.J.; and Fujikawa, G.: Interference Susceptibility Measurements for an MSK Satellite Communications Link, 14th AIAA Communications Satellite Systems Conference, 1992. (Also, NASA TM-105395.)
- Kerczewski, R.J.; Ponchak, G.E.; and Romanofsky, R.R.: Performance of Five 30 GHz Satellite Receivers. 1989 IEEE MTT-S International Microwave Symposium, IEEE, 1989, pp. 1079-1082 (Also, NASA TM-101960).
- Rummier, W.D.: A Simplified Method for the Laboratory Determination of Multipath Outage of Digital Radios in the Presence of Thermal Noise. *IEEE Trans. Commun.*, vol. COM-30, no. 3, Mar. 1982, pp. 487-494.
- Saunier, P.; and Nelson, S.: 30/20 GHz Spacecraft GaAs FET Solid State Transmitter for Trunking and Customer-Premises-Service Application. (TI-08-83-42, Texas Instruments Inc.; NASA Contract NAS3-22504), NASA CR-168276, 1983.
- Tamashiro, R.N.: The 20 GHz, 75 Watt, Helix Traveling Wave Tube for Space Communications. NASA CR-168271, 1984.

REPORT DOCUMENTATION PAGE			Form Approved OMB No. 0704-0188	
Public reporting burden for this collection of information is estimated to average 1 hour per response, including the time for reviewing instructions, searching existing data sources, gathering and maintaining the data needed, and completing and reviewing the collection of information. Send comments regarding this burden estimate or any other aspect of this collection of information, including suggestions for reducing this burden, to Washington Headquarters Services, Directorate for Information Operations and Reports, 1215 Jefferson Davis Highway, Suite 1204, Arlington, VA 22202-4302, and to the Office of Management and Budget, Paperwork Reduction Project (0704-0188), Washington, DC 20503.				
1. AGENCY USE ONLY (Leave blank)	2. REPORT DATE September 1992	3. REPORT TYPE AND DATES COVERED Technical Publication		
4. TITLE AND SUBTITLE Phase I Final Report of the SITE Project: Continuous Data Bit-Error-Rate Testing		5. FUNDING NUMBERS WU-650-60-23		
6. AUTHOR(S) Gene Fujikawa and Robert J. Kerczewski				
7. PERFORMING ORGANIZATION NAME(S) AND ADDRESS(ES) National Aeronautics and Space Administration Lewis Research Center Cleveland, Ohio 44135-3191		8. PERFORMING ORGANIZATION REPORT NUMBER E-6513		
9. SPONSORING/MONITORING AGENCY NAMES(S) AND ADDRESS(ES) National Aeronautics and Space Administration Washington, D.C. 20546-0001		10. SPONSORING/MONITORING AGENCY REPORT NUMBER NASA TP-3279		
11. SUPPLEMENTARY NOTES Responsible person, Robert J. Kerczewski, (216) 433-3434.				
12a. DISTRIBUTION/AVAILABILITY STATEMENT Unclassified - Unlimited Subject Category 18			12b. DISTRIBUTION CODE	
13. ABSTRACT (Maximum 200 words) The Systems Integration, Test, and Evaluation (SITE) Project at the NASA Lewis Research Center encompasses a number of research and technology areas of satellite communications systems. Phase I of this project established a complete satellite link simulator system. The evaluation of proof-of-concept microwave devices, radiofrequency (RF) and bit-error-rate (BER) testing of hardware, testing of remote airlinks, and other tests were performed as part of this first testing phase. This final report covers the test results produced in phase I of the SITE Project. The data presented include 20-GHz high-power-amplifier testing, 30-GHz low-noise-receiver testing, amplitude equalization, transponder baseline testing, switch matrix tests, and continuous-wave and modulated interference tests. The report also presents the methods used to measure the RF and BER performance of the complete system. Correlations of the RF and BER data are summarized to note the effects of the RF responses on the BER.				
14. SUBJECT TERMS Satellite communications systems; Microwave frequencies; Bit error rate			15. NUMBER OF PAGES 92	
			16. PRICE CODE A05	
17. SECURITY CLASSIFICATION OF REPORT Unclassified	18. SECURITY CLASSIFICATION OF THIS PAGE Unclassified	19. SECURITY CLASSIFICATION OF ABSTRACT Unclassified	20. LIMITATION OF ABSTRACT	

National Aeronautics and
Space Administration
Code JTT
Washington, D.C.
20546-0001
Official Business
Penalty for Private Use, \$300

BULK RATE
POSTAGE & FEES PAID
NASA
Permit No. G-27



POSTMASTER: If Undeliverable (Section 158
Postal Manual) Do Not Return
